NASA CONTRACTOR REPORT

NASA CR

NASA CR-641

DEVELOPMENT OF A GENERAL PURPOSE AIRBORNE SIMULATOR

by John Kroll, Rudy H. Arendt, and Francis E. Pritchard

Prepared by
CORNELL AERONAUTICAL LABORATORY, INC.
Buffalo, N. Y.
for Flight Research Center

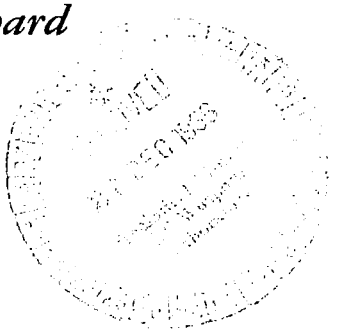

NATIONAL AERONAUTICS AND SPACE ADMINISTRATION • WASHINGTON, D. C. • NOVEMBER 1966

DEVELOPMENT OF A GENERAL PURPOSE AIRBORNE SIMULATOR

By John Kroll, Rudy H. Arendt,
and Francis E. Pritchard

Prepared under Contract No. NAS 4-607 by
CORNELL AERONAUTICAL LABORATORY, INC.
Buffalo, N.Y.

for Flight Research Center

NATIONAL AERONAUTICS AND SPACE ADMINISTRATION

For sale by the Clearinghouse for Federal Scientific and Technical Information
Springfield, Virginia 22151 – Price $3.00

ABSTRACT

This report summarizes the major design, analysis, and test efforts performed by the Cornell Aeronautical Laboratory, Inc., during the development of the variable stability system for the General Purpose Airborne Simulator (GPAS). The GPAS is a NASA-owned Lockheed JetStar incorporating a variable stability system that can operate in two modes, as a model-controlled system (MCS) and as a response feedback system (RFS). The theory and operation of both systems are discussed, but since the MCS is considered the primary system, it is given the most attention. The RFS is considered a backup system but it can also be used to augment MCS performance. Methods for computing MCS control loop gains are described. Functional and detailed designs are described for the major GPAS subsystems, the flight control system, variable feel system, pilot's instruments and control panels, airborne computer, test engineer's console, and data acquisition system. In addition, results are presented from the preliminary ground and flight test programs which illustrate the performance of the GPAS variable stability system.

FOREWORD

This report discusses the development, general theory of operation, description, and capabilities of a General Purpose Airborne Simulator (GPAS) constructed for the NASA Flight Research Center, Edwards AFB, California, under contract NAS 4-607. Mr. Jack Fischel and Mr. Dwain A. Deets served as program managers for NASA-FRC during this program.

Program management at CAL was under the direction of Mr. Robert C. Kidder. The aerodynamic, mechanical, and electronic design aspects were under the technical direction of Messrs. John M. Schuler, William Close, and William R. Deazley, respectively. Mr. William Wilcox was responsible for installations. Mr. Daniel C. Clark was the engineer responsible for the conceptual design analysis, and Mr. Arno E. Schelhorn was the lead electronic engineer.

CONTENTS

CONTENTS (Cont.)

TABLES

ILLUSTRATIONS

ILLUSTRATIONS (Cont.)

LIST OF SYMBOLS

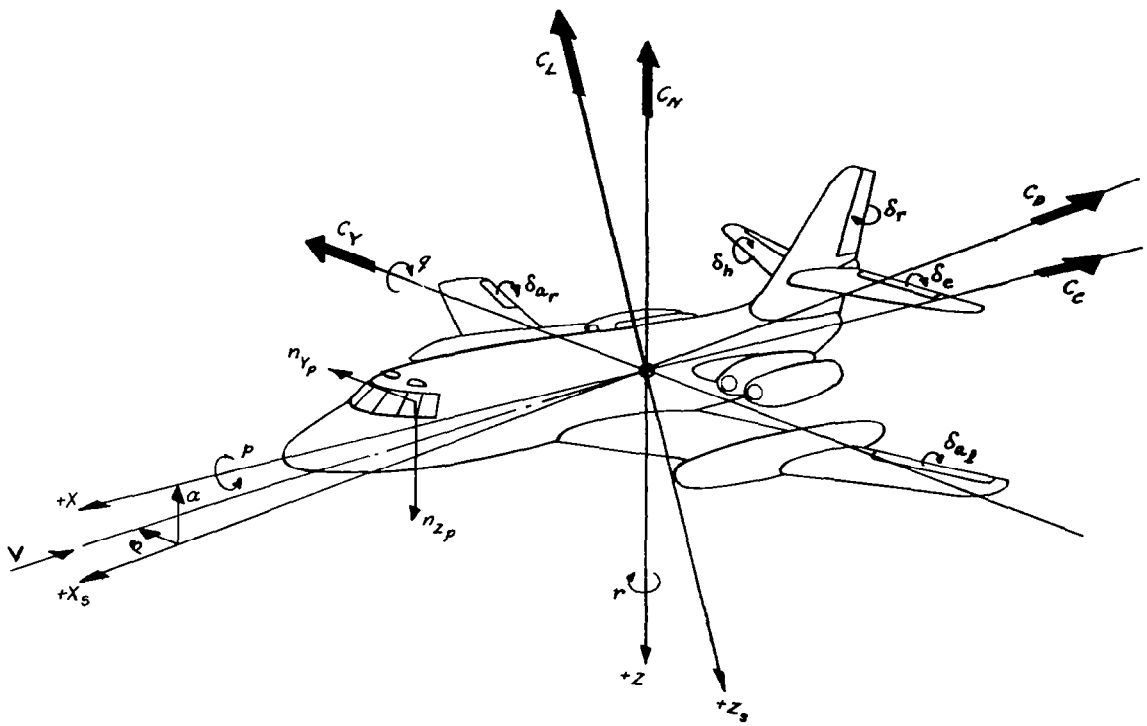

I. Aircraft Geometry, Mass, and Inertia

X, Y, Z	reference body axes
m	aircraft mass, slugs
W	aircraft weight, lb
g	gravitational constant, 32.17 ft/sec^2
S	wing area, ft^2
I_x, I_y, I_z	moments of inertia referred to body axes X, Y and Z, slug-ft^2

I_{xz} product of inertia referred to body X, Y and Z axes, slug-ft^2

$\bar{c}$ mean aerodynamic chord, ft

b wing span, ft

z_T thrust moment arm (positive along + Z axis), ft

II. Aircraft Motion Variables

V total velocity of c.g., ft/sec

α, β angle of attack and sideslip, rad or deg

γ flight path angle, rad or deg

h altitude, ft

M Mach number

a speed of sound, ft/sec

$\bar{q}$ dynamic pressure, $q = \frac{1}{2}\rho V^2$, lb/ft^2

p, q, r angular velocities (roll, pitch, yaw) about X, Y, and Z body axes, rad/sec or deg/sec

ψ, θ, ϕ orientation angles (heading, elevation, bank) defining body axes with respect to inertial space, rad or deg

ρ mass density of air, slugs/ft^3

α_I, β_I inertial angle of attack and sideslip (i.e. $\alpha_I = \alpha - \alpha$ gust), rad or deg

n_x, n_y, n_z accelerometer measured rigid body accelerations at the c.g. along X, Y, and Z body axes, g's

III. Aircraft Modal Properties

ω_{θ_S} undamped natural frequency of the longitudinal short period mode, rad/sec

ζ_{θ_s}	damping ratio of longitudinal short period mode
ω_{θ_p}	undamped natural frequency of the phugoid mode, rad/sec
ζ_{θ_p}	damping ratio of the phugoid mode
ω_ψ	undamped natural frequency of the Dutch roll mode, rad/sec
ζ_ψ	damping ratio of the Dutch roll mode
τ_s	time constant of the spiral mode, sec
τ_r	time constant of the roll mode, sec

IV. Forces and Moments

T	thrust, lb
L	lift, lb, or rolling moment about x-body axis, ft-lb
D	drag, lb
L, M, N	moments (roll, pitch, yaw) about X, Y, and Z body axes, ft-lb
X, Y, Z	components of force along X, Y and Z body axes, lb
C_L	lift coefficient, $C_L = L/\bar{q}S$
C_D	drag coefficient
C_N	normal force coefficient, along negative z-body axis
C_y	side force coefficient, along Y-body axis
C_ℓ	rolling moment coefficient, $C_\ell = L/\bar{q}Sb$
C_m	pitching moment coefficient, $C_m = M/\bar{q}S\bar{c}$
C_n	yawing moment coefficient, $C_n = N/\bar{q}Sb$
$C_{m_{(A)}}$	aerodynamic pitching moment coefficient at trim angle of attack; approximately equal to $-(\bar{z}_T/\bar{c})C_D$

V. Control System Variables

δ_e	elevator deflection, positive T. E. down, rad or deg
δ_a	total aileron deflection ($\delta_a = \delta_{a_\ell} - \delta_{a_r}$), positive left aileron T. E. down, rad or deg
δ_r	rudder deflection, positive T. E. left, rad or deg
δ_h	JetStar stabilizer deflection, positive L. E. up, rad or deg
δ_T	throttle deflection, deg
$\delta_{a_\ell}, \delta_{a_r}$	individual left and right aileron deflections, positive T. E. down, rad or deg
δ_{e_p}	pilot's fore-and-aft (elevator) wheel position, positive aft, in.
δ_{a_p}	pilot's lateral (aileron) wheel position, positive clockwise, deg
δ_{r_p}	rudder pedal position, positive for right pedal forward, in.
δ_{t_p}	simulation throttle position, positive forward, in.
F_e	pilot's longitudinal control force, positive aft, lb
F_a	pilot's lateral control force, positive clockwise, lb
F_r	rudder pedal control force, positive forward on right pedal, lb
ΔT	increment in thrust for thrust control system
EPR	engine pressure ratio, p_{t_5} / p_{t_2}
p_{t_2}	correlated compressor inlet pressure, in. Hg
p_{t_5}	turbine discharge total pressure, in. Hg
p_o	sea-level (standard conditions) static pressure
p_s	free-stream static pressure
p_t	total pressure as measured by a pitot tube
$\bar{q}_c$	impact pressure, compressible dynamic pressure, $p_t - p_s$

h_p	pressure altitude, ft
h_I	inertial altitude, as obtained from acceleration measurements in the air-data system, ft
V_I	inertial velocity, as obtained from acceleration measurements in the air-data system, ft/sec or knots
$V_{\bar{q}_c}$	true airspeed, as generated by the air-data system using standard conditions, ft/sec or knots
V_i	indicated airspeed, as displayed on pilot's panel, knots
x	arbitrary input in elevator feel system
e	error, command minus measured variable, with variable as subscript (e.g., $e_p = p_c - p$)
δ_e/α, etc.	RFS gain (e.g., elevator/angle of attack)
δ_e/e_α, etc.	MCS gain (e.g., elevator/error in angle of attack)
α_V	fuselage-mounted angle of attack vane deflection, deg
β_V	fuselage-mounted sideslip vane deflection, deg
$(\delta_e/e_{\dot{\alpha}})'$	$\delta_e/e_{\dot{\alpha}}$ gain used for damping with MCS normal acceleration (n_z) loop
$\delta_e', \delta_a', \delta_r'$	command signals feeding elevator, aileron, and rudder servos but without the automatic balance input and control interconnect signals (e.g., δ_e/δ_h, δ_a/δ_r', δ_r/δ_a')
$(\delta_r/e_{\dot{\beta}})'$	$\delta_r/e_{\dot{\beta}}$ gain used for damping with MCS lateral acceleration (n_y) loop
τ_V	time constant in MCS $\Delta T/e_V$ control loop

VI Stability Derivatives in Coefficient Form

The derivatives in normalized form for the equations of motion are presented in the Appendix.

$C_{L_\alpha} = \partial C_L / \partial \alpha$

$C_{L_{\delta_e}} = \partial C_L / \partial \delta_e$

$C_{D_\alpha} = \partial C_D / \partial \alpha$

$C_{m_\alpha} = \partial C_m / \partial \alpha$

$C_{m_{\dot{\alpha}}} = \partial C_m / \partial \left(\frac{\dot{\alpha}\bar{c}}{2V}\right)$

$C_{m_q} = \partial C_m / \partial \left(\frac{q\bar{c}}{2V}\right)$

$C_{m_{\delta_e}} = \partial C_m / \partial \delta_e$

$C_{Y_\beta} = \partial C_Y / \partial \beta$

$C_{Y_{\delta_r}} = \partial C_Y / \partial \delta_r$

$C_{\ell_p} = \partial C_\ell / \partial \left(\frac{pb}{2V}\right)$

$C_{\ell_r} = \partial C_\ell / \partial \left(\frac{rb}{2V}\right)$

$C_{\ell_\beta} = \partial C_\ell / \partial \beta$

$C_{\ell_{\delta_r}} = \partial C_\ell / \partial \delta_r$

$C_{\ell_{\delta_a}} = \partial C_\ell / \partial \delta_a$

$C_{n_p} = \partial C_n / \partial \left(\frac{pb}{2V}\right)$

$C_{n_r} = \partial C_n / \partial \left(\frac{rb}{2V}\right)$

$C_{n_\beta} = \partial C_n / \partial \beta$

$C_{n_{\delta_r}} = \partial C_n / \partial \delta_r$

$C_{n_{\delta_a}} = \partial C_n / \partial \delta_a$

$C_{L_{\delta_h}} = \partial C_L / \partial \delta_h$

$C_{m_{\delta_h}} = \partial C_m / \partial \delta_h$

VII. Additional Symbols and Subscripts

s Laplace Transform variable, rad/sec

Δ incremental change from a reference condition

$u(t)$ the unit step-function

$\bar{\alpha}/\delta_e$ short-period steady-state angle of attack per unit elevator deflection, $\frac{M_{\delta_e} - M_q Z_{\delta_e}}{-M_\alpha + M_q Z_\alpha}$ (see Appendix for $M_\alpha, M_q, M_{\delta_e}, Z_\alpha, Z_{\delta_e}$)

Z'_{δ_e} equivalent elevator normal-force parameter, $(Z_\alpha + Z_\theta)\frac{\bar{\alpha}}{\delta_e} + Z_{\delta_e}$ (see Appendix for $Z_\alpha, Z_\theta, Z_{\delta_e}$)

t real time, sec

$(\dot{})$ dot over symbol indicates differentiation with respect to time

sub e	elevator or elevon
sub a	aileron
sub r	rudder
sub m	refers to model
sub t	indicates trim conditions
sub p	refers to pilot or cockpit location
sub c	command
MCS	model controlled system
RFS	response feedback system
GPAS	General Purpose Airborne Simulator
CAL	Cornell Aeronautical Laboratory
NASA	National Aeronautics and Space Administration
FRC	Flight Research Center
H	"heavy" JetStar weight condition, 38,200 lb
L	"light" JetStar weight condition, 23,900 lb

SECTION 1

INTRODUCTION

1.1 HISTORY

Variable stability airplanes have been used for well over a decade to investigate the particular flying qualities problems of specific configurations, and to help in the quest for a better understanding of the dynamic behavior of pilot-airframe combinations. As aircraft designers have expanded flight boundaries to cover wider ranges of conditions, new and challenging problems in flight dynamics have been uncovered. To cope with these problems, researchers using variable stability aircraft have also expanded the capabilities of their research aircraft. More effective analytical and computational techniques have been developed; in-flight calibration, identification and experimental techniques have been improved as have the dynamic performance and reliability of system components. This report describes the most recent major effort in the continuing development of variable stability technology.

In 1964 the NASA Flight Research Center awarded Cornell Aeronautical Laboratory, Inc. (CAL) a contract to develop a new variable stability system for installation in a Lockheed JetStar (NASA 814). Under this contract CAL was responsible for the complete design, fabrication and installation of the variable stability system and ancillary equipment. The system developed for the JetStar is the most comprehensive variable stability system built so far, providing a versatile general purpose in-flight simulation capability. Accordingly, NASA refers to this research facility as the General Purpose Airborne Simulator, or GPAS.

1.2 BRIEF DESCRIPTION OF GPAS

The variable stability system developed for GPAS is unusual because it incorporates a relatively new type of variable stability system, called the "model controlled system" (MCS). This new approach essentially involves

forcing the airplane, through high-gain control loops, to literally follow the response of the simulated airplane as computed by an airborne analog computer. In addition to this model-following capability, the ability to operate GPAS as a "response feedback system" (RFS) is also provided. The response feedback approach is the one most commonly used in the past, and essentially involves matching aerodynamic derivatives (or combinations of derivatives) using feedback gains. The two techniques are illustrated by the simplified block diagrams in Figures 1-1 and 1-2 and are described in Section 2.

The GPAS variable stability system is comprised of the following major elements: the flight control system, variable feel system, pilot's instruments and control panels, airborne computer, test engineer's console, and data acquisition system.

The variable stability system employs the normal JetStar aerodynamic control surfaces and jet engines to vary the moments about all three axes and the forces along the longitudinal (x) axis. New irreversible electrohydraulic servos position the aerodynamic controls (the elevator, ailerons, and rudder) while electromechanical servos position the four jet engine throttle controls. The right-hand or safety pilot's controls and the normal throttle levers remain connected to the control surfaces and engine throttle controls as in a normal JetStar. Thus, in variable stability operation the airplane motions and the safety pilot's control motions correspond as they would in a normal JetStar. The test or evaluation pilot sits in the left-hand seat, and his controls represent those of the simulated airplane. The evaluation pilot's controls have been mechanically disconnected from the JetStar control surfaces (a ground adjustable link is provided to restore normal JetStar operation for ferry flights, etc.) and electrical signals from the left-hand controls are used in variable stability operation. A new, single simulation throttle lever is provided for the evaluation pilot. Thus, in variable stability operation the airplane motions and the evaluation pilot's control motions, including the throttle lever, correspond as they would in the simulated airplane.

The evaluation pilot's flight controls are connected, with the exception of the throttle, to electrohydraulic variable-feel servos. Feel for the simulation throttle lever is provided by a variable friction lock. Both force

and position outputs are available from the wheel and rudder pedals for use as inputs to the rest of the variable stability system; only a position output is available from the throttle handle. The feel systems for the wheel and rudder pedals provide not only variable force per deflection gradients but also such nonlinear effects as friction, break-out forces, and nonlinear variations of force with deflection. Also, the effect of bob weights in the elevator system can be simulated.

The flight instruments on the left-hand or evaluation pilot's panel are simulation instruments. They can indicate the actual JetStar conditions as obtained directly from sensors; or they can indicate the simulated conditions as obtained from the airborne computer, which may be different from the actual JetStar conditions. The safety pilot's instruments on the right are normal JetStar flight instruments. Instruments and controls for engaging and monitoring the variable stability system are provided in the cockpit. The feel system control panel is located on the evaluation pilot's left side panel. The main control panel is located near the center of the front instrument panel. System disengage buttons are located on both pilot's wheels as well as on the center control panel.

The airborne computer, test engineer's console, data acquisition system, and the system electronic modules (amplifiers, differentiator, demodulators, safety trip circuits, etc.) comprise the bulk of the variable stability equipment located in the JetStar cabin. The airborne computer is a moderate size, general purpose analog computer suitable for solving six-degree-of-freedom airplane equations of motion. Its primary function is to serve as the analog model when the system is operated in the MCS mode. The test engineer's console contains all the MCS and RFS gains and controls, variable feel system gains and controls, instruments for monitoring the airplane and model responses, a direct writing 12-channel recorder for in-flight use, and miscellaneous control panels for variable stability system operation. The data acquisition system consists of the various sensors, signal processing and computing equipment, and the recording system with its one 50-channel and two 26-channel oscillographs.

The GPAS system was designed to be flexible and to readily accommodate future expansion. Accordingly, patch panels have been incorporated into the system where appropriate. Provisions have been made to add additional MCS loops, to expand the airborne computer to a digital-analog hybrid, and to add a magnetic tape system to the primary recording system.

Reliability and safety of operation were stressed during the design and development of the GPAS system. Various automatic features are incorporated to facilitate system operation. Where practical, use has been made of components and techniques already proved satisfactory in CAL variable stability aircraft. Where the variable stability system mates with the primary flight control system (e.g., the variable-stability control-surface servos) so that safety of flight is concerned, fail-safe components and redundancy are employed to assure that single failures cannot lead to hazardous conditions.

Each variable stability aircraft is different from those built in the past, and presents its own special problems that must be solved during the early development phase and, later on, as the aircraft is used in research programs. GPAS, with its many innovations, certainly is no exception. However, based on the limited testing and modification already performed by CAL and NASA, it seems clear that the GPAS system essentially meets the design requirements and that it will prove to be an excellent variable stability system.

1.3 REPORT CONTENTS

The overall design approach for the GPAS variable stability system is described in Section 2. Emphasis is placed on MCS design, as compared to RFS design, because the MCS is considered the primary GPAS system. Also, the RFS design is straightforward, as it rests on a wealth of background and experience, while MCS design is new and not well understood. Because of its importance, a considerable portion of Section 2 is devoted to control loop design and the calculation of system gains in terms of performance.

The functions of the various major GPAS subsystems are described in Section 3. The detailed design of the electrical, mechanical, and hydraulic components are described in Section 4.

The performance of the GPAS variable stability system, as determined from the initial ground and flight tests performed at CAL, are described in Section 5. Key aspects of these tests are the determination of the performance of the variable stability servos, and the determination of the maximum gains realizable in flight and their attendant effect on the dynamics of the closed-loop airplane.

SECTION 2

DESIGN APPROACH

2.1 COMPARISON OF MCS AND RFS CHARACTERISTICS

An airplane with a model controlled variable stability system (Figure 1-1) duplicates the dynamic motions of a mathematical model programmed on an airborne analog computer. The pilot's cockpit control motions generate signals which become inputs to the computer model. The variables in the computer model then respond according to the programmed equations of motion. That is, the pilot flies the computer model.

To make the airplane duplicate the computer model response, the computer outputs representing various motion variables are used as command inputs to the airplane control system. These command inputs are compared with the corresponding airplane motion variables and the resulting errors are appropriately combined in high gain control loops to actuate the airplane control surfaces so that the airplane response follows that of the computer model. The airplane is now a closed loop system whose dynamics depend on the control gains used to reduce the errors between the airplane response and the model response. The dynamics of this closed-loop portion of the MCS system (Figure 1-1) are entirely different from the dynamics of the computer model. Ideally, the closed-loop dynamics would have a unity transfer function for model inputs and a null transfer function for disturbance inputs. Practically, with the proper set of feedback variables and control gains, the dynamic characteristics of the closed-loop portion of the MCS will be such that the airplane can follow or duplicate the responses of many different types of models.

A response feedback variable stability system (Figure 1-2) uses a feedback control system to move control surfaces proportionally to airplane response variables. The pilot's cockpit control motions generate signals that command specific control surface deflections. The feedback signals

cause additional control surface deflections that are superimposed on those commanded by the pilot. The control surface motions caused by the feedback signals generate incremental stability derivatives that are effectively added to, or subtracted from, the stability derivatives inherent to the airplane. With proper control loop gains and feedback variables, the effective derivatives of the closed-loop portion of the RFS will match those of the particular mathematical model which is being simulated. The RFS system then, is basically a derivative matching approach. Conventional pitch and yaw dampers are simplified versions of a response feedback system. Considering a pitch damper for example, the airplane's inherent pitch damping (M_q or C_{mq}) is augmented by the increment due to the elevator motion proportional to pitch rate.

Both systems have advantages and disadvantages. The MCS system has the flexibility of analog computer operation. Different sets of model equations of motion can be easily programmed on the analog computer. Aerodynamic derivatives and nonlinearities can be specified with the accuracy of analog potentiometer settings and can also be varied, introduced, or removed at will. The important feature here is that conduct of in-flight simulation centers around analog manipulations with the model -- the dynamics of the closed-loop portion of the MCS system are not tampered with.

Because of the high gain control loops, the dynamics of the closed-loop portion of the MCS system are relatively insensitive to changes in basic airframe stability characteristics which are caused by, say, c.g. shifts or weight changes. In particular, such changes will not significantly degrade model following performance when low frequency analog models are used. That is, the closed-loop airframe will accurately reproduce low frequency model dynamics even though the basic or open-loop airframe stability and control derivatives are not accurately known. The model derivatives, on the other hand, are known within the accuracy of analog potentiometer settings.

Flight calibrations, then, are largely a matter of judging whether the errors between the model response variables and the corresponding airplane response variables fall within acceptable limits. There is no need to identify

from flight test data the dynamic characteristics of the closed-loop portion of the MCS system. They bear no resemblance to those of the model and the pilot is unaware of them for a wide range of model dynamics.

The MCS system has a weight disadvantage caused primarily by the airborne analog computer which must have sufficient capacity for programming reasonably complex mathematical models.

High frequency model simulations pose a fundamental limitation for an MCS. If the model dynamics are too fast, the airplane simply cannot reproduce them with the necessary fidelity. Although the MCS control loops and their attendant high gains are designed to accommodate a wide range of models, the consequences of the high gains can detract from simulation. One of these consequences is the sensitivity to noise and, in particular, to rough air. While the computer model responds only to pilot commands, the closed-loop airplane responds to both analog computer signals and noise that enters any of the control loops, rough air being the most important source. When this occurs, the pilot feels a response which is a combination of smooth air analog model dynamics and rough air airplane dynamics. This combination may differ significantly from the turbulence response of the model. There are several possible means for alleviating this problem (e.g., electronic filtering, proper control loop selection, inserting measured or simulated turbulence into the analog model) but until more MCS flight experience is accumulated, high fidelity simulations in rough air are not expected.

A response feedback variable stability system has good capability for simulating high frequency dynamics. Since the RFS feedback loop gains are adjusted to give the closed-loop airplane a given set of the dynamics, they are, in general, lower than the gains of an MCS system whose analog model had these same dynamics.

As stated before, the RFS system is based on the derivative matching approach. The feedback loop variables and the control gains are used to change the effective derivatives of the basic airframe. The closed-loop airplane has, then, within the limitations of the system, the same transfer functions as the airplane whose dynamics are being simulated. The closed-loop airplane will, therefore, exhibit a closed-loop response to turbulence

similar to that of the simulated airplane. In other words, the fidelity of simulation in rough air is not unduly compromised.

A fundamental shortcoming of the RFS is that it requires calibration and identification of closed-loop airplane dynamics. At a given flight condition it is generally necessary to change many RFS gains in order to vary a single parameter and still keep other parameters constant. After control gains are computed, calibration flights are necessary to prove that the desired dynamics are actually being achieved in flight. If proper dynamics are not being achieved, then gains must be re-evaluated and calibration flights again flown. The difficulty with the RFS stems from the inaccuracy of the methods used for measuring and extracting airplane dynamic characteristics and parameters from flight tests. The stability derivatives of the open-loop airplane are not always known to the accuracy necessary for gain calculations. In particular, when simulating low frequency dynamics, several important open-loop stability derivatives such as M_α and N_β must be reduced to very small magnitudes by subtracting increments due to control surface motions. Small changes in control gains, therefore, have a large effect on the magnitude of the simulated derivatives. Thus, it is difficult to arrive at a set of control gains which will give sufficiently accurate low-frequency simulations.

On the other hand, for high-frequency simulations the incremental derivatives created by the moving control surfaces are added to those of the open-loop airplane. The accuracy in the simulated dynamic characteristics is then much better because the error between the assumed and actual values of the open-loop derivatives is a small percentage of the desired, closed-loop values of these same derivatives.

In summary, the desirable attributes of MCS and RFS variable stability aircraft are complementary. The RFS has the capabilities for simulating high-frequency aircraft beyond the capabilities of the MCS. On the other hand, the MCS has special advantages which make it preferable for simulating sluggish aircraft. Within its applicable range, the MCS has the potential for greatly simplifying flight operations, allowing the simulation of complex aircraft characteristics and sophisticated aircraft flight control systems with relative ease. The inclusion of both MCS and RFS modes in GPAS contributes importantly to its overall capability for in-flight simulation.

2.2 MCS PERFORMANCE REQUIREMENTS

The control loop configuration (i.e., the choice of feedback variables) greatly influences the performance characteristics of a model controlled variable stability system. Studies at CAL have indicated that the high-gain feedback loops should usually incorporate those variables which the airplane is required to match. For example, angle-of-attack should be a feedback loop variable if the airplane is required to match it. However, it is not always possible or practical to feed back a particular variable and occasionally variables related to those quantities being matched are used. Note that additional loops are usually required to obtain adquate matching, either those that provide lead for high frequency matching or those that reduce steady-state or long-term errors.

Once the control loop configuration is selected, the proper control gains must be established. For the given configuration, these gains define the closed-loop dynamic behavior so their values must be based on the requirements established for the system performance.

In designing the system, two very real types of limitations on system operation must be considered. The first type may be defined as those limitations which can be predicted beforehand and can be dealt with analytically. For example, if for the longitudinal system only two controls are available, the elevator and throttle, then it will not be possible to simultaneously control all three longitudinal degrees of freedom, and the system must be designed to perform as best it can within this limitation. A variety of limitations fall within this first class, and mathematical and computer analyses generally suggest courses of action to remove, modify, or live within such limitations.

The second type of limitation may be defined as those which can not be predicted with sufficient precision and can not be analytically treated prior to actually testing the system. These types range from those which are known but are too complicated to analyze (i.e., gain limitations imposed by structural feedback) to those which are unknown or totally unexpected. Past experience provides the basis for dealing with this type of limitation. For example,

maximum allowable gains for the various feedback variables can be estimated on the basis of values that have been realized in past variable stability airplanes. However, the actual values of the gains that can be used can only be determined practically from flight test. The appropriate course of action is to design the system based on the estimated maximum gains, and build and flight test the system to determine the actual limits. If any of the limits are too low, then the system must be redesigned (e.g., filters introduced, sensors modified, new loops selected) to accommodate the situation. The important point is that design for this second type of limitation does not warrant sophisticated and lengthy analyses. Because of the unique character of each variable stability airplane, simple considerations based on past experience, coupled with redesign when a real problem is uncovered in flight test, becomes the most expedient and effective method for handling many limitations in the design and development of a variable stability system.

Basically, the GPAS model controlled system (MCS) design involves the problem of a multi-input, multi-output control system. From a linear point of view, the ideal design goal is to mechanize the control loops and establish control gains so that the transfer function, which relates a closed-loop airplane response variable to the corresponding analog model response variable, is unity over the frequency range pertinent to the model.

The design of a versatile and practical MCS, then, depends on choosing a model whose dynamics serve as a reference or base. If these reference dynamics are too severe (too fast), it may be impossible to design a practical variable stability system. Moreover, if they represent only a small class of existing or proposed airplane designs, then the simulation capability will be unduly restricted.

NASA specifications state that the MCS must be capable of following a model with at least the following characteristics:

ω_{θ_s}	=	2π rad/sec	longitudinal
ζ_{θ_s}	=	0.1	
ω_{ψ}	=	5 rad/sec	lateral-directional
ζ_{ψ}	=	0.1	
τ_r	=	0.1 sec	

The GPAS must duplicate such a model at selected points within the JetStar's flight envelope. At low speeds and low altitudes, the model short-period and Dutch-roll frequency requirements are each relaxed to 3 rad/sec.

Early CAL analog investigations of the model controlled concept (performed prior to the GPAS program) showed that when the bandwidth of the closed-loop MCS airplane is approximately three times that of the highest model frequency, the airplane will follow the model with very little error. Furthermore, these same analog studies showed that a factor as low as 1.5 will also give acceptable performance. Thus the choice of closed-loop bandwidth is not based on rigid criteria but evolves from engineering judgment.

Several factors limit the closed-loop bandwidth, the most important of which are structural vibration feedback, sensor dynamics and noise, and actuator dynamics and nonlinearities. Structural vibration perhaps the most troublesome factor, depends on the particular airplane in which the system is installed. The other factors depend more on the nature of specific design, installation and environmental details and often do not appear until the system is actually used.

To make the JetStar follow a model having the dynamics listed above within acceptable error, the following MCS closed-loop dynamics have been selected as design objectives:

$$\omega_{\theta_s} = 9 \text{ rad/sec}$$
$$\zeta_{\theta_s} = 0.5$$
$$\omega_{\psi} = 7.5 \text{ rad/sec}$$
$$\zeta_{\psi} = 0.5$$
$$\tau_r = 0.067$$

The damping ratios and time constants were chosen to give good transient response of the closed-loop system.

2.3 LONGITUDINAL LOOP DESIGN

Figure 2-1 is a block diagram of the longitudinal MCS control loops. Design calculations for these loops are based on the three-degree-of-freedom linearized equations of motion given in the appendix. Both the elevator and throttle receive command inputs to produce the forces and moments necessary to make the JetStar respond like the computer model.

There are actually two loop configurations in Figure 2-1. One is used when matching angle-of-attack, velocity, and altitude; the other is used when matching normal acceleration, velocity, and altitude. Although the angle-of-attack and normal acceleration loops can be used jointly, the design calculations consider each loop configuration separately (i.e., either an α - loop or an n_z - loop).

The angle-of-attack and angle-of-attack rate loops are used to increase the short-period dynamics of the closed-loop system from those of the basic JetStar to those having a frequency of 9 rad/sec and a damping ratio of 0.5.

The angle-of-attack gain, $\frac{\delta_e}{e_\alpha}$, is computed from the equation

$$\frac{\delta_e}{e_\alpha} = \frac{\Delta(\omega_{\theta_s}^2)}{M_{\delta_e}} \tag{2-1}$$

where $\Delta(\omega_{\theta_s}^2)$ is the difference between the square of the desired closed-loop natural frequency (9 rad/sec) and the square of the natural frequency of the basic, open-loop JetStar.

The angle-of-attack rate gain, $\frac{\delta_e}{e_{\dot\alpha}}$, is given by

$$\frac{\delta_e}{e_{\dot\alpha}} = \frac{\Delta(2\zeta_{\theta_s}\omega_{\theta_s})}{M_{\delta_e}}, \tag{2-2}$$

where $\Delta(2\zeta_{\theta_s}\omega_{\theta_s})$ is the difference between the desired $2\zeta_{\theta_s}\omega_{\theta_s}$ and the open-loop JetStar $2\zeta_{\theta_s}\omega_{\theta_s}$. Note that $\frac{\delta_e}{e_{\dot\alpha}}$ depends on the closed-loop natural frequency desired (ω_{θ_s}) and, therefore, on the gain $\frac{\delta_e}{e_\alpha}$.

If normal acceleration is used as a feedback variable rather than angle of attack, then the desired short-period frequency can be achieved by

using normal acceleration feedback to the elevator, with the gain being given by

$$\frac{\delta_e}{e_{n_z}} = \frac{g}{V_t} \cdot \frac{\left(\frac{\delta_e}{e_\alpha}\right)}{\bar{z}_\alpha - \bar{z}_{\delta_e}\left(\frac{\delta_e}{e_\alpha}\right)} \tag{2-3}$$

This equation provides a simple algebraic relation for calculating δ_e/e_{n_z} from δ_e/e_α . The short-period damping ratio is still controlled by the angle-of-attack rate gain, whose magnitude is now computed from the equation

$$\left(\frac{\delta_e}{e_{\dot{\alpha}}}\right)' = \frac{\bar{z}_\alpha\left(\frac{\delta_e}{e_{\dot{\alpha}}}\right)}{\bar{z}_\alpha - \bar{z}_{\delta_e}\left(\frac{\delta_e}{e_\alpha}\right)} \tag{2-4}$$

The prime is used to indicate that the gain applies to the acceleration loop configuration(n_z - loop) rather than the angle-of-attack loop (α - loop) configuration.

The short-period characteristics can be completely altered by using only the elevator, but the phugoid and flight-path characteristics must be altered by both the elevator and the throttle.

The following equations give the elevator and throttle loop gains. Note that altitude error is fed to the elevator and velocity error is fed to the throttle

$$\frac{\delta_e}{e_{\dot{h}}} = -\frac{\sqrt{\Delta(\omega^2_{\theta_p})}}{V\bar{z}'_{\delta_e}} \tag{2-5}$$

where $\bar{z}'_{\delta_e} = (\bar{z}_\alpha + \bar{z}_\theta)\left(\frac{\bar{\alpha}}{\delta_e}\right) + \bar{z}_{\delta_e}$ and $\frac{\bar{\alpha}}{\delta_e} = \frac{M_{\delta_e} - M_q\ \bar{z}_{\delta_e}}{-M_\alpha + M_q\ \bar{z}_\alpha}$

$$\frac{\delta_e}{e_h} = 0.05\,\frac{\delta_e}{e_{\dot{h}}} \tag{2-6}$$

$$\frac{\Delta T}{e_V} = m\left\{\sqrt{\Delta(\omega^2_{\theta_p})} - D_V\right\} \tag{2-7}$$

In these equations, $\Delta(\omega^2_{\theta_p})$ is the difference between the square of the desired phugoid frequency and the square of the phugoid frequency of the open-loop JetStar. The desired phugoid frequency was established empirically from

CAL analog computer studies since NASA requirements did not quantitatively specify MCS phugoid characteristics that GPAS was to simulate. The gain $\frac{\delta_e}{e_{\dot{h}}}$ was established as one-twentieth of $\frac{\delta_e}{e_{\dot{h}}}$ on the basis of analog studies. Although the phugoid loops perform satisfactorily without using the $\dot{V}$-loop shown in Figure 2-1, the loop was incorporated to provide flexibility in the choice of phugoid control systems.

The results of the longitudinal gain calculations are shown in Figures 2-2 through 2-8. On these graphs, the theoretical values computed from the previous equations are plotted as a function of $1000/\bar{q}$, where $\bar{q}$ is dynamic pressure. In most cases the relationship is linear, and in some cases gross weight is a parameter.

The numbers along the abscissa ($1000/\bar{q}$ coordinate) in Figures 2-2 through 2-8 are codes which identify the Mach number and altitude. For example, ".55 - 20" means Mach .55 and 20,000 ft. Elsewhere, the letters "H" or "L" appear in the code and refer to the two weight conditions selected for the study. The letter "H" refers to the heavyweight condition of 38,200 lb, and "L" refers to the lightweight condition of 23,900 lb. Therefore, .55H20 indicates a Mach number of .55, a gross weight of 38,200 lb, and an altitude of 20,000 ft.

In addition to the theoretical gains, Figures 2-2 through 2-8 have curves labeled "limit value" or "estimated limit gain." These limit gains are the results of a study made to determine whether the theoretical gains, which in many cases seemed quite high, could actually be achieved in flight. Approximately thirty gains used during past in-flight research simulations were scrutinized, and the reasons for the maximum values used fell into three categories:

1. gain levels were limited by structural instability
2. gain levels were limited by noise (usually turbulence)
3. gain levels were sufficient for the particular simulation tasks for which the gains were used

The GPAS limited gain values, which occur primarily at the lower dynamic pressure flight conditions, do not necessarily imply poor model-following performance. Rather, they imply that the closed-loop JetStar will have dynamic characteristics different from those used to compute theoretical gain levels. For example, the short-period natural frequency will be less than the 9 rad/sec established as desirable for following models having short-period frequencies up to 6 rad/sec. At low speeds and altitudes, the GPAS cannot follow a 6 rad/sec model. Normal airplanes, however, are also much slower than 6 rad/sec; hence, a realistic analog model would not be this fast. Therefore, the inability to follow the reference model used as a basis for design calculations does not represent a severe limitation for low dynamic pressure simulations.

Figures 2-2 and 2-3 show the gains calculated to control the short-period dynamics of the closed-loop JetStar. These gains, $\frac{\delta_e}{e_\alpha}$ and $\frac{\delta_e}{e_{\dot{\alpha}}}$, yield short-period dynamics with a natural frequency of 9 rad/sec and a damping ratio of 0.5 and were computed using Equations 2-1 and 2-2.

Figure 2-4 through 2-6 show the gains calculated to control phugoid dynamics. The gain $\frac{\delta_e}{e_{\dot{h}}}$ is strongly influenced by the short-period gain $\frac{\delta_e}{e_\alpha}$. Figure 2-4 shows the manner in which $\frac{\delta_e}{e_{\dot{h}}}$ varies with $1000/\bar{q}$ and gross weight when there is no short-period gain. Figure 2-5 shows what happens to this gain when the theoretical and limit values of short-period gain $\frac{\delta_e}{e_\alpha}$ are used to compute $\frac{\delta_e}{e_{\dot{h}}}$. Note that $\frac{\delta_e}{e_\alpha}$ affects both the magnitude and shape of the phugoid gain function (Figures 2-4 and 2-5). The theoretical values of phugoid gains $\frac{\delta_e}{e_{\dot{h}}}$ are calculated to yield closed-loop phugoid frequency of $\omega_{\theta_p} = 0.3$ rad/sec. The closed-loop damping will be $\zeta_{\theta_p} > 1.0$

The thrust also influences the phugoid characteristics. Figure 2-6 shows the throttle gains which are required in conjunction with the elevator gains to yield the desired phugoid characteristics. This gain is practically independent of dynamic pressure, but does depend on gross weight.

As mentioned previously, normal acceleration signals can be used instead of angle-of-attack in the feedback loops. Figure 2-7 shows the normal acceleration gain that achieves the same effect as the angle-of-attack

gain of Figure 2-2. Figure 2-8 shows the phugoid gain $\frac{\delta_e}{e_{\dot{h}}}$ which must be used with the normal acceleration gains of Figure 2-7. These gains were computed using Equation 2-5. The remaining phugoid gains ($\frac{\delta_e}{e_h}$ and $\frac{\Delta T}{e_V}$) are the same for either α or n_z control loops.

Figures 2-9 and 2-10 are examples of model-following performance obtained on an analog computer. The time histories show the JetStar following motions of an SST configuration whose dynamics have been excited by an elevator input and a thrust command. In particular, note that the control gains used in the GPAS loops are not those computed from the theoretical equations but are, rather, the lower or limited values which are more realistic in terms of numerical values that can actually be achieved in flight. These lower gain values still give good model-following performance.

The analog computer studies of GPAS model-following performance, of which Figures 2-9 and 2-10 are examples, utilized six-degree-of-freedom nonlinear equations with full Euler angle representations and variations of aerodynamic coefficients with angle-of-attack, airspeed, and altitude. Also, the elevator and throttle dynamics were represented on the analog, although they were neglected in the approximate equations used to compute gains.

Actuator dynamic characteristics, which can have a serious influence on the performance of automatic feedback control systems, were accounted for in root locus studies performed on the ESIAC computer. Whereas on the ESIAC these important effects were easily studied, much analytical labor and complexity would have been required to include these actuator dynamics in the approximate equations for the gains. The ESIAC results showed that elevator and throttle dynamics did not significantly alter the results predicted with the approximate equations.

Figure 2-11 is an example of a root locus in which actuator dynamics are included and shows how the poles of the $\frac{n_z}{\delta_e}$ transfer function migrate as gain $\frac{\delta_e}{e_{n_z}}$ increases. The locus on the far right begins at the poles of the elevator actuator transfer function. The short-period locus actually goes unstable for a gain between 21 and 35 deg/g because the damping gain $\frac{\delta_e}{e_{\dot{\alpha}}}$ is zero in this particular case.

2.4 LATERAL-DIRECTIONAL LOOP DESIGN

Stability calculations made for normal airplanes, based on linearized lateral-directional equations of motion, show that the lateral-directional mode characteristics can vary over wide ranges for different configurations and flight conditions. Furthermore, the results of flight research have shown that these characteristics are important to flying qualities. To be of value for general-purpose airborne simulation, the GPAS model-following system must be capable of following many different types of models exhibiting different lateral-directional characteristics. This wide range of characteristics must be simulated with fidelity and realism so that useful results and conclusions may be drawn from in-flight research studies.

Figure 2-12, a block diagram of the lateral-directional MCS system, shows the control loops designed to provide the GPAS with the desired capability. The following feedback variables are incorporated in the control loop:

sideslip angle (or lateral acceleration)

sideslip rate

bank angle

roll rate

The primary purpose of the sideslip (or lateral acceleration) loop is to increase the frequency of the basic JetStar's Dutch roll. The sideslip rate loop provides Dutch roll damping for the closed-loop JetStar. The roll rate and bank angle loop provide a rapid roll subsidence and spiral mode. The theoretical gains for each control loop were calculated to provide the closed-loop JetStar with lateral-directional closed-loop dynamics having natural frequency bandwidths 1.5 times those of the design model in each of the modes of motion.

The linearized lateral-directional equations of motion shown in the Appendix yield a characteristic equation which can be written as a product of approximate factors for the Dutch roll, roll subsidence and spiral modes.

The control-loop gains can be computed using these approximate factors. The following equations define these gains:

$$\frac{\delta_r}{e_\beta} = \frac{\omega_\psi^2 - N_\beta}{-N_{\delta_r}} \tag{2-8}$$

where ω_ψ is the desired Dutch roll natural frequency (7.5 rad/sec) and N_β is the basic JetStar directional stability, and

$$\frac{\delta_r}{e_{\dot\beta}} = -\frac{2\zeta_\psi \omega_\psi + N_r + Y_\beta - Y_{\delta_r}(\delta_r/e_\beta)}{N_{\delta_r} + Y_{\delta_r}(N_r + 2\zeta_\psi \omega_\psi)} \tag{2-9}$$

Equations 2-8 and 2-9 apply to the sideslip control-loop configuration. When an acceleration loop is used, the gain $\frac{\delta_r}{e_{n_y}}$ is used to achieve the same effect as $\frac{\delta_r}{e_\beta}$ and is computed from

$$\frac{\delta_r}{e_{n_y}} = \frac{V_t}{g} \cdot \frac{\frac{\delta_r}{e_\beta}}{Y_\beta - Y_{\delta_r}\left(\frac{\delta_r}{e_\beta}\right)} \tag{2-10}$$

The corresponding $\dot\beta$ gain, marked with a prime to show that its value applies to the acceleration loop configuration, is given by

$$\left(\frac{\delta_r}{e_{\dot\beta}}\right)' = \frac{Y_\beta\left(\frac{\delta_r}{e_{\dot\beta}}\right)}{Y_\beta - Y_{\delta_r}\left(\frac{\delta_r}{e_\beta}\right)} \tag{2-11}$$

Roll rate and bank angle comprise the aileron control-loop feedback signals. The gains are given by

$$\frac{\delta_a}{e_p} = \frac{\frac{1}{\tau_r} + L_p}{L_{\delta_a}} \tag{2-12}$$

and

$$\frac{\delta_a}{e_\phi} = \frac{1}{10} \cdot \frac{\delta_a}{e_p} \tag{2-13}$$

In Equation 2-12, τ_r is the desired time constant for the roll-subsidence mode, and L_p is the roll damping of the basic JetStar. There is no simple expression which relates the spiral mode characteristics to a given control system gain. To insure a reasonable level of spiral stability and acceptable bank angle-following, the gain $\frac{\delta_a}{e_\phi}$ was taken as one-tenth of the gain $\frac{\delta_a}{e_p}$, as established from analog computer studies.

The results of these gain computations are shown in Figures 2-13 through 2-17. The limit gain values shown in these figures were established for the same reasons discussed previously for the longitudinal gains.

Figure 2-13 shows the theoretical values of the gain $\frac{\delta_r}{e_\beta}$ which make the Dutch roll natural frequency approximately constant at 7.5 rad/sec throughout the JetStar flight envelope. Damping of the Dutch roll is controlled by the gain $\frac{\delta_r}{e_{\dot\beta}}$ whose theoretical gain program, shown in Figure 2-14, yields a damping ratio of about 0.5 throughout the JetStar flight envelope. The gains $\frac{\delta_r}{e_\beta}$ and $\frac{\delta_r}{e_{\dot\beta}}$ shown in these two figures are used together in the β - loop configuration.

When lateral acceleration is used to increase Dutch roll frequency instead of sideslip, the gain program for $\frac{\delta_r}{e_{n_y}}$ shown in Figure 2-15 must be used. The $\dot\beta$ - gain is still used for damping, but its gain program changes to that of Figure 2-16, which shows that $\left(\frac{\delta_r}{e_{\dot\beta}}\right)'$ is relatively independent of weight and dynamic pressure as compared to $\frac{\delta_r}{e_{\dot\beta}}$.

Figure 2-17 shows the gain program for $\frac{\delta_a}{e_p}$ which is used to produce the roll model-following. It is linear with $1000/\bar q$ and is strongly influenced by weight. This gain schedule holds the roll mode time constant of the closed-loop JetStar constant at $\tau_r = .067$ sec throughout the flight envelope.

Figures 2-18 through 2-21 are examples of lateral-directional model-following performance obtained on an analog computer. Figures 2-18 and 2-20 show the performance with the theoretical values of the MCS loop gains (those computed to give $\omega_\psi = 7.5$ rad/sec, $\zeta_\psi = 0.5$, and $\tau_r = 0.067$ sec) for the closed-loop JetStar. Figures 2-19 and 2-21 show the same response with the gains set at the lower values estimated to be achievable in flight.

The difference between the responses with theoretical gains and limited gains is almost imperceptible for both aileron and rudder inputs to the model.

2.5 RESPONSE FEEDBACK SYSTEM DESIGN

Since response feedback is a derivative matching technique, the RFS system design must incorporate enough loops so that all significant stability derivatives and control parameters in the equations of motion can be independently varied over wide ranges. One gain often changes more than a single derivative, and a single derivative can change more than one significant flying-qualities parameter. However, with the proper number and types of control loops, the simulated stability and control characteristics can be varied with the RFS feedback gains in somewhat the same manner that derivatives are varied on the MCS analog computer model.

Table 2-1 lists the design values of the GPAS RFS gains. Also listed are the primary derivatives which each gain affects, the primary function of the gain and the reasons for choosing the particular numerical ranges of the gains.

The RFS loops can be used in conjunction with the MCS loops when performing flight research. For example, the RFS system has a pitch rate loop to the elevator through the gain $\frac{\delta_e}{q}$ which will augment the short-period damping provided by $\frac{\delta_e}{e_{\dot{\alpha}}}$ in the MCS system. Thus, by using the $\frac{\delta_e}{q}$ gain, a given value of short-period damping can be obtained with a lower value of $\delta_e/e_{\dot{\alpha}}$. This might be desirable, for example, when performing in-flight simulations in rough air.

SECTION 3
SYSTEM FUNCTIONAL DESIGN

3.1 GENERAL

Calculating the control loop gains to achieve the desired dynamic characteristics of the closed-loop JetStar is only part of the GPAS system design problem. There are several other aspects which are necessary for the system to perform its final intended job -- in-flight simulation. The complete system is composed of subsystems, each of which must receive detailed design considerations because overall system operation depends on their special functions.

The complete GPAS system can be considered as a well integrated unit consisting of the following subsystems:

Flight Control System

Variable Feel System

Pilot's Instrument and Control Panel

Airborne Computer

Test Engineer's Console

Data Acquisition System

3.2 FLIGHT CONTROL SYSTEM

The cockpit controls for the right-hand or safety pilot are always connected directly to the airplane control surfaces through the JetStar's primary mechanical or hydromechanical system. The test or the evaluation pilot, who sits in the left-hand seat, however, flies by wire. When he moves his cockpit controls, electrical signals are transmitted to either the computer model (MCS) or directly to electrohydraulic servo valves (RFS). These servos, called simulation servos, position the aerodynamic control surfaces. During MCS operation the servo commands

are error signals which are the difference between the computer model response and the JetStar response. During RFS operation the servo commands are signals comprising pilot inputs and appropriate JetStar response variables.

The GPAS flight control system is designed to permit smooth and safe transfer of airplane control to and from the test pilot. Nulling circuits reduce the level of electrical signals at critical points in the system, thereby preventing "jump" of the aerodynamic control surfaces (and consequent dangerous airplane responses) when the MCS system is engaged for fly-by-wire operation. The alternative, manual nulling by the safety pilot, takes considerable time.

An automatic trim system, which operates when the GPAS system is engaged and controlling the elevator, positions the all-movable stabilizer to maintain zero aerodynamic hinge moments on the elevator in equilibrium flight (including steady turns). Since the variable stability servos are irreversible, large aerodynamic elevator hinge moments can exist (without automatic stabilizer trim) even though the evaluation pilot has the airplane trimmed with zero stick forces. If the variable stability system disengages when such elevator hinge moments exist, large and dangerous transients can occur and the safety pilot may not be able to cope with the out-of-trim forces. Such situations can develop if large speed, altitude, or c.g. changes occur while the GPAS system is engaged. The automatic trim system prevents such an occurrence by moving the stabilizer to keep elevator hinge moments near zero. A cockpit indicator allows the safety pilot to monitor the amount and nature of the unbalance. If the automatic trim system fails to function properly, the pilot can use manual trim to avoid dangerous disengage transients.

An automatic disengage feature, which disengages the system whenever certain signals exceed a predetermined maximum limit, eliminates the possibility of losing control or incurring structural damage when simulating aircraft whose undesirable characteristics cause extreme or violent motions. Before a dangerous situation can manifest itself, the system will disengage, allowing the safety pilot to resume control of the basic JetStar.

3.3 VARIABLE FEEL SYSTEM

The control systems of all airplanes are carefully designed to provide a pilot with proper cockpit control force or feel characteristics. The forces and deflections of the controls are important cues which aid him in flying the airplane. In conventional airplanes, the feel is determined by mechanical design of the mechanism connecting the stick, or control column, and the rudder pedals to the elevator, ailerons, and rudder, and by the aerodynamic loads on the control surfaces. The mechanical linkage is often combined with an irreversible or boost hydraulic system on larger, high-speed aircraft.

The cockpit controls of the GPAS test pilot are not mechanically connected in this way when the variable stability system is operative. Therefore, an artificial feel system is used to generate the control-force characteristics for him. By using electrohydraulic servos which can receive a wide variety of inputs, the feel characteristics of the cockpit controls can be made to vary in almost every conceivable manner. For example, the GPAS variable feel system can behave like a system having aerodynamic feel, or like an irreversible control system or a zero-deflection pure-force control system. The effective gearing between cockpit control motion and control-surface deflection can be easily altered, and linear or nonlinear force gradients can be provided. Breakout forces, friction, hysteresis, and deadband can all be adjusted.

Since the variable feel system is capable of varying many important feel characteristics, it contributes greatly to the capability of the overall system. An important feature is the ability to change these feel characteristics in flight by simple manipulation of dials on the Test Engineer's Console. The force-deflection performance capabilities provided by the elevator, aileron, and rudder feel systems are described in Section 4.3.2.

3.4 PILOT'S INSTRUMENT AND CONTROL PANEL

An instrument panel which is removable and easily modified offers flexibility for conducting in-flight simulations and general-purpose pilot display research. Also, the variable stability and control system cannot always modify the airplane dynamics exactly as desired, and, in certain cases, changes in the apparent display statics and dynamics can make the simulation appear more realistic to the pilot. Frequently the JetStar will be at flight conditions which differ from those of the simulated airplane. The evaluation pilot's display must indicate the speed, altitude, attitude, etc., of the simulated airplane rather than those of the JetStar.

The present GPAS simulation display panel instruments, listed below, are normal-appearing instruments, but most of them are electrically driven and can receive inputs either from the analog computer model or from the actual JetStar sensors.

Mach meter

Normal acceleration

Angle-of-attack

Altimeter

Rate-of-climb

Gyro horizon indicator

Course indicator (receives limited computer inputs only)

Airspeed

RMI compass (does not receive analog inputs)

Turn and slip

Another panel containing standard JetStar instruments can replace the simulation panel for ferry flights. These instruments, in contrast to the instruments on the simulation panel, are normal JetStar flight instruments and cannot be driven by electrical signals from the computer.

There are two variable stability control panels in the cockpit. One is the simulation servo control panel which is mounted on the instrument panel between the two pilots; this panel contains null meters, manual trim controls, engage and disengage switches, and operational and safety indicators. The other, the feel system control panel, which is mounted on a side panel to the left of the evaluation pilot, is used for engaging and disengaging the variable feel servos. Photographs of these two control panels are shown in Figure 3-1.

3.5 AIRBORNE COMPUTER

The airborne computer is a key element in MCS operation, for on it are programmed the equations of motion representing the dynamics of another airplane, the model, whose motions the JetStar must duplicate. Movement of the test pilot's cockpit controls provides inputs to the computer model, and the response variables of the model are compared with the corresponding variables of the JetStar. The resulting error signals become inputs to the JetStar control system. The GPAS airborne computer, which is an EAI PC-12 special-purpose computer, has the capacity for representing the dynamics of a reasonably complex model. A complete set of six-degrees-of-freedom nonlinear equations can be programmed. Thus, a wide range of realistic airframe dynamics can be simulated in flight.

The computer is properly integrated into the overall GPAS system design by providing both proper scaling and circuitry which insures that initial conditions of the model at the time of system engagement are the same as those of the JetStar. This circuitry eliminates control-system transients which would surely occur if the model and the JetStar were at different trim conditions.

Figure 3-2 is a photograph of the airborne computer installation.

3.6 TEST ENGINEER'S CONSOLE

The test engineer's console is the central monitoring station for the entire JetStar variable stability system. Here the test engineer can select the variable stability operating modes. A particular simulation may require MCS operation, RFS operation, or a combination of the two. Four switches are used to place the elevator-, aileron-, rudder-, and throttle-control channels in the proper operating mode.

Null meters located on the instrument panel show the status of the input signal levels for the various control servos. Thus, the test engineer knows if the system can be engaged smoothly, and he can detect any impending malfunctions.

The gain control panels permit the test engineer to change the various gain levels for both MCS and RFS operation. He has a strip-chart recorder with which he can make in-flight data evaluations if unusual circumstances so require, or he can simply perform routine evaluations on the progress of in-flight simulations. He can easily reach the variable feel system controls and quickly adjust the many combinations of force gradients, breakout, deadbands, etc., for the longitudinal, lateral, and directional cockpit controls.

Figure 3-3 is a photograph of the test engineer's console, and Figure 3-4 shows the grouping of the various functional control panels.

3.7 DATA ACQUISITION SYSTEM

The entire operation of the GPAS variable stability system depends on accurate measurement, recording, and monitoring of many quantities. During both MCS and RFS operation, the variables defining the dynamic motions of the JetStar must be sensed and measured before they can be recorded or properly transmitted through the various control loop channels as electrical signals. By comparison, every variable defining the dynamics of the computer model is directly available as a voltage, and there is no need for sensing devices.

Both angle-of-attack and sideslip of the JetStar are sensed by vanes mounted on the fuselage. Since these vanes are responsive to the local flow angles in the immediate vicinity of their fuselage mountings, corrections are made for static position error and dynamic errors due to angular velocities. The signal which is finally transmitted to the system control loops is, therefore, indicative of the total or overall effective airplane angle-of-attack or sideslip.

A rate gyro package is used to sense the angular velocities of airplane pitch, roll, and yaw, and a two-axis attitude gyro senses pitch attitude and bank angle. There are two linear accelerometer packages. One, which is located near the center of gravity, senses longitudinal, lateral, and normal accelerations. The other, which is located in the nose wheel well, senses the lateral and normal accelerations experienced by the pilot.

The altitude, rate-of-climb, and airspeeds of the JetStar are obtained from a composite system which uses both air-pressure and acceleration measurements. This composite configuration, called the air data system, yields correct long-term values from the air-pressure measurements and correct short-term values from the inertial measurements, thus providing a frequency response that gives satisfactory variable stability system performance.

SECTION 4
DETAIL DESIGN

4.1 FLIGHT CONTROL SYSTEM

The GPAS uses the normal JetStar control surfaces and engine controls in variable stability operation. The evaluation pilot's cockpit controls (control column, rudder pedals, and special throttle lever) are not mechanically connected to the JetStar flight controls, but the safety pilot's cockpit controls (including the engine controls) are connected in the normal manner. The GPAS variable stability system uses specially installed servos (called simulation servos) to drive the JetStar control system during variable stability operation. Thus, during such operation, the safety pilot's controls are also driven by the simulation servos, and the airplane responds to these control motions as a normal JetStar. When the variable stability system is not operating, its special servos are disengaged from the Jet Star controls, and the safety pilot then flies the airplane using the normal JetStar control system.

The approach used to design the variable stability system has several important advantages. One advantage is that with the exception of the servo engage and disengage mechanisms, the variable stability system is not a part of the JetStar primary control system, so its design does not affect safety of flight. Accordingly, certain liberties in design, which would not be allowed in designing a primary flight control system, may be taken. For example, the high performance of the simulation servos is obtained by using electronic feedback rather than mechanical feedback around the actuators. In addition, the actuators are sized so they can exert static forces about three times greater than the largest static load expected from external or aerodynamic forces. They can still accelerate the control surfaces at these expected aerodynamic loads. Although the actuators are sized to provide high forces, these maximum forces cannot be transmitted to the aircraft structure because hydraulic pressure limit valves are placed across the actuator.

The design approach also provides an important safety feature during variable stability operation. Since the safety pilot's controls move with the JetStar control surfaces and engine controls, and since the Jet Star responds in the normal fashion to these control motions, the control positions give the

safety pilot advance information concerning the impending airplane motions. Knowing this, he can anticipate dangerous situations before they develop and take over control from the evaluation pilot. Also, experience has shown that the safety pilot can often detect system malfunctions or simple errors in system setup by looking at the control motions produced by the variable stability system. Noise in the system, most usually due to turbulence, can also be evaluated by the safety pilot if he can see the control motions. The safety pilot can decide whether operation should be continued, or discontinued because the control system is being subjected to excessive vibrations and loads.

4.1.1 Mechanical Description

The mechanical arrangement of the elevator position servo system is shown in Figure 4-1. A bell crank and push-pull rods transmit the output force of the linear servo actuator to the torque tube assemblies at the inner ends of each elevator. Strain gages bonded to the torque tube assemblies of each elevator sense the hinge moment required for the auto trim system. The signal from a pressure transducer, which senses the differential pressure across the servo actuator piston, is used for pressure feedback. It is also transmitted to a null meter and an auto trim system safety alarm. Rotary position potentiometers, which are belt-driven from the torque tubes, sense the angular position of each elevator and provide position feedback for the actuator. The elevator position stops are those of the standard JetStar, which are incorporated in the elevator booster unit.

The mechanical arrangement of the aileron position servo system is shown in Figure 4-2. The output force of the linear electrohydraulic actuator is transmitted to an idler lever and thence, by push-pull rods and levers, to both aileron horns. The aileron position stops are those of the standard JetStar, which are located at the booster unit. A linear position potentiometer, linked to the servo actuator idler lever, senses the angular position of the ailerons and provides position feedback for the actuator. The signal from a differential pressure transducer is used for pressure feedback.

The mechanical arrangement of the rudder position servo system is shown in Figure 4-3. The output force of the linear electrohydraulic actuator is transmitted, via a rod end and double lever, to the rudder torque shaft. The rudder position stops are those of the standard JetStar, which are located at the quadrant on the lower end of the torque tube assembly. A rotary position potentiometer which is belt-driven from the torque shaft senses the angular position of the rudder and provides position feedback to the actuator. Pressure feedback is also used for the rudder actuator.

4.1.2 Electrical Description

Figure 4-4 is a block diagram of the elevator surface servo. This servo employs conventional position feedback plus a somewhat unusual approach for stabilization. The position command signal is compared to the measured surface position, and the difference is fed through a high gain amplifier to the servo control valve. This amplified error signal activates a hydraulic flow control valve which, in turn, drives the elevator surface in the direction which reduces this error. This process continues until the measured position signal cancels the electrical command signal.

The differential pressure signal is used to improve the frequency response at the resonant load of the elevator servo. The high pass filter washes out the signal at low frequencies to preserve static stiffness.

Additional features of the servo loop include an authority limiter, a balance servo, and a manual trim. The authority levels available are 1/4, 1/2, and full elevator command.

The balance servo consists of a servo amplifier driving a servo motor and attached potentiometer with an electrically controlled brake. Prior to system engagement, the balance servo nulls the elevator command signal. On engagement, the brake holds the balance servo fixed, thus holding constant the null bias to the elevator command at its initial value.

The manual trim is a safety feature which allows manual balancing of the signal to the control valve. Before the system is engaged, a manual input can be used to test the nulling capabilities of the balance servo.

Aileron and rudder servo block diagrams are identical to the elevator block diagram, Figure 4-4.

4.2 THROTTLE DESIGN

4.2.1 Mechanical Description

The throttle servo system is illustrated in Figure 4-5. The simulation throttle lever is mounted to the left of the standard JetStar throttles on the center console. Movement of this lever by the pilot produces electrical signals which correspond to thrust commands to the analog computer model. A rotary position potentiometer measures the angular movement of the simulation throttle lever which also has a variable friction adjustment.

Four electromechanical rotary actuators move the engine throttle controls using capstans attached to each actuator to move the four throttle control cables. A rotary position potentiometer located on the throttle linkage of each engine measures the power lever angle. Pressure transducers are mounted at the inlet and tailpipe of each of the engines to measure ram air pressure and tailpipe pressure. The outputs of these pressure transducers are used to obtain engine pressure ratio (EPR) which is used as the primary (outer-loop) feedback for the throttle servo system.

4.2.2 Electrical Description

Figure 4-6 shows a block diagram of a typical throttle servo system. For MCS operation, the error between the JetStar velocity and model velocity becomes a thrust command signal. This thrust command signal is converted to an engine pressure ratio signal by a function generator that represents engine operating characteristics as a function of altitude. This signal is used as the EPR command signal to each of the four engine throttle servos. Each throttle actuator consists of a constant speed motor and two dry magnetic-particle clutches which transmit the motor torque to the cable capstan. The clutch operation provides an angular acceleration output at the capstan

proportional to the throttle servo amplifier input, thus providing an acceleration actuator. Inner-loop feedbacks, rate feedback measured directly at the capstan, and position feedback measured at the throttle linkage on the engine, produce an accurate high-performance position servo for the engine throttle lever. The outer-loop feedback of engine pressure ratio (EPR) converts the control system to a direct thrust command system. The integrator in the EPR forward loop eliminates steady-state errors.

4.3 VARIABLE FEEL SYSTEM

4.3.1 Mechanical Description

The mechanical components of the elevator feel system are illustrated in Figure 4-7. For simulation flights, the test pilot's control column is disconnected mechanically from the remainder of the elevator primary flight control system. It can be reconnected for nonsimulation flights. When set up for simulation flights, the test pilot's input forces produce position commands to an electrohydraulic actuator connected to the control column by a mechanical linkage. The input forces are sensed by strain gages bonded to the spokes of the test pilot's control wheel. The position of the test pilot's control column is measured with a rotary potentiometer driven by a belt from the pivoting lower end of the control column.

The mechanical components of the aileron feel system are illustrated in Figure 4-8. The test pilot's control wheel is connected by a cable system to an intermediate torque shaft assembly which is connected by another cable system to an electrohydraulic actuator. For nonsimulation flights, the intermediate torque shaft assembly can be connected through the aileron torque shaft assembly to the aileron primary control system. For simulation flights, the intermediate torque shaft assembly is disconnected from the main aileron torque shaft assembly. The test pilot's input forces then command the electrohydraulic actuator. The input forces are sensed by strain gages bonded to the spokes of the test pilot's control wheel. The position of the control wheel is measured with a rotary position potentiometer driven by a belt from the intermediate torque shaft.

The mechanical components of the rudder feel system are illustrated in Figure 4-9. The test pilot's rudder pedals are connected through a torque shaft assembly, a push-pull rod, an idler lever assembly, and a cable system to an electrohydraulic actuator. A mechanical disconnect is provided on the control torque shaft assembly so that the test pilot's controls may be connected to the primary control system for nonsimulation flights and disconnected for simulation flights. The input forces on the rudder pedals are sensed by pedal dynamometers. The pedal position is measured by a rotary position potentiometer driven by a belt from the torque shaft assembly.

4.3.2 Electrical Description

A block diagram of the elevator feel system is shown in Figure 4-10. The basic operation of the feel system is as follows. Elevator wheel forces are measured, and (neglecting the effects of the active filter, hysteresis, breakout force, nonlinear force, deadband, and $f(u)$ function) the signal is passed through the force gradient gain control, δ_{e_p}/F_e, thus converting the signal from a force to a deflection measurement. This signal is now the position command for the elevator feel servo. The feel servo itself is a position control system consisting of a rate actuator (servo control valve and actuator) with wheel position and rate feedback. The natural frequency of the feel servo is controlled by the loop gain, and its damping ratio, by the rate feedback gain $\delta_{e_p}/\dot{\delta}_{e_p}$. Function generators, indicated by the $f(u)$ blocks in Figure 4-10, are provided to vary the elevator wheel force gradient, natural frequency, and damping ratio as a function of the variable u, which could represent, for example, the indicated airspeed.

A wide variety of optional characteristics are available for use with the elevator feel system, as indicated in Figure 4-10. Linear and angular acceleration bob weights can be simulated using the $F_e/\Delta n_z$ and $F_e/\dot{q}$ gains, respectively. The F_e/x gain allows any computer signal x to be patched in to affect the feel system (e.g., an α signal would provide for the effects of C_{h_α} in the simulation of an unpowered control system). Breakout forces, hysteresis, a dead band, and a nonsymmetrical, nonlinear variation of force with deflection can be simulated. Either force or position commands can be

used for the elevator command signal (model ζ_e for MCS, increment to JetStar ζ_e for RFS). Rate trim, operated by the trim button on the test pilot's wheel, is available, using either force or position commands to the elevator; the trim rate is adjustable. The wheel position trim can be used by the test pilot to adjust the fore-and-aft position of the control column without producing a control input to the system. The active filter, which is a combination of a low pass filter and a notch filter at the control column resonant frequency, provides feel system stability rather than a simulation capability.

The aileron and rudder feel systems are similar to the elevator feel systems, and their block diagrams would be identical to Figure 4-10, with the following exceptions: No independent aileron wheel or rudder pedal position trim is provided (not to be confused with aileron or rudder rate trim, the controls for which are mounted on the test pilot's console). Only symmetrical, nonlinear variations of aileron wheel and rudder pedal forces with deflection can be accommodated. Also, no bob weight simulation is provided for aileron and rudder feel systems (i.e., equivalent to the $F_e/\Delta n_z$ and $F_e/\dot{q}$ gains in the elevator feel system).

Force-versus-position plots, presented for the elevator, aileron, and rudder in Figures 4-11, 4-12, and 4-13, respectively, summarize the performance capabilities of the feel system. These plots indicate the maximum and minimum linear slopes available; the maximum deadband, breakout force, and hysteresis available; and the range of increasing and decreasing function generator slopes available.

4.4 HYDRAULIC SYSTEM

The GPAS JetStar utilizes four 3000 psi hydraulic systems. Of these, the No. 1 normal system, the No. 2 standby system, and the No. 3 auxiliary system are standard JetStar installations. The No. 4 system is peculiar to the GPAS JetStar and, except for the engine bleed air supply used to pressurize the reservoir, is completely independent of the other systems.

The No. 4 system, shown in Figure 4-14, is supplied by an engine-driven pump on the No. 1 engine and powers the three variable feel servos (Figure 4-15) and the three surface position servos (Figure 4-16).

Separate solenoid-operated shutoff valves of the normally closed type are provided for the feel servo pressure supply and the surface position servo pressure supply. This enables the feel servo system to be operated independently of the surface position servo system.

The pump is identical with those mounted on the No. 2 and No. 3 engines, which power the No. 1 and No. 2 systems, respectively. For ground checkout work, connections labeled PRESSURE and SUCTION in the speed brake opening framing are provided for connection of an external hydraulic power supply; these connections are accessible when the speed brake is in the extended position.

The reservoir is pressurized to 8.5 (±0.6) psi air pressure to prevent pump cavitation. This pressure is supplied by tapping off the engine bleed air system used for the No. 1 and No. 2 hydraulic systems.

Controls and indicators for the No. 4 hydraulic system are situated on the simulation-system control panel and the feel-engage panel in the cockpit. The GPAS OIL PRESSURE LOW warning light on the cockpit annunciator panel is illuminated when the system supply pressure drops below 2200 psi.

There are two filters in the No. 4 hydraulic system: a pressure filter and a return filter. Two accumulators are installed in the No. 4 hydraulic system to minimize surges.

Two groups of safeguards are provided to ensure that the flight control surfaces can be easily operated by the safety pilot when the GPAS system is "off". The first consists of a solenoid-operated shutoff valve fitted as a bypass control in each surface position servo piping system (see Figure 4-16). When de-energized, these valves are normally open, and there are neither differential pressures across the servo actuator pistons nor any impediment to the free flow of fluid from one side of each piston to the other side. The second safeguard is provided in case any one of the shutoff valves just mentioned fails to open when de-energized. This consists of another solenoid-operated shutoff valve connecting the surface position servo pressure supply to the return line, together with a pair of check valves (shown in Figure 4-16) fitted

in each position-servo manifold block. The latter shutoff valve, also normally open when de-energized, dumps the supply pressure, thus permitting flow through the check valves. Should any servo bypass fail to operate, fluid can escape freely through one of the check valves when movement of the relevant surface by the safety pilot causes the servo piston to move in the cylinder.

4.5 AIR DATA SYSTEM

The JetStar air data system, shown schematically in Figure 4-17, contains the instrumentation necessary to obtain altitude, rate-of-climb, true airspeed, and indicated airspeed with the resolution necessary for phugoid and flight-path model following. In order to meet GPAS requirements, the system was designed to use both air pressure measurements and inertial acceleration measurements.

Pressure measurements have good low frequency response characteristics, but pneumatic lags caused by compressibility and tubing length deteriorate high frequency performance. By combining the pressure signals with accelerometer signals which have favorable high frequency characteristics, a composite system with improved overall frequency response is achieved.

Static and dynamic pressures are measured by two PACE pressure transducers, located on the left side of the forward nose section. Accelerations are measured with a three-axis accelerometer package. The table below lists the sensor output variables, the sensor type, and the sensor location.

Variable	Sensor	Sensor Location
$P_o - P_s$	PACE Engineering Co. Model P21A - 15 psi	Left-hand side nose section; approx. Station No. 162
$P_t - P_s$	PACE Engineering Co. Model P21D - 4 psi	Left-hand side nose section; approx. Station No. 162
n_x, n_y, n_z	UNICO Controls, Inc. 3-axis acceleration Sensing Package	Sensor Platform; approx. Station No. 475

The operation of the system can be explained by referring to Figure 4-17. Signals from the pressure transducers pass through appropriate function generators and are converted into pressure altitude, h_p, and true airspeed, $V_{\bar{q}_c}$. The function generators are designed with the appropriate standard atmosphere functional relationships for converting pressure measurements into altitude and velocity.

The outputs of the function generators are transmitted to complementary filters where they combine with signals derived from the accelerometers. These latter signals come from a computer which transforms body axis accelerations into earth axis components by Euler angle transformations. The altitude signal for use in the system is simply filtered pressure altitude. Figure 4-18 shows the frequency response of the altitude signal, h

Figures 4-19 and 4-20 show the frequency response characteristics of the rate-of-climb signal. These figures, in particular, show how the complementary filter combines the pressure and acceleration inputs to achieve an improved high frequency response characteristic.

Figures 4-21 and 4-22 show the similar frequency response curves for true airspeed and rate of change of true airspeed.

Figure 4-17 also shows the provision for field elevation barometric adjustment. This provision duplicates the altimeter setting function of standard aircraft altimeters.

SECTION 5
GROUND AND FLIGHT TEST DATA

5.1 GENERAL

This section presents the ground and flight test data which substantiate the performance capabilities of the major GPAS subsystems. Although the test programs were of limited scope, they did provide some performance data prior to the delivery of the JetStar to the NASA Flight Research Center. The data, which are indicative of system performance, are presented and are compared with the GPAS design requirements.

The discussions that follow are organized in the following way:

(1) ground test results of surface servos, feel system, and throttle servos, with some flight test verification included:

(2) open- and closed-loop flight test results and RFS performance;

(3) model-following (MCS) performance from flight tests.

5.2 GROUND TEST RESULTS

5.2.1 Surface Servo Performance

The amplitude and phase responses for each surface servo are presented in Figures 5-1 through 5-3. The crosses faired through by continuous lines represent the actual ground-measured responses, and the dashed lines indicate the design specifications. In addition, a few flight test points are also shown.

The amplitude and phase responses for the rudder servo contain two sets of curves. One was plotted from data taken at CAL, and the other is from data taken at the NASA Flight Research Center. The rudder servo performance was improved on the ground at NASA by applying 2.0 volts of

60 cps dither to the hydraulic valve. For small amplitude, low-frequency motions of the rudder servo, a hysteresis effect was noticed on the response, as shown in Figure 5-4. This "flat topping" was attributed to actuator friction. When the 60 cps dither voltage was applied to the valve, the effect was to break the actuator friction, and the small amplitude response was improved as shown in Figure 5-5.

The amplitude and phase responses of the aileron and elevator servos fall within the envelope specified in the work statement. The phase response of the rudder servo slightly exceeds the specification envelope due to the low resonant frequency of the rudder surface and torque tube assembly. The rudder amplitude response is within the specification.

Typical elevator, aileron, and rudder time responses to a step command are shown in Figures 5-6, 5-7, and 5-8, respectively.

The surface servo rate limits were obtained from responses to large amplitude commands during ground tests by manually turning the balance potentiometers associated with each surface servo. The rate limits represent minimum values because the commands were manually generated and may not have resulted in a good approximation to an ideal step. These rate limits are:

Elevator - 80 deg/sec,
Aileron - 170 deg diff/sec (or 85 deg/sec for one aileron),
Rudder - 109 deg/sec,

all of which exceed the specified 60 deg/sec.

5.2.2 Feel System Performance

Figures 4-11, 4-12, and 4-13 show the design boundaries for the force feel characteristics of the cockpit controls. These boundaries were not verified by tests at CAL. Lateral feel characteristics, however, were evaluated at the NASA Flight Research Center. Since the feel system electronic circuitry is identical for all three controls, tests of the longitudinal and directional feel characteristics should yield results similar to those obtained for lateral feel.

The test results obtained at NASA-FRC are shown in Figure 5-9 and are representative of the lateral force feel characteristics that can be attained.

5.2.3 Throttle Servo Performance

The GPAS throttle servos use engine pressure ratio (EPR) as a feedback signal to control the JetStar engine thrust. Pressure transducers measure the inlet and exhaust pressures of each engine, and electronic circuits compute engine pressure ratio from the transducer signals.

Throttle servo tests were conducted at CAL to obtain frequency response and rate limit data. Frequency response data were obtained from both ground and flight tests.

The throttle position loop frequency response shown in Figure 5-10 was obtained from ground tests with the engines inoperative. The amplitude ratio is the ratio of the actual engine power lever angle to the commanded power lever angle, which was a sinusoidal input signal.

Figure 5-11 shows the frequency response characteristics of the entire thrust loop for ground operation with the engines running. The amplitude ratio is the actual engine pressure ratio divided by the commanded engine pressure ratio for descending step commands. The data were obtained by performing a Fourier harmonic analysis of engine pressure ratio transient response to step command inputs. Each part of Figure 5-11 corresponds to a different initial and final steady state engine pressure ratio as indicated in the figure.

Figure 5-12 shows flight test frequency response data for a command of engine pressure ratio which raised the EPR from 1.35 to 1.64. The dashed line is the predicted frequency response, based on the thrust model derived from engine operating curves and data. The solid line has been rather loosely faired through the plotted test points.

The throttle servo rate limit was obtained from the throttle linkage position time response to a large step command in EPR. The time history shown in Figure 5-13 was obtained from ground tests, performed with the

engines running. The rate limit is determined by the time constant of the integrator in the throttle servo loop. The measured rate limit of 37.4 deg/sec agrees with a calculated value of 36.6 deg/sec.

The response shown in Figure 5-13 was caused by a command excursion from an EPR of 1.05 (engine idle) to an EPR of 1.56. It is noted from the EPR response that the engine acceleration from idle is quite slow. However, small command excursions at higher EPR's produce a much faster EPR (thrust) response. This increased response at higher EPR's is shown in Figure 5-14. These tests were performed on the ramp with the engine running. The frequency responses of Figure 5-11 were calculated from the time histories of Figure 5-14.

5.3 OPEN- AND CLOSED-LOOP FLIGHT TEST RESULTS

5.3.1 Purpose

The GPAS variable stability control loops were designed on the basis of only the rigid body motions of the JetStar. The structural bending modes and noise in the variable stability system limit system performance. Neither bending modes nor noise can be satisfactorily accounted for in analytical design studies and analog computer simulations. Hence, the open- and closed-loop flight tests were intended, first, to assess the limitations imposed by bending modes and noise, and, second, to demonstrate the performance of the GPAS variable stability system. In particular, the open-loop tests were to provide certain helpful information (e.g., estimates of maximum allowable gains) for the closed-loop tests.

As an aid to proper understanding of these tests, schematics for the control systems for elevator, aileron, and rudder as used in the tests are shown in Figures 5-15 and 5-16.

5.3.2 Open-Loop Flight Tests

The open-loop transient tests for elevator, aileron, and rudder control loops were performed at one representative flight condition of the JetStar, specifically at 20,000 ft altitude and 0.55 Mach number during Flight 4. The airplane weight varied from approximately 31,200 lb to about 25,000 lb as

the test segment of the 2 hour flight progressed.

In variable stability operation, one or more of the appropriate sensor signals is weighted by the feedback gains and summed to form each of the three command signals $\Delta\delta_{e_c}$, δ_{a_c} , and δ_{r_c} which drive the elevator, aileron, and rudder control surface servos, respectively. For stability analyses of the control loops, the following transfer functions should be obtained:

Elevator [‡] - $\frac{\Delta\alpha}{\Delta\delta_{e_c}}$ $\frac{\dot{\alpha}}{\Delta\delta_{e_c}}$ $\frac{\Delta n_{z_{cg}}}{\Delta\delta_{e_c}}$ $\frac{\Delta h}{\Delta\delta_{e_c}}$ $\frac{\dot{h}}{\Delta\delta_{e_c}}$

Aileron - $\frac{\phi}{\delta_{a_c}}$ $\frac{p}{\delta_{a_c}}$

Rudder - $\frac{\beta}{\delta_{r_c}}$ $\frac{\dot{\beta}}{\delta_{r_c}}$ $\frac{n_{y_{cg}}}{\delta_{r_c}}$.

Briefly, the open-loop tests were accomplished by having the test pilot put a force pulse into one of his controls and simultaneously recording the transient time histories of the input and the airplane responses. The entire forward path of the particular GPAS control loop was intentionally involved. The recorded transients were subsequently reduced to Fourier series coefficients from which transfer functions (frequency responses) were calculated for each of the several pertinent responses to the given input.

With the transfer functions in hand, gain margins [*] could be determined for each transfer function, and, from the gain margins, the gain at which a given loop would become unstable could be calculated. Unfortunately, for control loop stability analyses, meaningful results could not be obtained because of an error in the experimental setup. In particular, the proper input signals ($\Delta\delta_{e_c}$, δ_{a_c} , δ_{r_c}) for elevator, aileron, and rudder control loops were not recorded. Although the force inputs ΔF_{e_c} , F_{a_c} , and F_{r_c} were measured, the transfer functions for these inputs could not be used to determine GPAS variable stability system control loop stability. These transfer functions include the breakout force nonlinearities and the filters, indicated in Figures 5-15 and 5-16, which are elements external to the control loops.

[‡] Since the air data system was not yet operational at the time of the flight tests, the $\Delta h/\Delta\delta_{e_c}$ and $\dot{h}/\Delta\delta_{e_c}$ transfer functions could not be obtained.

[*] Gain margin is defined at frequencies where the phase angle is ±180 deg ± n 360 deg and n = 1, 2, ... and is the amount by which the open-loop transfer function magnitude differs from unity.

Elimination of the effects of these elements from the measured data by analytical means would have been impractical.

As an illustration of the nature of the transfer function data obtained, three transfer functions for $\frac{\Delta\alpha_v}{\Delta\delta_e}$, $\frac{\Delta n_{z_{cg}}}{\Delta\delta_e}$, and $\frac{\Delta\delta_e}{\Delta F_{e_c}}$ - are presented in Figures 5-17, 5-18, and 5-19. These longitudinal transfer functions were calculated from the data of Flight 4, record 35. The first two are the usual airplane (JetStar) transfer functions themselves, and the third includes all electrical and hydraulic elements between the pilot input ΔF_{e_c} and the elevator displacement, including the feel system filter and the breakout force nonlinearity. Figure 5-20 presents time histories of $\Delta\alpha_v$, $\dot{\alpha}$, $\Delta n_{z_{cg}}$, Δn_{z_p}, $\Delta\delta_e$, and ΔF_{e_c} for a part of the 2.9 seconds of record analyzed for the transfer functions. Several features may be noted:

(1) A damped oscillation of about 10 cps, which is clearly seen in the Δn_z traces, is probably due to symmetric structural bending.

(2) The 60 cps oscillation seen in the $\Delta n_{z_{cg}}$ trace, and to a lesser degree in the Δn_{z_p} trace, is probably an accelerometer response, excited by a subharmonic of the JetStar engine vibrations.

(3) The moderately damped oscillation of about 14.3 cps, evident in the ΔF_{e_c} trace, is due to the control column natural resonance.

At this point, some general comments on the measured transfer functions are in order. It is quite clear that Figures 5-17 and 5-18, relating measured airplane responses to elevator inputs, are not so easy to interpret as Figure 5-19, which relates surface deflection to force input. The former appear to be noisier, especially at the higher frequencies (roughly above 5 cps), where the magnitudes are small compared to magnitudes at the rigid-body natural frequencies of the airplane. This behavior can, in part, be attributed to vane noisiness, of aerodynamic origin, which was subsequently corrected as described in the next section. Another contributing factor is that the feel system filters heavily attenuate the input signal and, hence, worsen the signal-to-noise ratio (elevator input to vane noise).
The presence of turbulence may have been a third factor. The transfer

function relating open-loop control surface deflections to elevator input is not affected by the vane noise or turbulence and, therefore, shows none of this degradation at the higher frequencies. Also, the normal acceleration transfer functions are somewhat better than the angle-of-attack transfer functions because any turbulence would directly affect the vane measurements, but only indirectly affect the accelerometer measurements. Of course, airplane structural bending modes exist in profusion from about 4 cps and on up. These bending modes would show up in the measured airplane responses and, therefore, would tend to make corresponding transfer functions appear "noisy," but they would not show up in the control surface transfer functions.

Despite the difficulties with the open-loop tests, the open-loop transfer functions were briefly analyzed in an attempt to determine rough gain limits prior to performing the closed-loop tests. Since these rough limits seemed reasonable, and since the automatic safety trip equipment was proved to be operating correctly during the open-loop flight tests, the closed-loop tests were undertaken. To ensure safety, the loops were closed starting at very low gain values, and then the gains were slowly increased until some indication of instability (rigid body or structural instability, or just plain noise) appeared. In this way the closed-loop tests were accomplished without having to repeat the open-loop tests to establish valid gain limits. However, it is recommended that the open-loop tests be repeated in the future to provide basic data which will benefit the operation of the GPAS system as a variable stability airplane.

5.3.3 Closed-Loop Flight Tests

The closed-loop tests consisted of a series of transients with the response feedback (RFS) loops closed--usually, two at a time; one loop controlled primarily the natural frequency, and the other controlled damping. These tests were kept to the minimum necessary to prove the adequacy of the variable stability system. Specifically, the tests were designed to demonstrate the natural frequency and damping characteristics of the variable stability systems as functions of the pertinent RFS gain settings. The closed-loop tests were also used to indicate possible deficiencies of the variable stability system, such as nonlinearities and noise, that would degrade the variable stability performance. Usually, visual inspection of the flight records reveals these deficiencies, and the recorded time history data are usually sufficient to locate the source of the trouble.

The basic closed-loop tests were run during Flights 5 and 6, for the same flight condition as the open-loop tests, with the airplane carefully trimmed before each test.

Briefly, the RFS tests during Flights 5 and 6 were accomplished by having the test pilot apply a pulse input (force) to a particular control while both the input and the various responses were being recorded. Natural frequency and damping were determined directly from the recorded transients; no digital computer data reduction or analysis was required.

Since the vane-measured α and β are larger than they should be because of induced flow at the vanes, the vane position errors effectively introduce gains into the α and β feedback loops. In order to ascertain the overall loop gain (position error gain plus electrical gain), the position error gain must be determined. For the JetStar, the position error gains were determined from data taken during Flight 6.

The position error gain of the angle of attack vane was determined by assuming the validity of the expression

$$\Delta\alpha_I = \Delta\theta - \Delta\gamma$$

which holds exactly when $\beta = \phi = 0$. During these calibration tests, the JetStar was flown so that β, ϕ, and $\Delta\gamma$ were all as close to zero as possible. Therefore, the incremental inertial angle of attack $\Delta\alpha_I$ is equal to the incremental pitch attitude, and the α vane position error calibration is

$$k_\alpha = \frac{\Delta\alpha_v}{\Delta\alpha_I} = \frac{\Delta\alpha_v}{\Delta\theta} \qquad \text{when } \beta = \phi = \Delta\gamma = 0$$

where $\Delta\alpha_v$ is the incremental angle of attack measured by the vane. About a dozen evaluations of k_α were made at carefully selected points in the flight records, and the average value $k_\alpha = 1.50$ was obtained. This value was subsequently verified using the entire equation of motion for $\dot{\alpha}_I$

Investigation of the entire $\dot{\beta}_I$ equation of motion showed, however, that no simple ways of obtaining the β vane calibration error k_β were valid.

Consequently, the equation

$$\dot{\beta}_I = \frac{57.3g}{V} n_{y_{CG}} + \frac{g}{V}\phi - r + \frac{\alpha_I}{57.3} p$$

was solved for $\dot{\beta}_I$ (DEG/SEC), using measured values of $n_{y_{CG}}$, ϕ, r, and p. Also, α_I was taken to be an average trim value, $\alpha_I = \alpha_{TRIM} = 3.7$ deg, and the nominal velocity was used, $V = 570$ ft/sec. The equation was solved for five points in each of six different records in Flight 6, and four incremental values $\Delta\dot{\beta}_I$ were formed from each set of five points. The position error gain was then calculated, using the formula:

$$k_\beta = \frac{\Delta\beta_V}{\Delta\beta_I} = \frac{\Delta\dot{\beta}_V}{\Delta\dot{\beta}_I}$$

The resulting average position error gain was $k_\beta = 1.66$.

With regard to the vanes, the closed-loop tests showed that the original α and β vane configurations were very noisy. On close inspection, this noisiness was evident even from the open-loop flight tests. However, the noise became totally unacceptable during the high-gain closed-loop tests of Flight 5. It was surmised, on the basis of past experience, that the trouble lay in the aerodynamics of the vanes themselves. Vortex shedding from the mounting shaft was thought to be primarily responsible for a disturbed airflow downstream at the vane surface position. Between Flights 5 and 6, the vane mounting shafts were lengthened, and fairing was added to smooth the flow. This action corrected the difficulty, as shown by subsequent Flight 6 closed-loop tests.

Certain RFS performance results from the closed-loop tests of Flight 5 are given in Table 5-1. This table correlates gains with resulting frequencies and damping for elevator, rudder, and aileron gains.

A typical rudder response transient due to a pedal position pulse input is shown in Figure 5-21. This figure shows the response in sideslip, bank angle, and roll rate to illustrate variable stability operation with the RFS. Figure 5-21 also illustrates an unacceptably large rudder nonlinearity due to actuator friction. Similar nonlinearities are present in the aileron and elevator actuators but are not nearly so objectionable. The application of a dither to these actuators may help in eliminating these nonlinearities.

5.4 MODEL-FOLLOWING RESULTS

The primary mode of operation of the GPAS is as a model-controlled system (MCS). It is important, therefore, to demonstrate the model-following capability of the GPAS variable stability system. To this end, brief tests were conducted both on the ground, using an analog computer to solve the JetStar equations of motion, and in flight. Although these tests were of very limited scope, and, as such, the results were not analyzed in detail, they did demonstrate that satisfactory model following was achieved. Moreover, the tests indicate that considerably better model following may be obtained when feedback gains are optimized and certain system deficiencies are corrected.

Since the ground-test model following indicates essentially the same performance as the flight-test model following, the former results are not shown in this report. The tests were run similarly except that ground tests used an analog computer to solve the JetStar's equations of motion.

The in-flight model-following tests undertaken at CAL were made during Flights 6 and 7. The JetStar was flown at the same flight condition as for the open- and closed-loop transient tests (0.55 Mach number and 20,000 ft altitude), but the airplane weight varied according to the time from the start of the flights. The model represented the supersonic transport at 0.55 Mach number, 20,000 ft altitude, and a weight of 240,000 lb (light weight). For the model-following tests shown here, from Flight 7, the pilot was flying the GPAS; that is, he was not using specialized inputs such as pulses.

Flight 7 results shown in Figures 5-22 and 5-23 are for pilot inputs to the elevator and ailerons during record 29. The actual pilot inputs are not shown since the figure is intended to show the model following. But, it is significant here that the inputs represent ordinary "flying" of the system involving non-specialized inputs. A CAL evaluation pilot flew the GPAS during these tests. Figure 5-22 shows model following with the α -loop, and Figure 5-23 shows sideslip, bank angle, and roll rate model following.

The results shown in Figures 5-22 and 5-23 are generally good, except for the sideslip model-following results shown in Figure 5-23. The GPAS sideslip response exhibits a 0.5 cps limit cycle, which is probably due to the rudder nonlinearity (friction) discussed before. In other model-following test results (not shown in this report) involving larger inputs, the sideslip limit cycle was not objectionable because it was much smaller relative to the commanded response.

The gains used for these model-following results may not necessarily be optimum. Very little time was available to experiment in flight with various combinations of gains. Although the Flight 7 tests involved the highest gains of all the model-following tests run at CAL, this does not mean that these tests necessarily had the best model following. Increased gain in MCS loops does not always guarantee increased performance. Careful in-flight optimization of gains should bring improved performance and is, therefore, recommended.

APPENDIX

LINEARIZED EQUATIONS OF MOTION

Linearized Longitudinal Equations (x-wind axis and y-, and z-body axes)

$$\Delta\dot{V} + D_V \Delta V + V_t D_\alpha \Delta\alpha + g\Delta\theta = \frac{\Delta T}{m}$$

$$\frac{\alpha_t}{V_t}\Delta\dot{V} - \frac{Z_V}{V_t}\Delta V + \Delta\dot{\alpha} - Z_\alpha \Delta\alpha - \Delta\dot{\theta} - Z_\theta \Delta\theta = Z_{\delta_e}\Delta\delta_e$$

$$-M_V \Delta V - M_{\dot{\alpha}}\Delta\dot{\alpha} - M_\alpha \Delta\alpha + \Delta\ddot{\theta} - M_q \Delta\dot{\theta} = M_{\delta_e}\Delta\delta_e + M_{\Delta T}\Delta T$$

$$D_V = \frac{1}{m}\left(\frac{\partial D}{\partial V} - \frac{\partial T}{\partial V}\right) \qquad \frac{\partial D}{\partial V} = C_{D_t}\rho V_t S$$

$$D_\alpha = \frac{1}{mV_t}\left(\frac{\partial D}{\partial \alpha} + \alpha_t T_t - W\right) \qquad \frac{\partial D}{\partial \alpha} = C_{D_\alpha}\frac{1}{2}\rho V_t^2 S$$

$$Z_V = -\frac{1}{m}\left(\frac{\partial L}{\partial V} + \alpha_t \frac{\partial D}{\partial V}\right) \qquad \frac{\partial L}{\partial V} = C_{L_t}\rho V_t S$$

$$Z_\alpha = -\frac{1}{mV_t}\left(\frac{\partial L}{\partial \alpha} + \alpha_t \frac{\partial D}{\partial \alpha} + T_t - W\theta_t\right) \qquad \frac{\partial L}{\partial \alpha} = C_{L_\alpha}\frac{1}{2}\rho V_t^2 S$$

$$Z_\theta = -\frac{g\alpha_t}{V_t}$$

$$Z_{\delta_e} = -\frac{1}{mV_t}\frac{\partial L}{\partial \delta_e} \qquad \frac{\partial L}{\partial \delta_e} = C_{L_{\delta_e}}\frac{1}{2}\rho V_t^2 S$$

$$M_V = \frac{1}{I_{YY}}\frac{\bar{q}S\bar{c}}{a}\left\{\frac{2}{M}C_{m_{(A)}} + \frac{\partial C_{m_{(A)}}}{\partial M}\right\} - \frac{y_T}{I_{YY}a}\frac{\partial T}{\partial M}$$

$$C_{m_{(A)}} \cong \frac{-y_T}{\bar{c}} C_D$$

$$M_{\dot{\alpha}} = \frac{1}{I_{yy}} \bar{q} S \bar{c} \cdot \frac{\bar{c}}{2V_t} C_{m_{\dot{\alpha}}}$$

$$M_{\alpha} = \frac{1}{I_{yy}} \bar{q} S \bar{c} \, C_{m_{\alpha}} .$$

$$M_{q} = \frac{1}{I_{yy}} \bar{q} S \bar{c} \cdot \frac{\bar{c}}{2V_t} C_{m_{q}}$$

$$M_{\delta_e} = \frac{1}{I_{yy}} \bar{q} S \bar{c} \, C_{m_{\delta_e}}$$

$$M_{\Delta T} = \frac{z_T}{I_{yy}}$$

a = speed of sound

z_T = thrust moment arm (along positive z body axis)

Linearized Lateral-Directional Equations (Body Axes)

Side Force

$$-\alpha_t \dot{\phi} - \frac{g}{V_t} \phi + (1+\alpha_t^2) r + \dot{\beta} - Y_\beta \beta = Y_{\delta_r} \delta_r$$

Rolling Moment

$$\ddot{\phi} - L_p \dot{\phi} - \left(\frac{I_{xz}}{I_{xx}} + \alpha_t \right) \dot{r} + (\alpha_t L_p - L_r) r - L_\beta \beta = L_{\delta_r} \delta_r + L_{\delta_a} \delta_a$$

Yawing Moment

$$-\frac{I_{xz}}{I_{zz}} \ddot{\phi} - N_p \dot{\phi} + \left(1 + \alpha_t \frac{I_{xz}}{I_{zz}} \right) \dot{r} + (\alpha_t N_p - N_r) r - N_\beta \beta = N_{\delta_r} \delta_r + N_{\delta_a} \delta_a$$

These equations, which have ϕ, r, and β as variables, were derived from the corresponding linear lateral-directional equation having p, r, and β as variables by using the relation $p \cong \dot{\phi} - r\alpha_t$. This relation was obtained from the basic equations $p = \dot{\phi} - \dot{\psi} \sin\theta$ and $\dot{\psi} = (q \sin\phi + r \cos\phi)/\cos\theta$ along with the small angle approximation:

$$\sin\theta = \sin\alpha_t \cong \alpha_t, \quad \cos\phi = \cos\theta \cong 1.$$

$$Y_\beta = \frac{1}{mV_t}\,\bar{q}\,S\,C_{Y_\beta} \qquad N_\beta = \frac{1}{I_{zz}}\,\bar{q}\,Sb\,C_{n_\beta}$$

$$Y_{\delta_r} = \frac{1}{mV_t}\,\bar{q}\,S\,C_{Y_{\delta_r}} \qquad N_{\delta_r} = \frac{1}{I_{zz}}\,\bar{q}\,Sb\,C_{n_{\delta_r}}$$

$$L_p = \frac{1}{I_{xx}}\,\bar{q}\,Sb \cdot \frac{b}{2V_t} \cdot C_{\ell_p} \qquad N_{\delta_a} = \frac{1}{I_{zz}}\,\bar{q}\,Sb\,C_{n_{\delta_a}}$$

$$L_r = \frac{1}{I_{xx}}\,\bar{q}\,Sb \cdot \frac{b}{2V_t} \cdot C_{\ell_r}$$

$$L_\beta = \frac{1}{I_{xx}}\,\bar{q}\,Sb\,C_{\ell_\beta}$$

$$L_{\delta_r} = \frac{1}{I_{xx}}\,\bar{q}\,Sb\,C_{\ell_{\delta_r}}$$

$$L_{\delta_a} = \frac{1}{I_{xx}}\,\bar{q}\,Sb\,C_{\ell_{\delta_a}}$$

$$N_p = \frac{1}{I_{zz}}\,\bar{q}\,Sb\,\frac{b}{2V_t}\,C_{n_p}$$

$$N_r = \frac{1}{I_{zz}}\,\bar{q}\,Sb\,\frac{b}{2V_t}\,C_{n_r}$$

Table 2-1

DESIGN VALUES OF GPAS RFS GAINS

Gain	Derivative Changed	Range	Units	Primary Function	Estimated Max. Established by*
δ_e/α	M_α	±10	-	short-period frequency	(1) and (2)
$\delta_e/\dot{\alpha}$	$M_{\dot{\alpha}}$	±1	sec	short-period damping	(2)
δ_e/q	M_q	±3	sec	short-period damping	(3)
$\delta_e/\dot{q}$	–	±.1	sec^2	elevator servo compensation	(2)
δ_e/V	M_V	±.5	deg-sec/ft	phugoid frequency	(2)
$\delta_e/\dot{V}$	$M_{\dot{V}}$	±1	$deg\text{-}sec^2/ft$	phugoid damping	(2)
δ_r/β	N_β	±10	-	Dutch-roll frequency; directional stability	(1) and (2)
$\delta_r/\dot{\beta}$	$N_{\dot{\beta}}$	±1	sec	Dutch-roll damping	(2)
δ_r/r	N_r	±4	sec	Dutch-roll damping	(3)
$\delta_r/\dot{r}$	–	±.1	sec^2	rudder servo compensation	(2)
δ_r/p	N_p	±4	sec	roll to yaw coupling	(3)
$\delta_r/\dot{p}$	–	±.1	sec^2	rudder servo compensation	(2)
δ_a/ϕ	L_ϕ	±5	-	roll attitude stabilization	(3)
δ_a/p	L_p	±2	sec	roll mode time constant	(1) and (2)
$\delta_a/\dot{p}$	–	±.1	sec^2	aileron servo compensation	(2)
δ_a/r	L_r	±4	sec	spiral mode time constant	(3)
$\delta_a/\dot{r}$	–	±.1	sec^2	aileron servo compensation	(1) and (2)
δ_a/β	L_β	±10		roll to yaw ratio; ω_ϕ/ω_ψ	(2)
$\delta_a/\dot{\beta}$	–	±1	sec	phase compensation	(2)
δ_e/δ_{e_p}	$M_{\delta_{e_c}}$	0 to 10	deg/in.	elevator control gearing	(3)
δ_a/δ_{a_p}	$L_{\delta_{a_c}}$	0 to 1	deg/deg	aileron control gearing	(3)
δ_r/δ_{r_p}	$N_{\delta_{r_c}}$	0 to 30	deg/in.	rudder control gearing	(3)
δ_e/F_e	–	0 to 1	deg/lb	elevator force command sensitivity	(3)
δ_a/F_a	–	0 to .2	deg/lb	aileron force command sensitivity	(3)
δ_r/F_r	–	0 to .5	deg/lb	rudder force command sensitivity	(3)
δ_a/δ_{r_p}	$L_{\delta_{r_c}}$	±5	deg/in.	roll due to yaw command	(3)
δ_r/δ_{a_p}	$N_{\delta_{a_c}}$	±1	deg/deg	yaw due to roll command	(3)
δ_{a_c}/δ'_r	L_{δ_r}	±2	deg/deg	roll due to yaw control derivative	(3)
δ_{r_c}/δ'_a	N_{δ_a}	±2	deg/deg	yaw due to roll control derivative	(3)

* 1) structural instability; 2) noise, 3) sufficient for the task

Table 5-I

RESPONSE FEEDBACK SYSTEM PERFORMANCE (FLIGHT 5)

RECORD NO.	RFS GAINS*		NATURAL FREQUENCY $\left(\frac{RAD}{SEC}\right)$	DAMPING RATIO
	$\frac{\delta e}{\Delta \alpha_V}$	$\frac{\delta e}{\dot{\alpha}_V}$	SHORT PERIOD	SHORT PERIOD
35	0	0	2.1	0.17
35	+0.8	+0.08	4.6	0.11
35	+2.0	+0.20	6.0	0.22
35	+2.4	+0.24	6.2	0.20
35	+3.0	+0.30	7.6	0.07
35	+3.6	+0.36	8.4	0.01
	$\frac{\delta r}{\beta_V}$	$\frac{\delta r}{\dot{\beta}_V}$	DUTCH ROLL	DUTCH ROLL
36	0	0	1.7	0.08
36	-0.4	-0.04	1.3	0.19
37	-0.6	-0.06	1.1	0.22
37	-0.8	-0.08	0.82	0.21
21	+1.0	+0.10	2.3	-0.05
	$\frac{\delta a}{\phi}$	$\frac{\delta a}{p}$	ROLL-SPIRAL	ROLL-SPIRAL
40	-2.5	-1.0	5.3	1.32

*VANE POSITION ERROR GAINS ARE NOT INCLUDED.

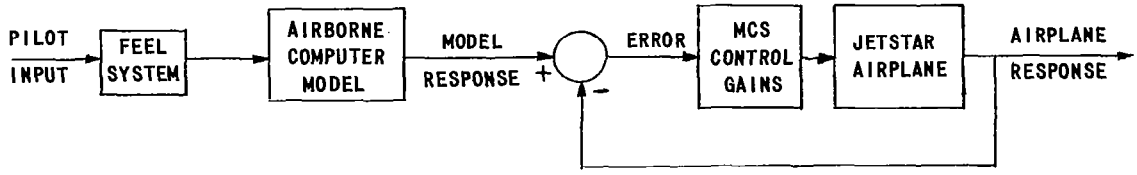

Figure I-1 SIMPLIFIED BLOCK DIAGRAM OF MODEL CONTROLLED (MCS) VARIABLE STABILITY SYSTEM

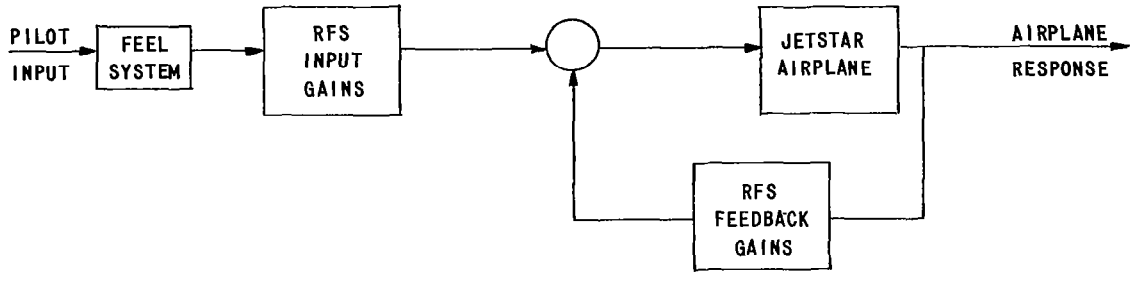

Figure I-2 SIMPLIFIED BLOCK DIAGRAM OF RESPONSE FEEDBACK (RFS) VARIABLE STABILITY SYSTEM

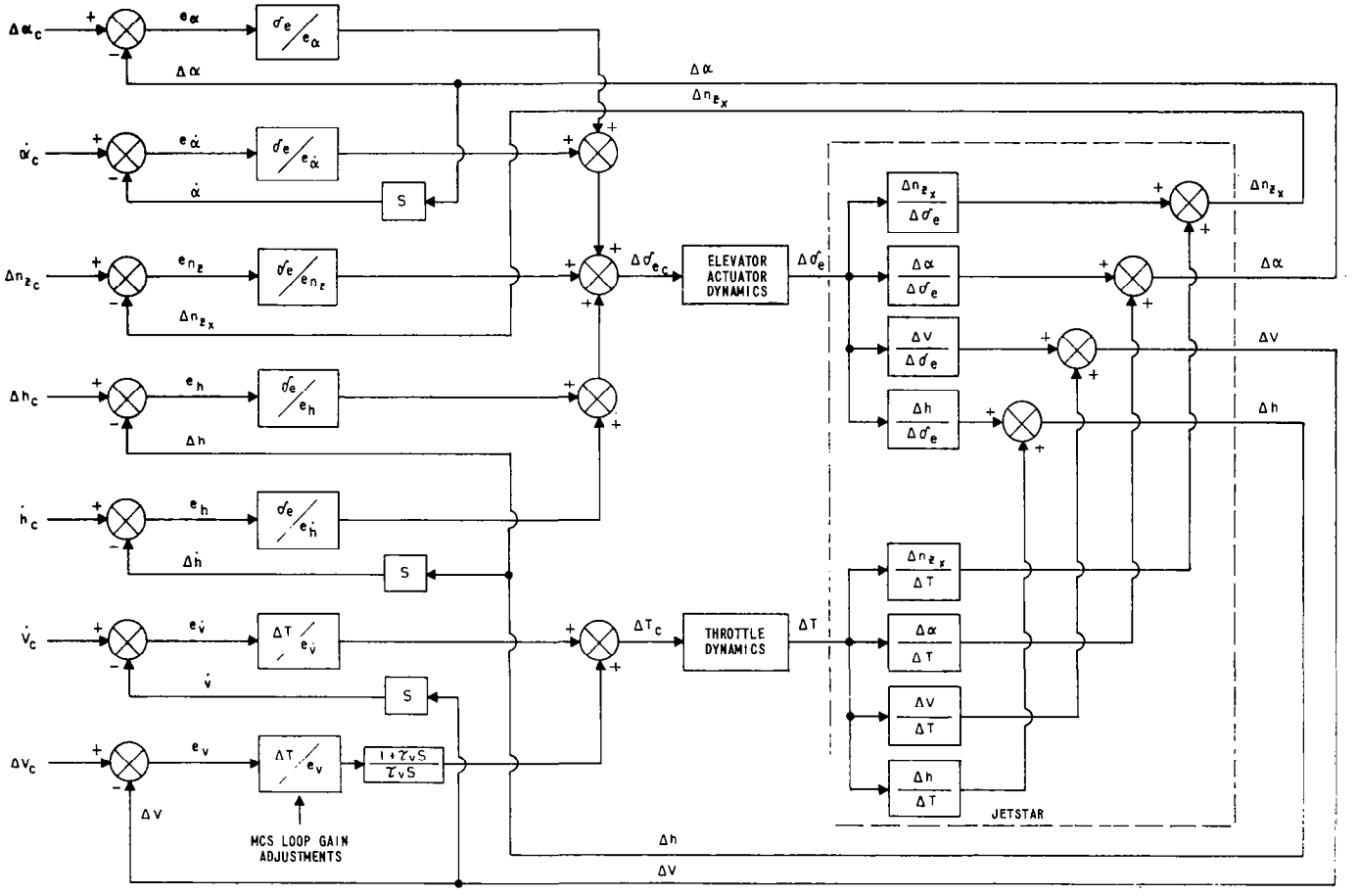

Figure 2-1 BLOCK DIAGRAM OF THE LONGITUDINAL MCS CONTROL LOOPS

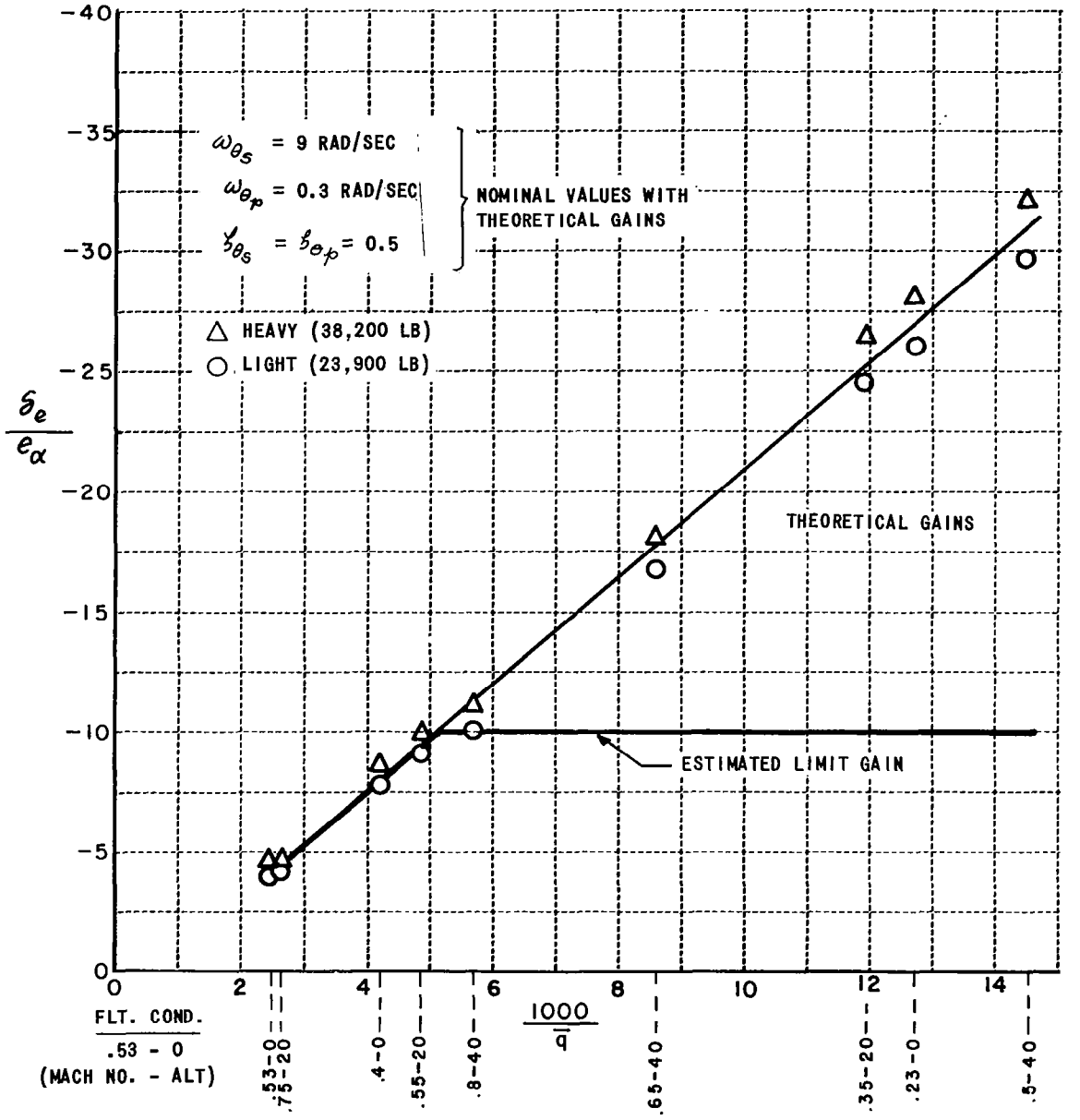

Figure 2-2 LONGITUDINAL SHORT-PERIOD ANGLE-OF-ATTACK GAIN

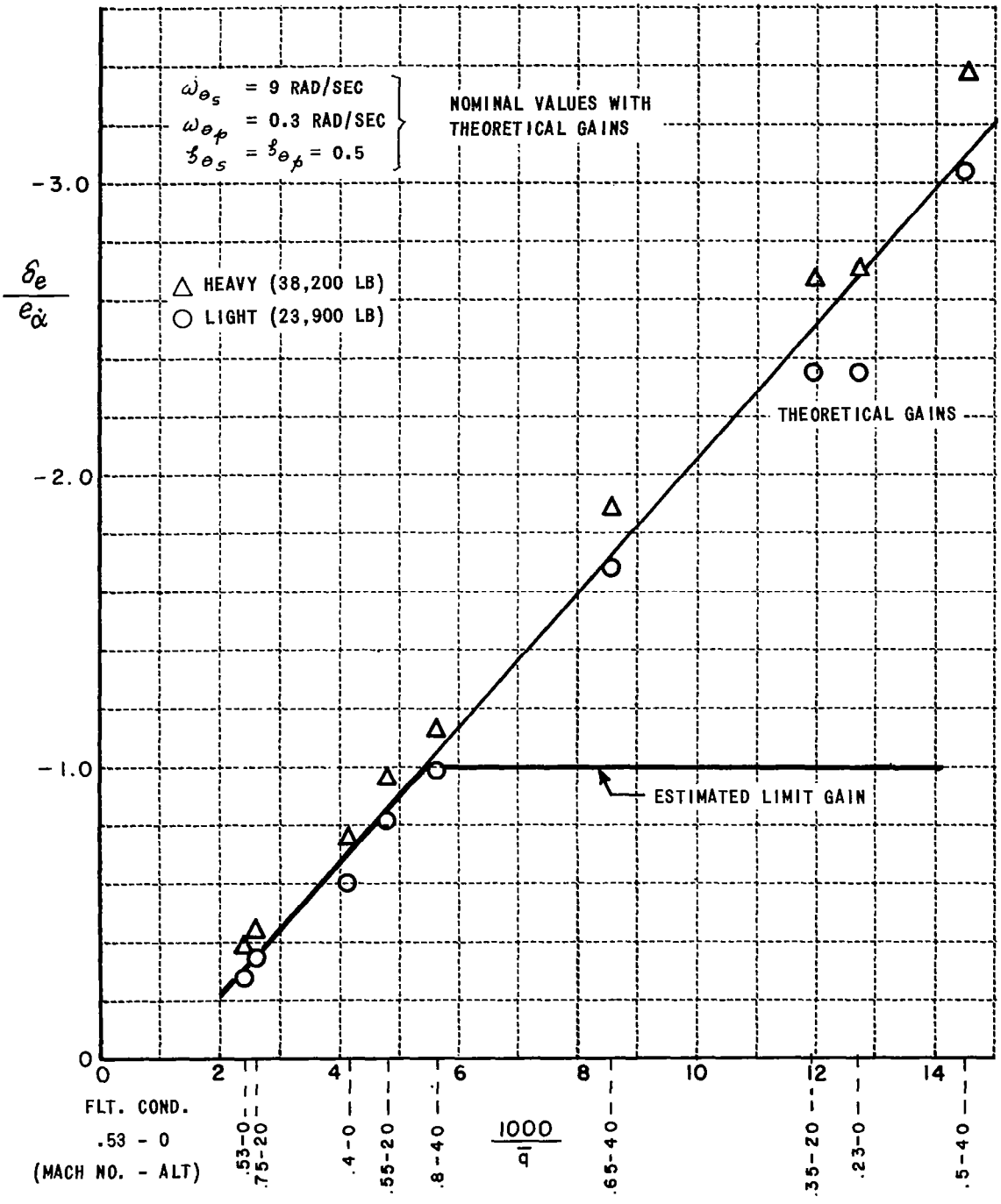

Figure 2-3 LONGITUDINAL SHORT-PERIOD DAMPING GAIN

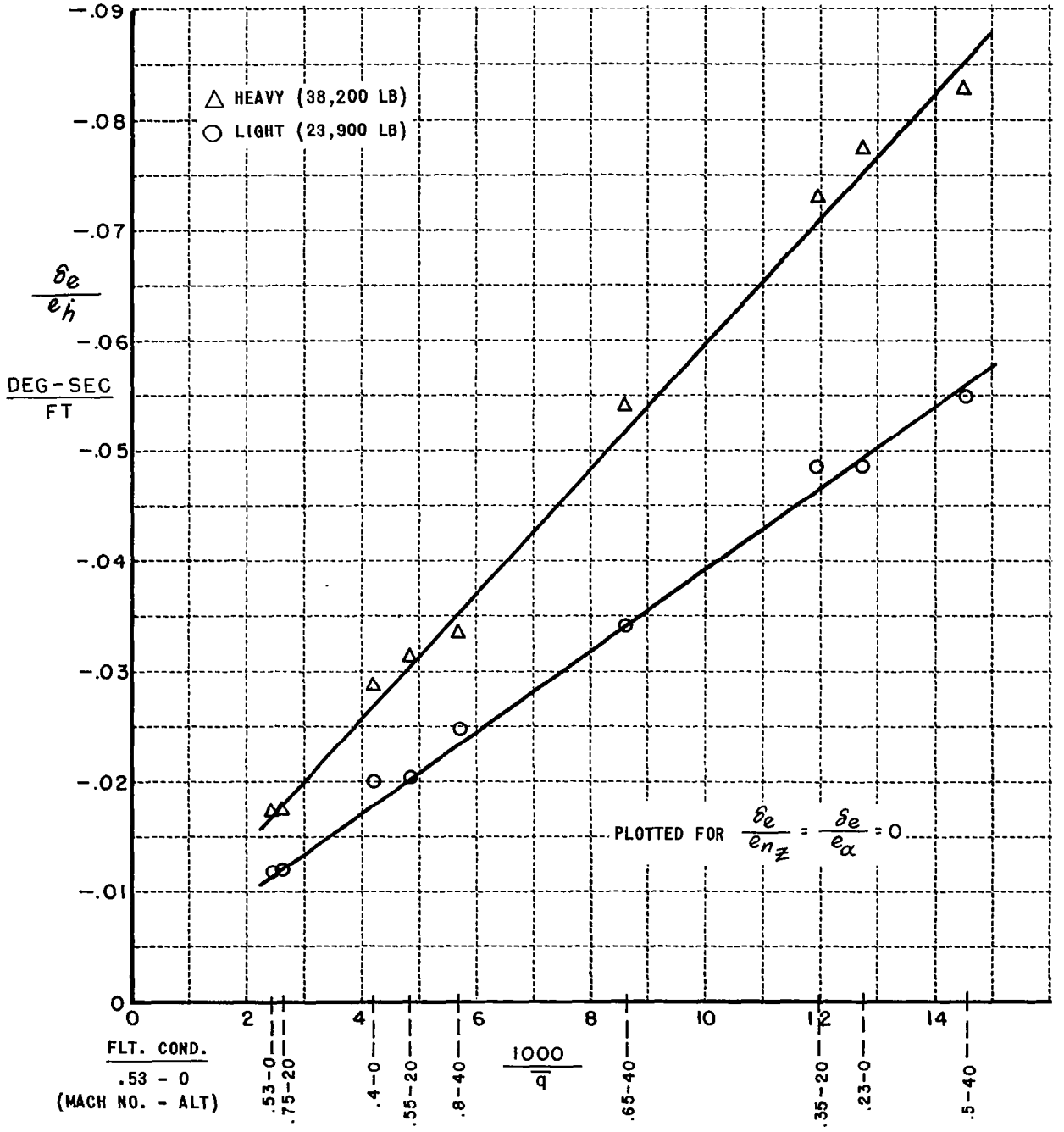

Figure 2-4 LONGITUDINAL δ_e/e_h PHUGOID CONTROL LOOP GAIN WITH SHORT-PERIOD LOOPS OPEN

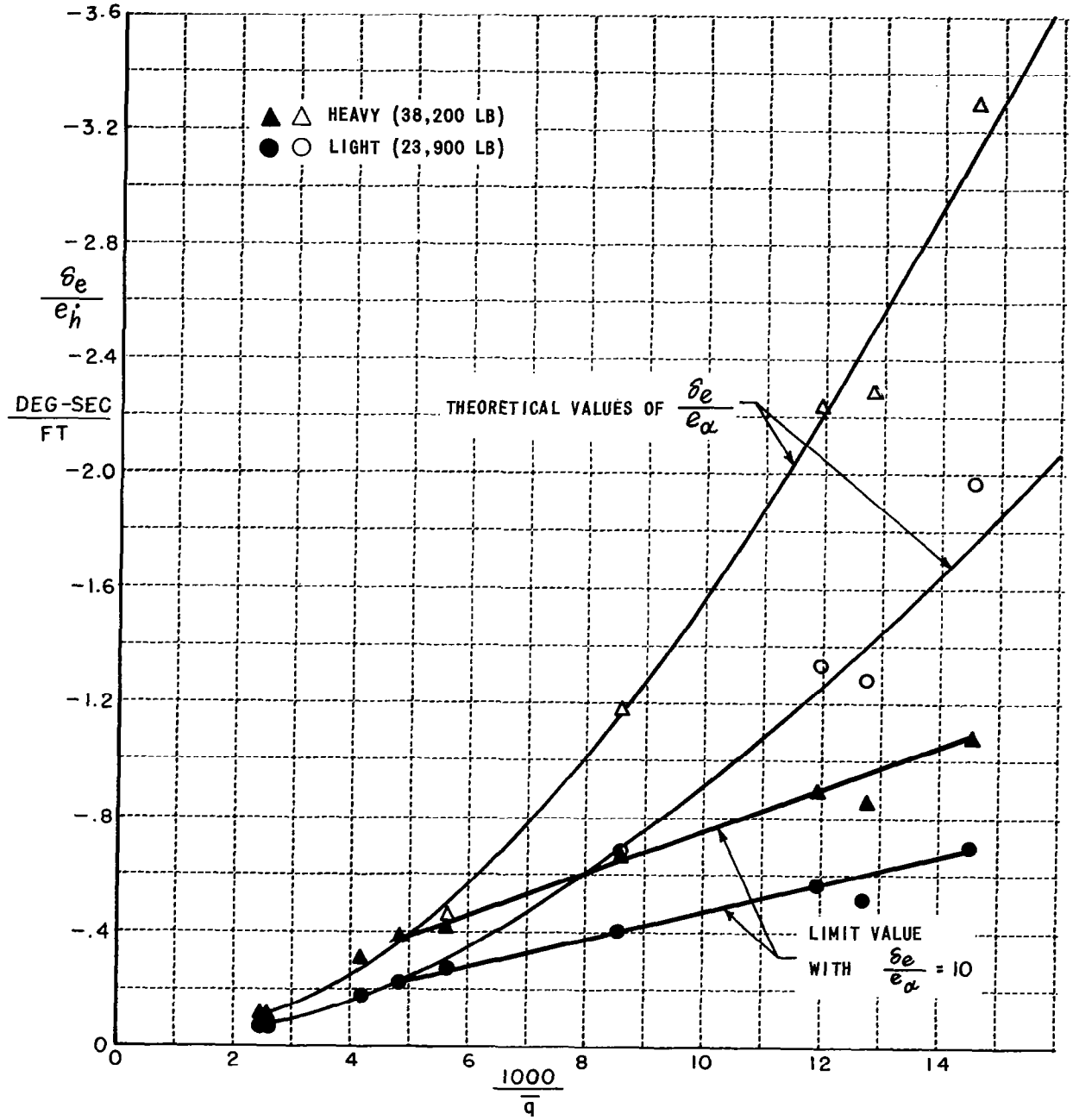

Figure 2-5 LONGITUDINAL $\delta_e/e_{\dot{h}}$ PHUGOID CONTROL LOOP GAIN WITH SHORT-PERIOD α-LOOP CLOSED

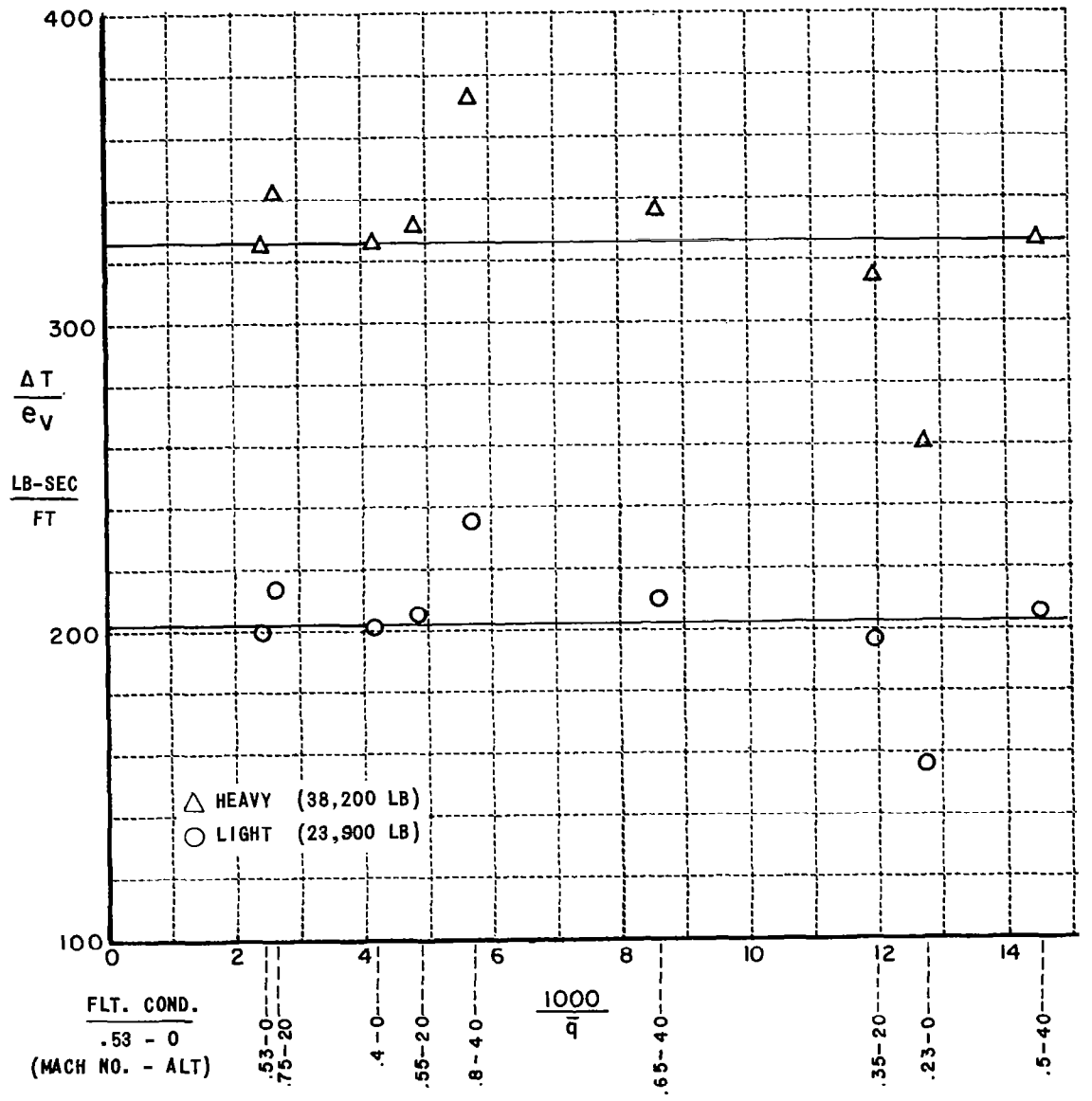

Figure 2-6 LONGITUDINAL THROTTLE PHUGOID CONTROL LOOP GAIN

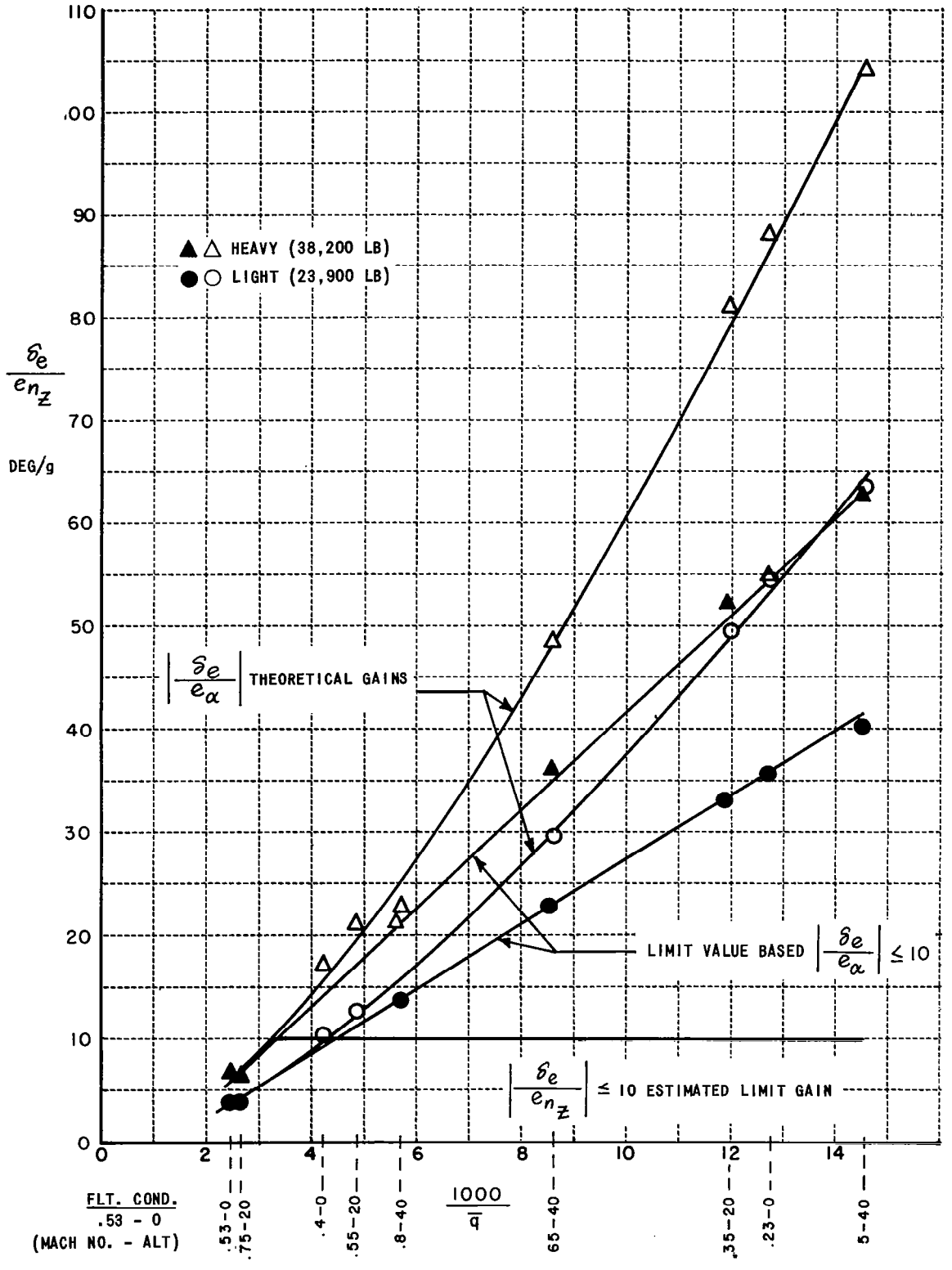

Figure 2-7 LONGITUDINAL NORMAL ACCELERATION GAIN

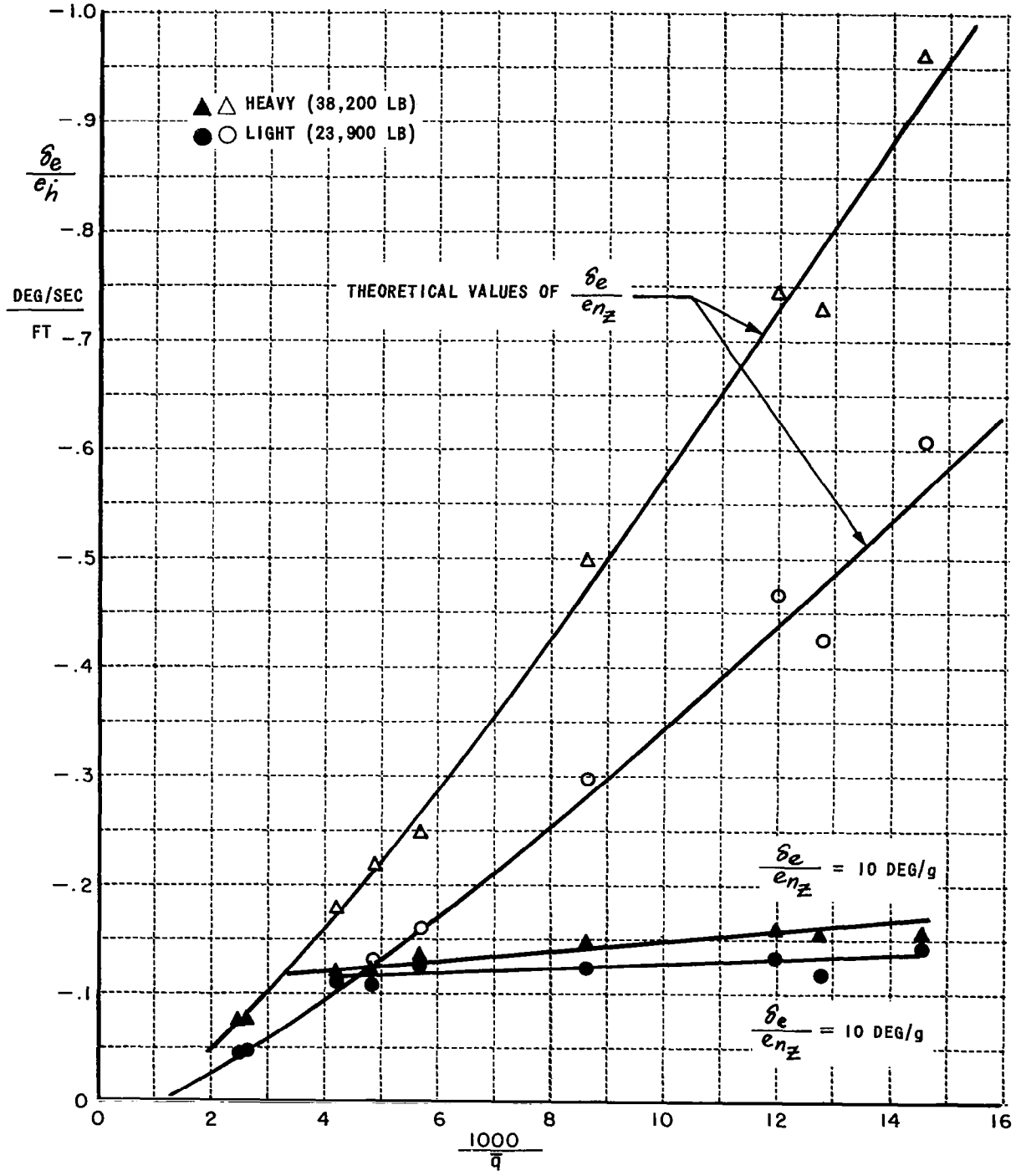

Figure 2-8 LONGITUDINAL $\delta_e/e_{\dot{h}}$ PHUGOID CONTROL LOOP GAIN WITH SHORT-PERIOD n_z LOOP CLOSED

Flight Condition .5H40 | Input Gains - 1.0 | Control Input $\Delta\delta_{e_m}$ = -0.5 u(t) deg

$\frac{\delta_e}{e_\alpha}$ = -10 $\frac{\delta_e}{e_h}$ = -0.05 deg/ft $\frac{\Delta T}{e_V}$ = 326 $\frac{\text{lb sec}}{\text{ft}}$

$\frac{\delta_e}{e_{\dot\alpha}}$ = - 1.0 sec $\frac{\delta_e}{e_{\dot h}}$ = - 1.0 deg sec/ft τ_v = 20 sec

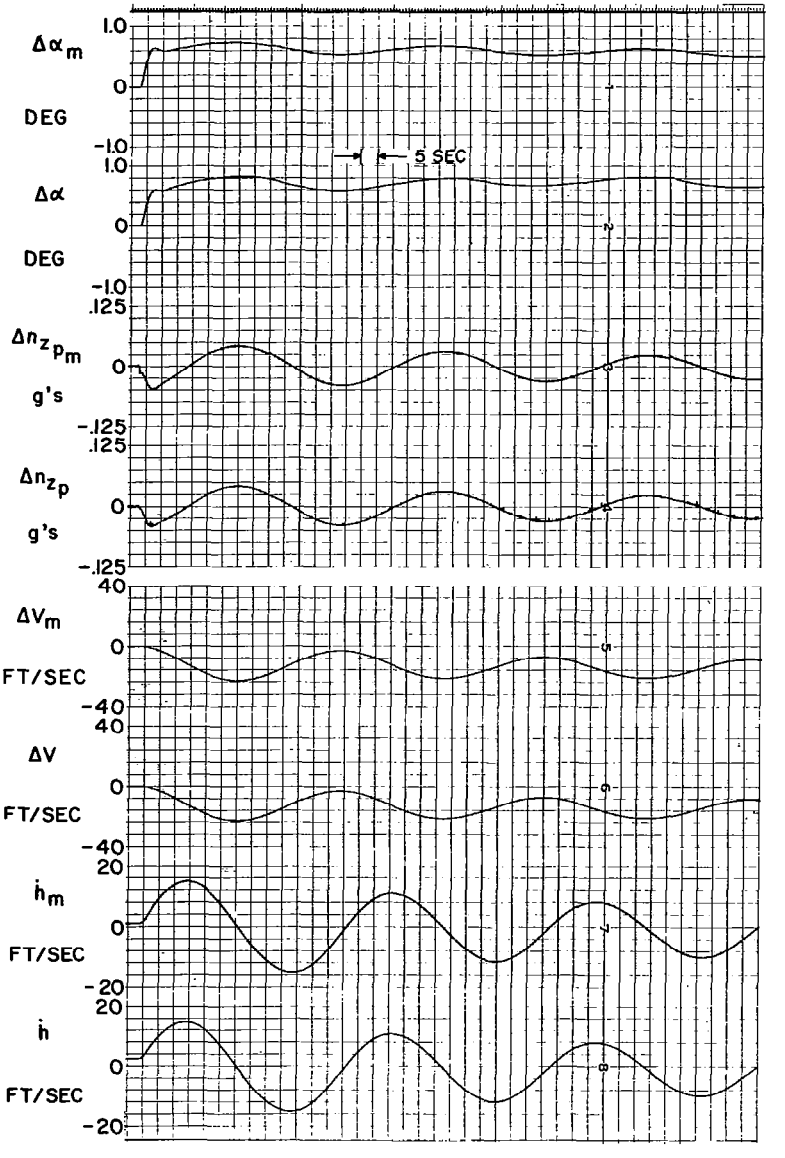

Figure 2-9 LONGITUDINAL MODEL FOLLOWING RESPONSE TO ELEVATOR INPUT WITH LIMITED GAINS FOR α-LOOP

Flight Condition

.5H40

Control Input

ΔT_m = 12,500 u(t) lb

Input Gains = 1.0

$\frac{\delta_e}{e_\alpha}$ = - 10

$\frac{\delta_e}{e_h}$ = - 0.05 deg sec/ft

$\frac{\Delta T}{e_V}$ = 326 lb sec/ft

$\frac{\delta_e}{e_{\dot{\alpha}}}$ = - 1.0 sec

$\frac{\delta_e}{e_{\dot{h}}}$ = - 1.0 deg sec/ft

τ_V = 20 sec

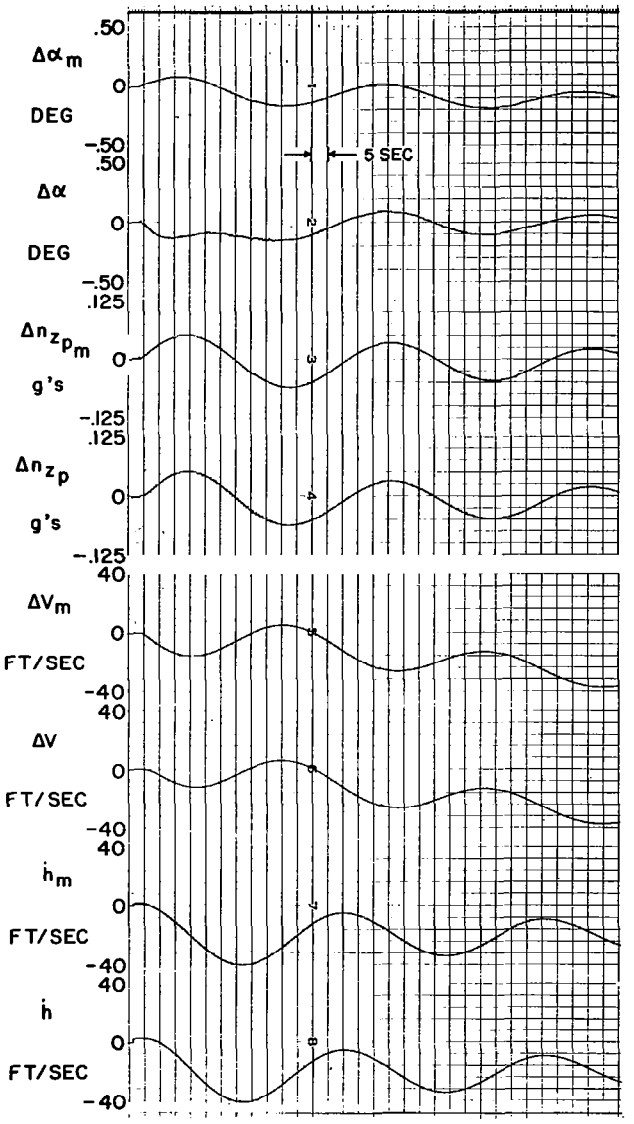

Figure 2-10 LONGITUDINAL MODEL FOLLOWING RESPONSE TO THROTTLE INPUT WITH LIMITED GAINS FOR α-LOOP

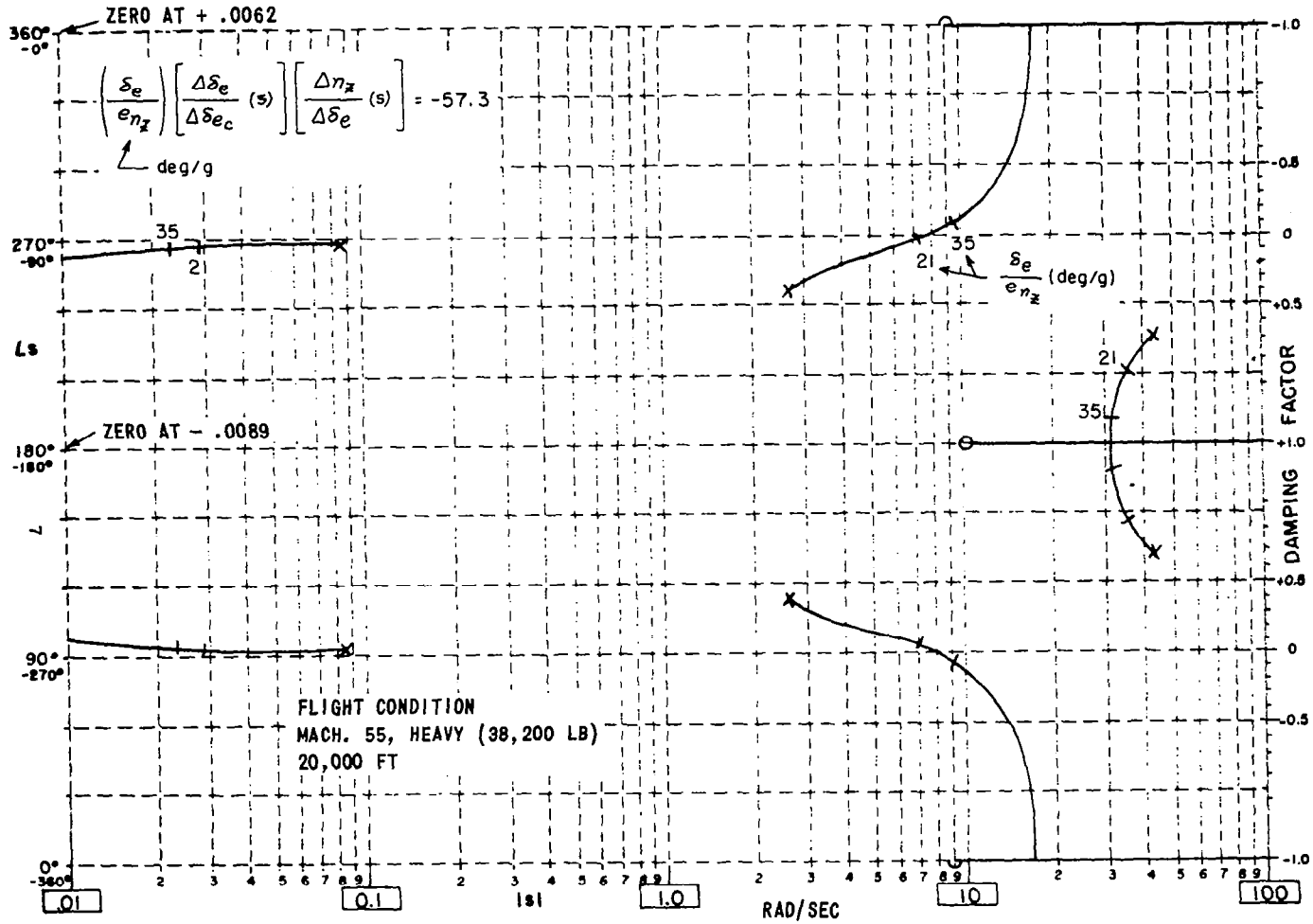

Figure 2-11 C.G. NORMAL ACCELERATION LOOP ROOT LOCUS

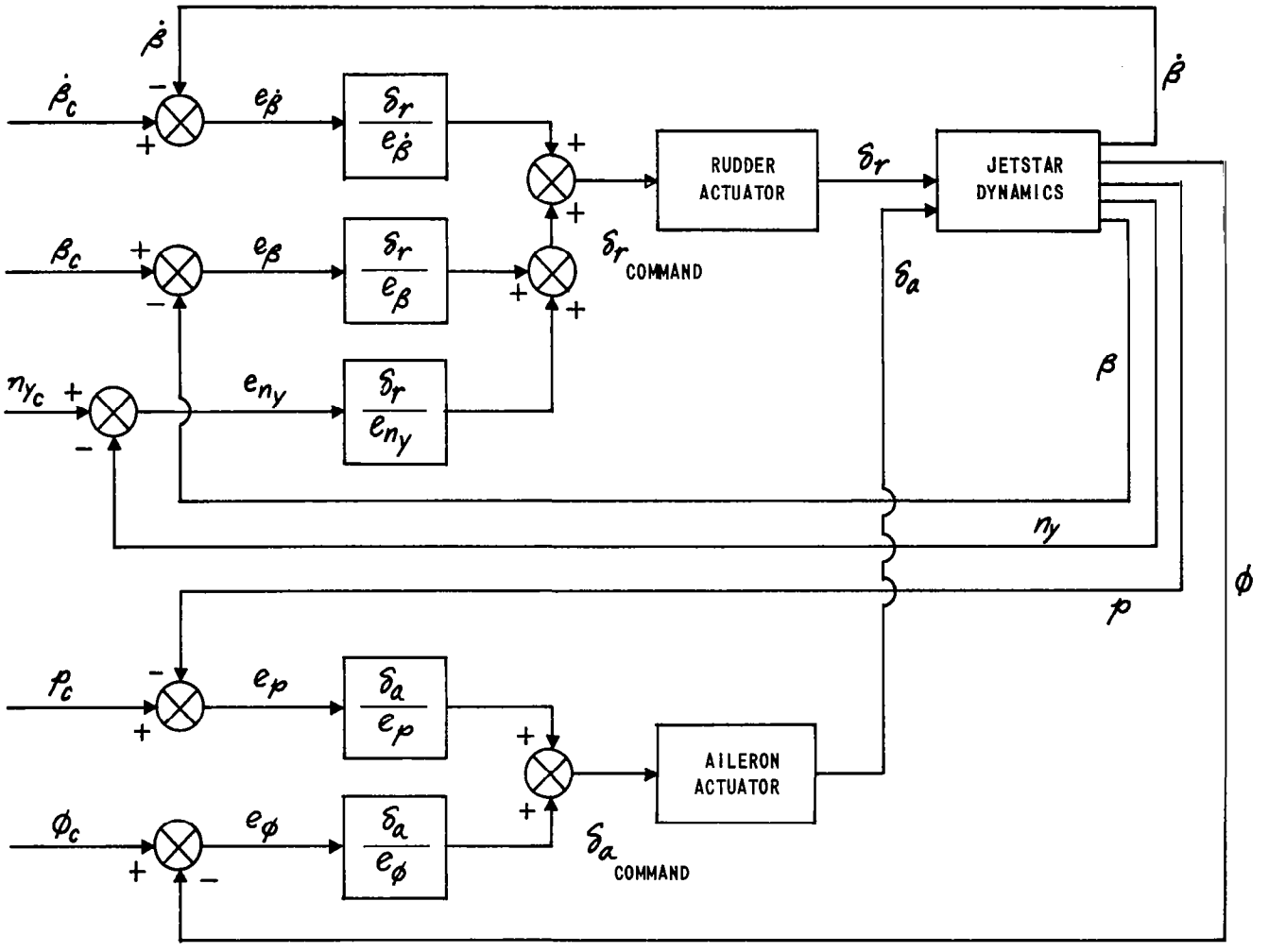

Figure 2-12 BLOCK DIAGRAM OF LATERAL-DIRECTIONAL MCS CONTROL LOOPS

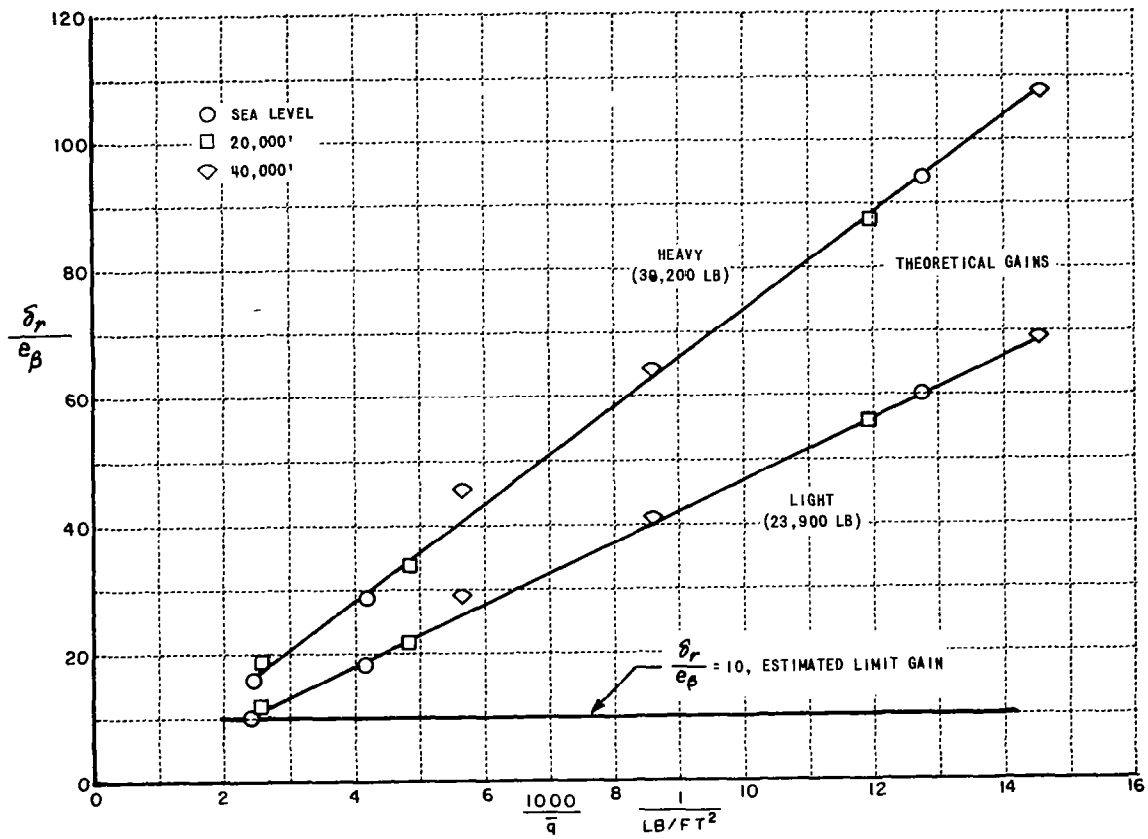

Figure 2-13 LATERAL-DIRECTIONAL ANGLE OF SIDESLIP GAIN

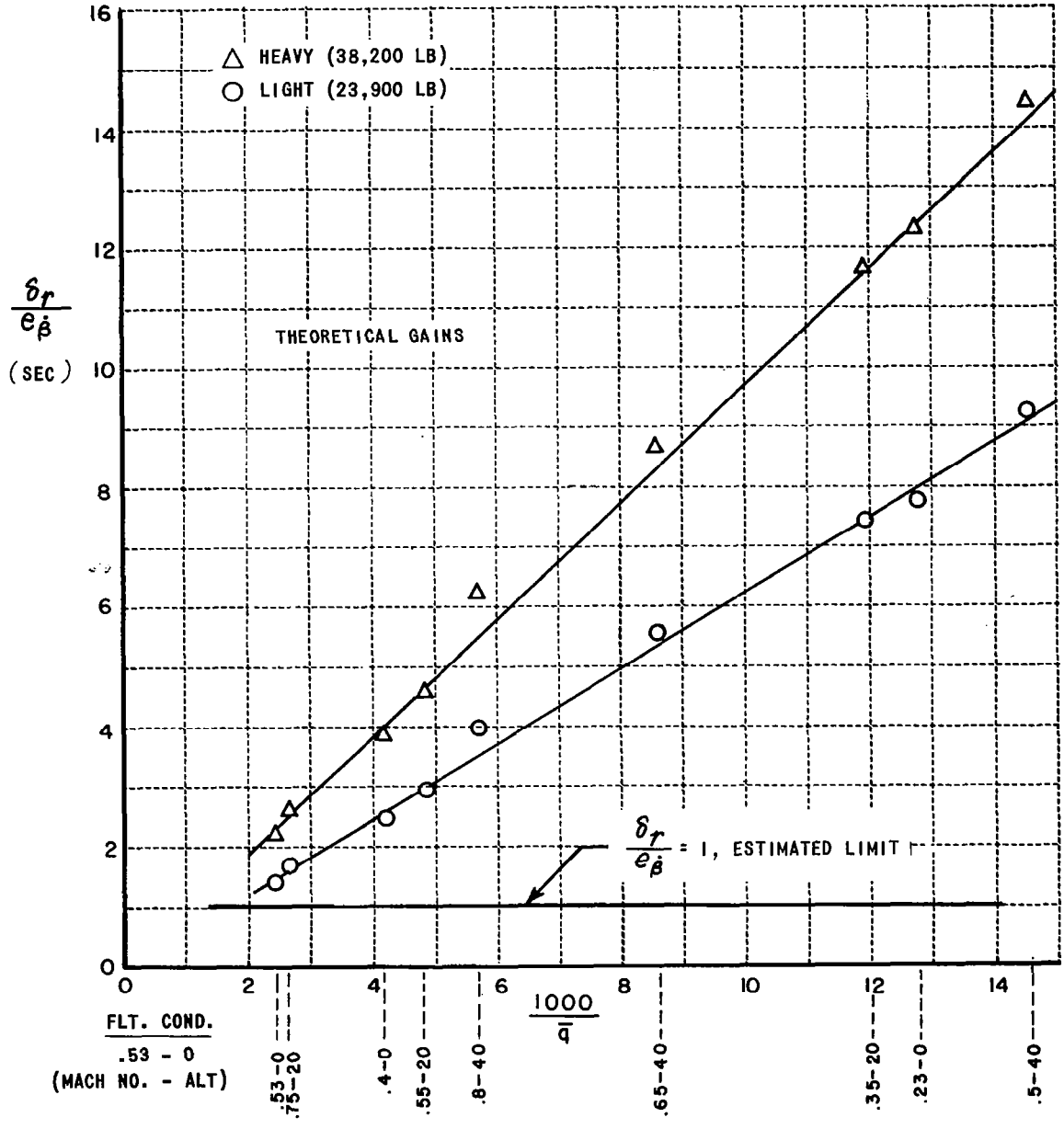

Figure 2-14 LATERAL-DIRECTIONAL DUTCH ROLL DAMPING GAIN FOR β-LOOP

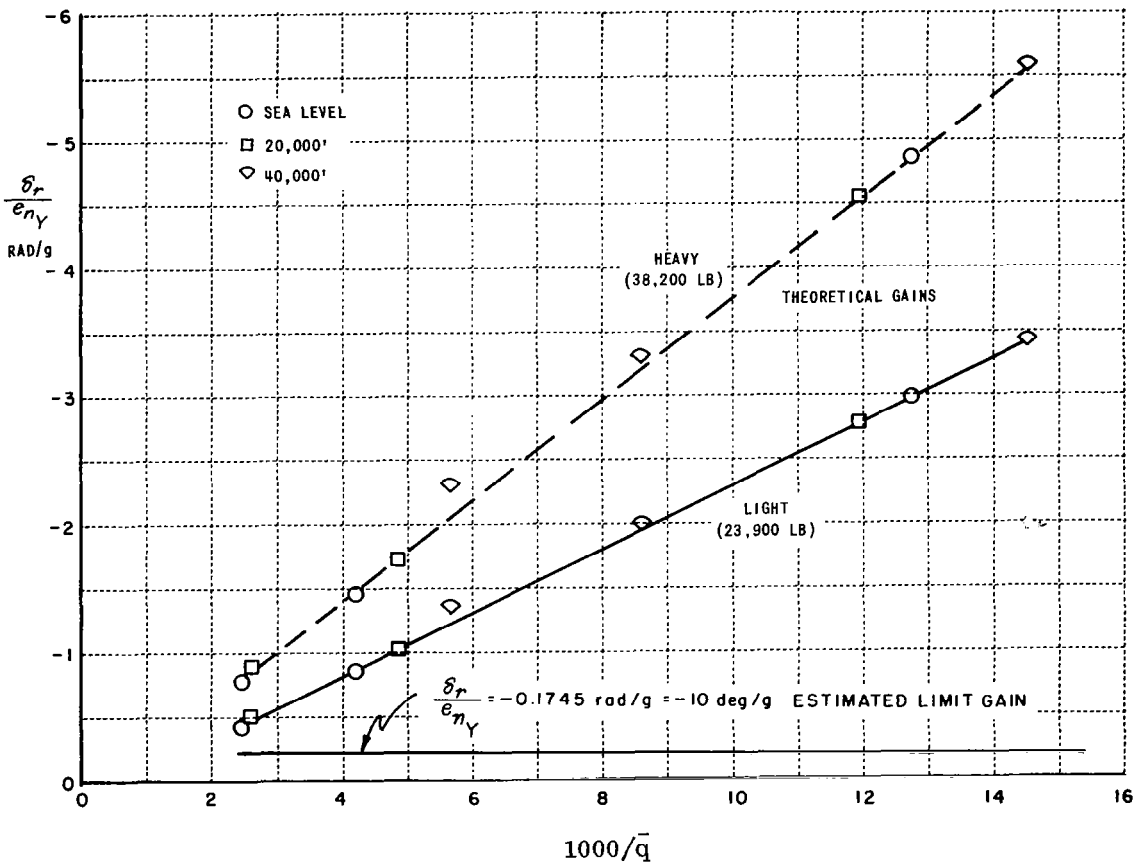

Figure 2-15 LATERAL-DIRECTIONAL LATERAL ACCELERATION GAIN

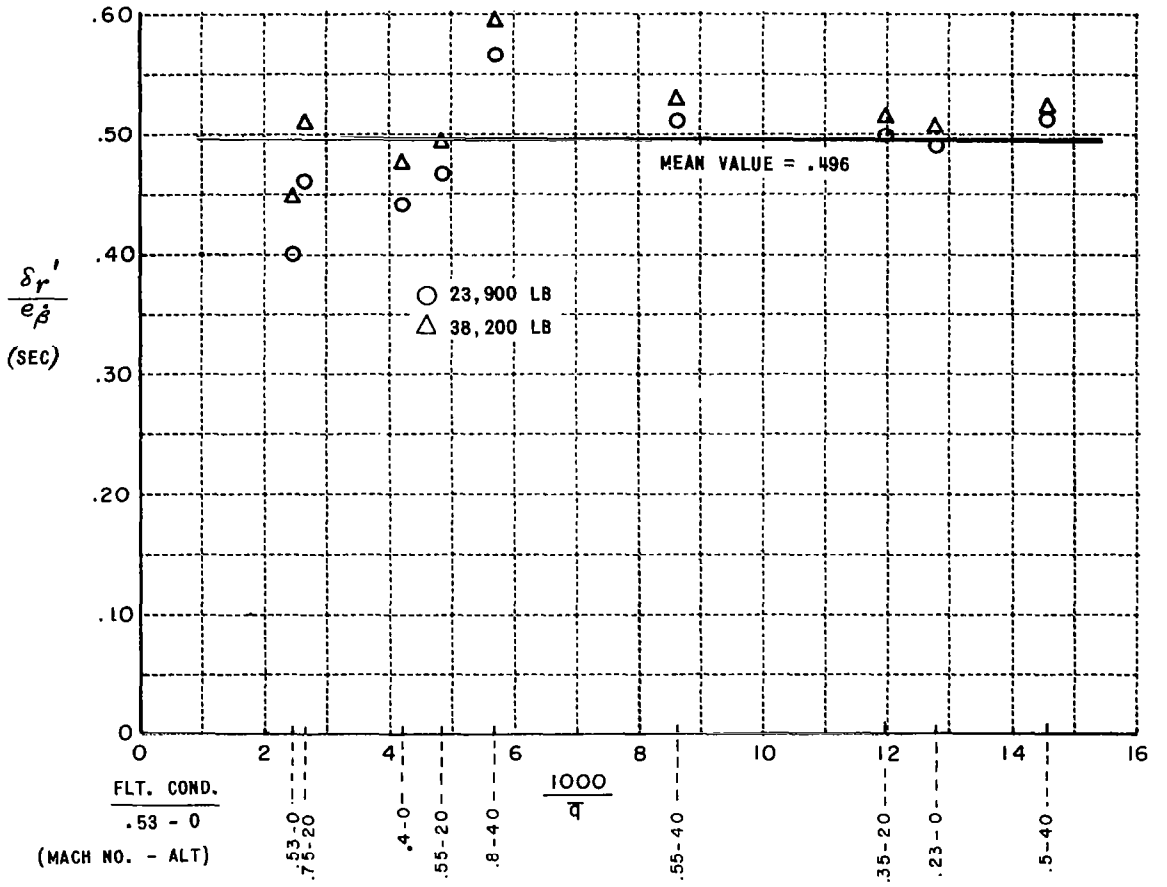

Figure 2-16 LATERAL-DIRECTIONAL DUTCH ROLL DAMPING GAIN FOR n_y-LOOP

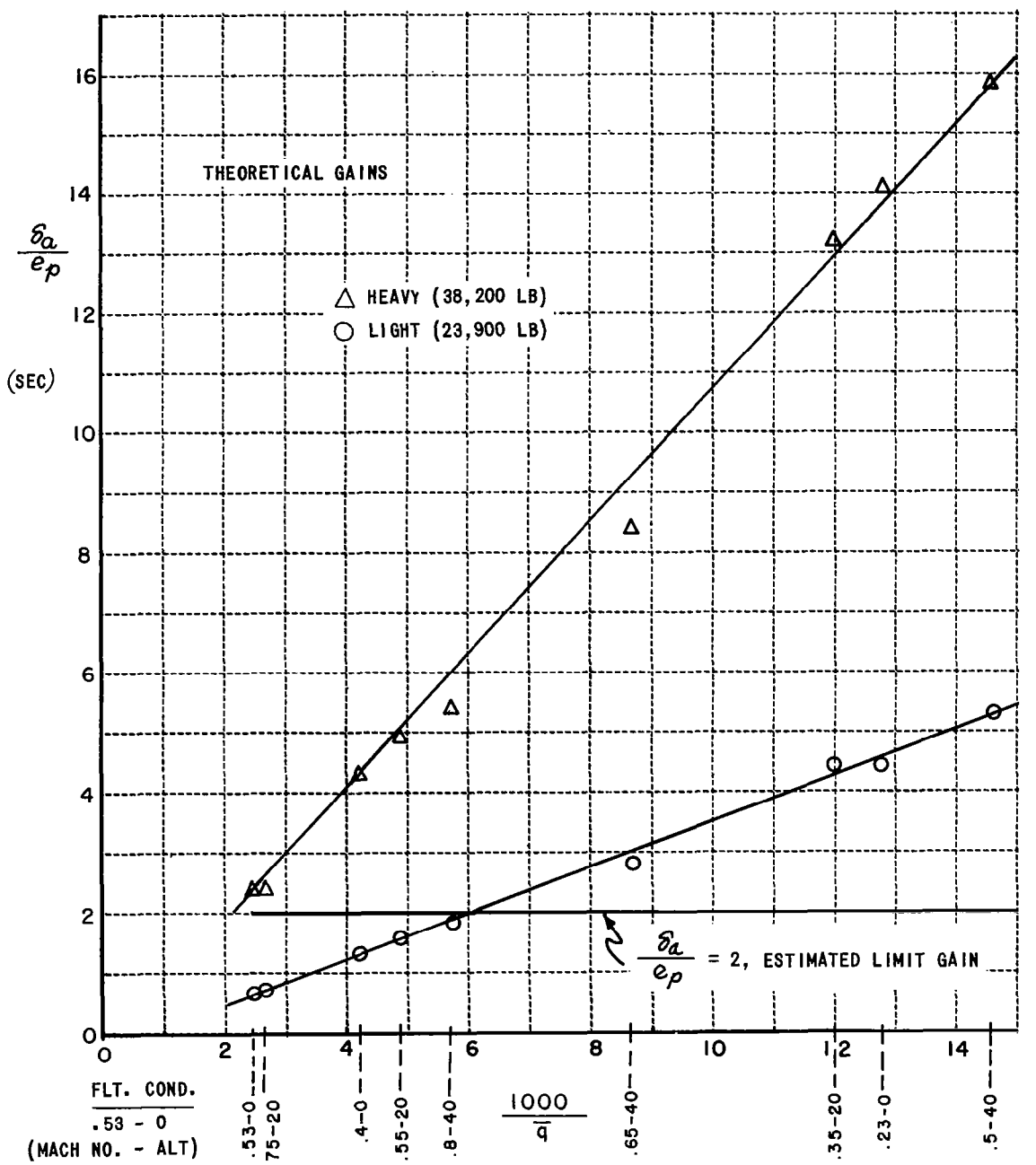

Figure 2-17 LATERAL-DIRECTIONAL ROLL RATE GAIN

Flight Condition
.5H40

All input gains equal 1.0.

Control Input
δ_a = 0.5 u(t) deg

Forward Loop Gains

$\frac{\delta_a}{e_p}$ = 10.5 sec $\frac{\delta_a}{e_\phi}$ = 1.05 $\frac{\delta_r}{e_\beta}$ = 108 $\frac{\delta_r}{e_{\dot{\beta}}}$ = 10.3 sec

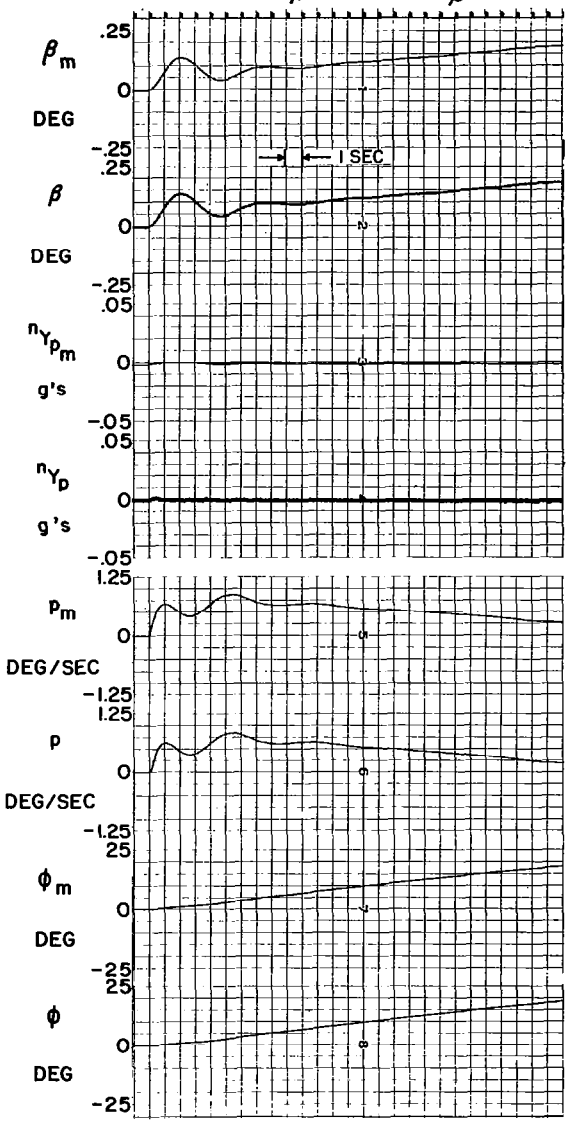

Figure 2-18 LATERAL-DIRECTIONAL MODEL FOLLOWING RESPONSE TO AILERON INPUT, SST MODEL, THEORETICAL GAINS WITH β -LOOP

Flight Condition

.5H40

Control input

$\delta_a = 0.5\ u(t)$ deg

$\frac{\delta_r}{e_\beta} = 10$ $\frac{\delta_r}{e_{\dot\beta}} = 1.0$ sec $\frac{\delta_a}{e_p} = 2.0$ sec $\frac{\delta_a}{e_\phi} = 1.05$

All input gains equal 1.0.

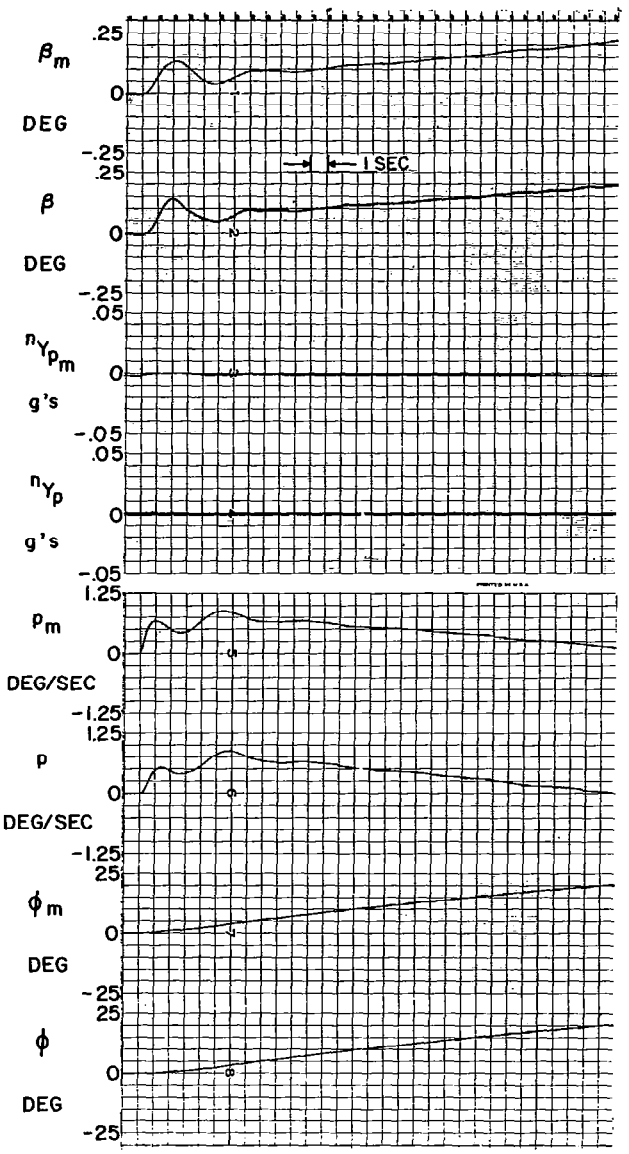

Figure 2-19 LATERAL-DIRECTIONAL MODEL FOLLOWING RESPONSE TO AILERON INPUT, SST MODEL, LIMITED GAINS WITH β -LOOP

Flight Condition

.5H40

Control Input

$\delta_R = 0.5\ u(t)$ deg

$\frac{\delta_r}{e_\beta} = 108$ $\quad \frac{\delta_r}{e_{\dot\beta}} = 10.3$ sec $\quad \frac{\delta_a}{e_p} = 10.5$ sec $\quad \frac{\delta_a}{e_\phi} = 1.05$

All input gains equal 1.0.

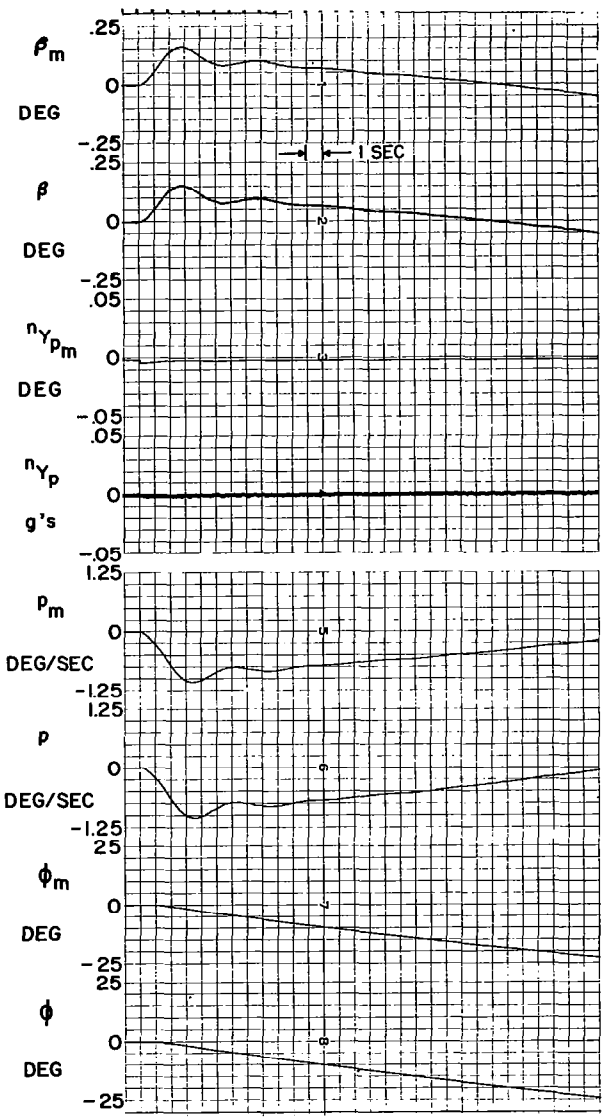

Figure 2-20 LATERAL-DIRECTIONAL MODEL FOLLOWING RESPONSE TO RUDDER INPUT, SST MODEL, THEORETICAL GAINS WITH β-LOOP

Flight Condition

.5H40

Control Input

$\delta_r = 0.5\ u(t)$ deg

$\frac{\delta_r}{e_\beta} = 10$ $\quad \frac{\delta_r}{e_{\dot{\beta}}} = 1.0$ sec $\quad \frac{\delta_a}{e_p} = 2.0$ sec $\quad \frac{\delta_a}{e_\phi} = 1.05$

All input gains equal 1.0.

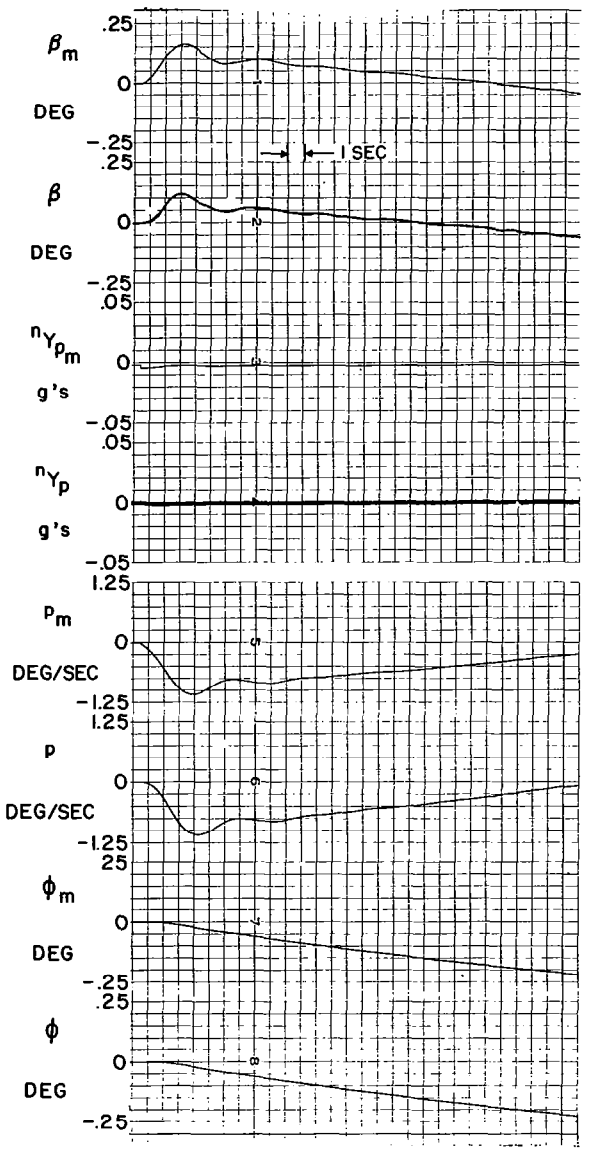

Figure 2-21 LATERAL-DIRECTIONAL MODEL FOLLOWING RESPONSE TO RUDDER INPUT, SST MODEL, LIMITED GAINS WITH β -LOOP

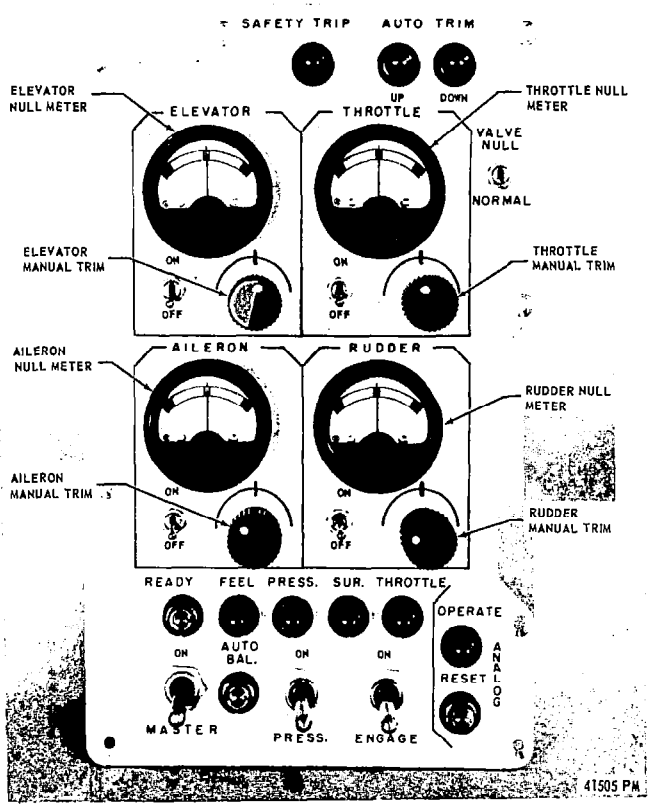

SIMULATION SERVO SYSTEM
ENGAGE PANEL

VARIABLE FEEL SYSTEM
ENGAGE PANEL

Figure 3-1 COCKPIT VARIABLE STABILITY CONTROL PANELS

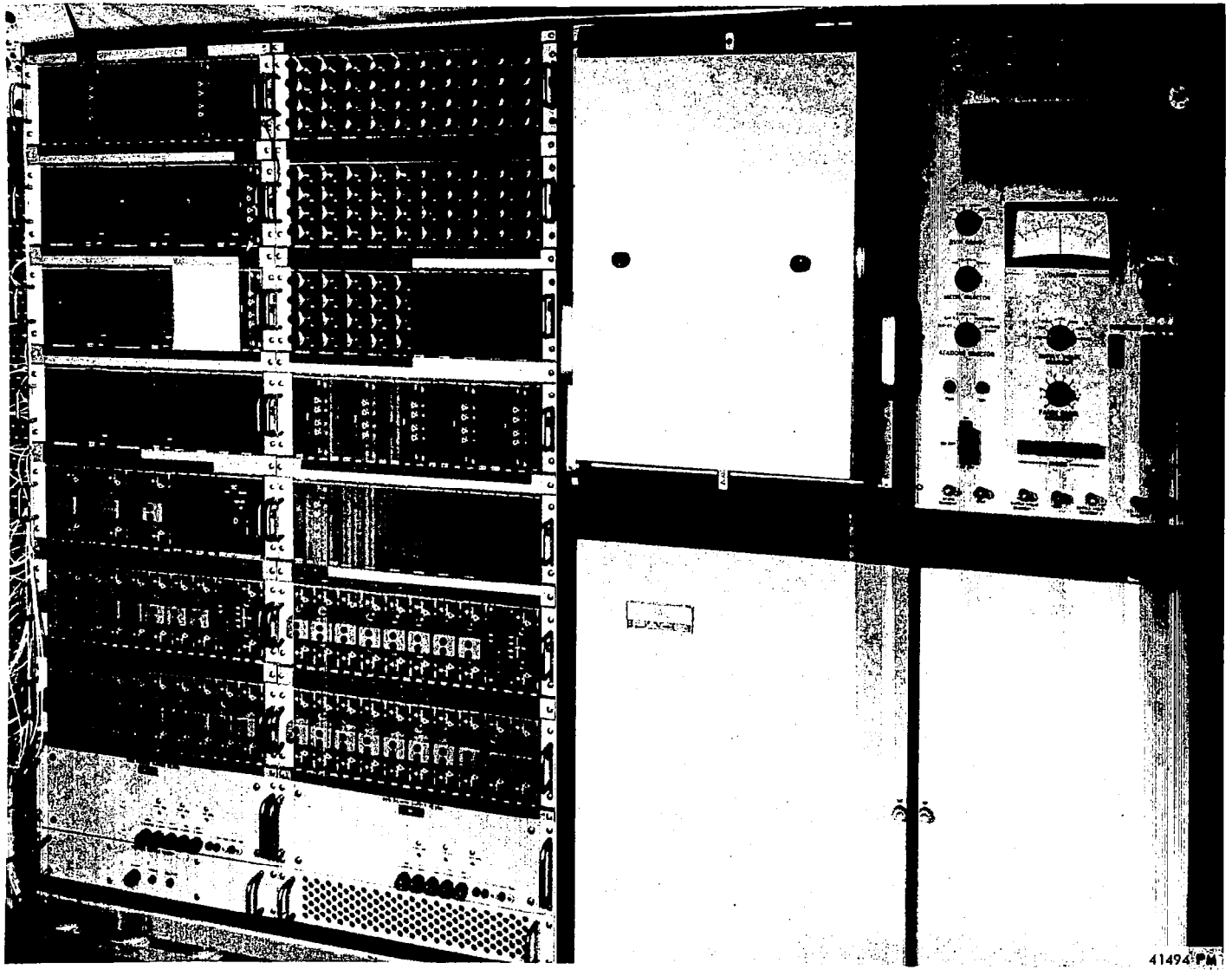

Figure 3-2 AIRBORNE COMPUTER

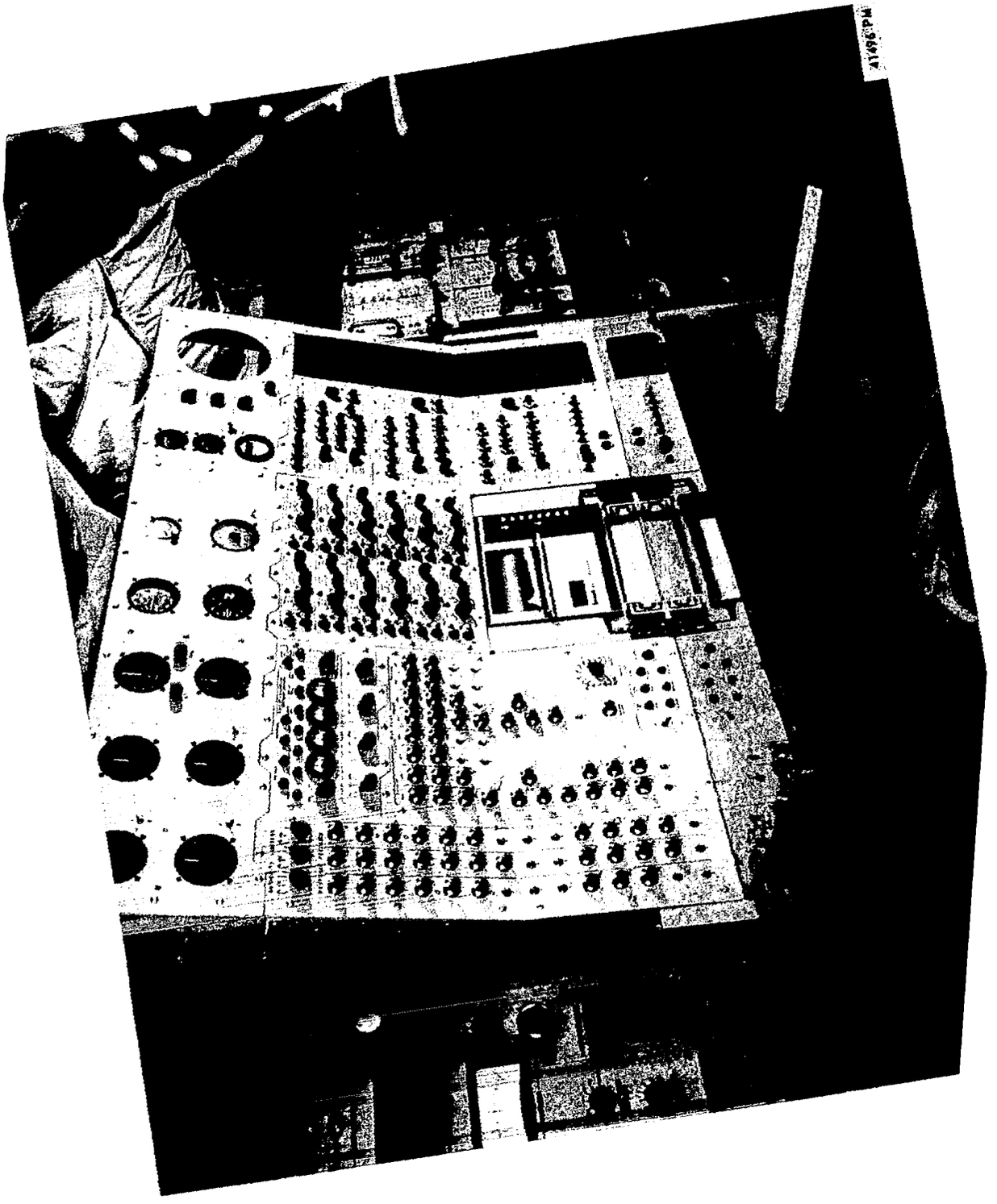

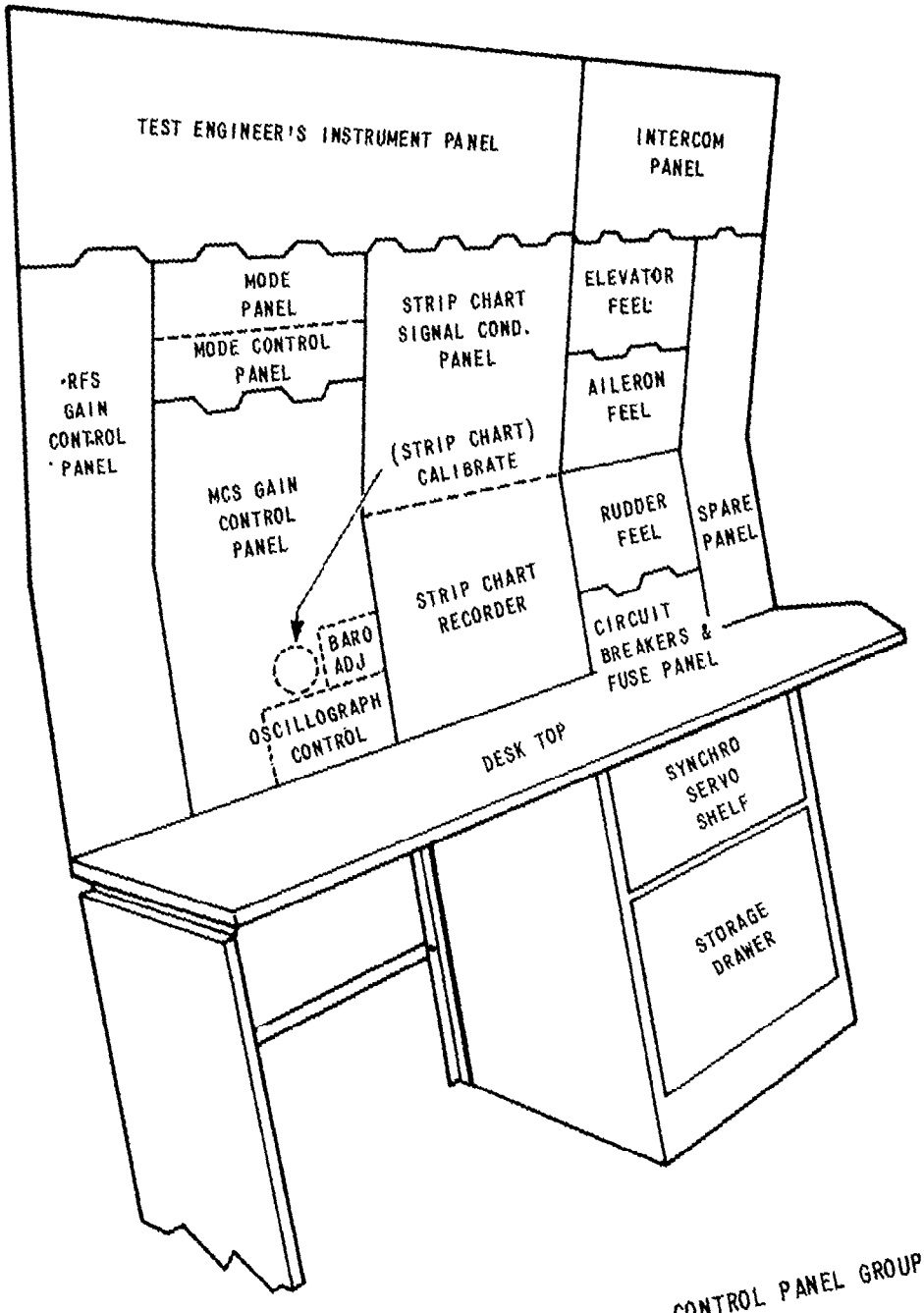

CONSOLE - CONTROL PANEL GROUPING

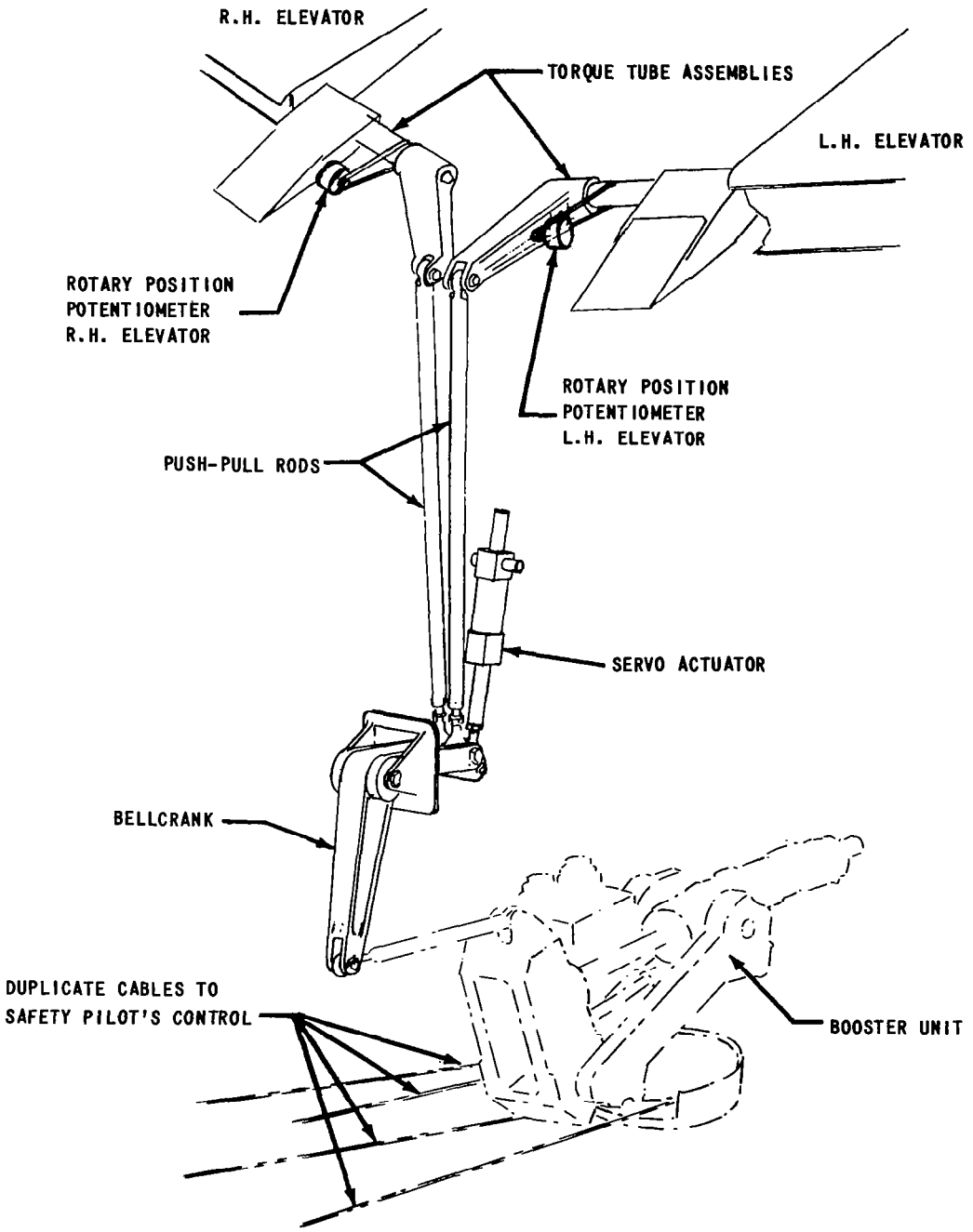

Figure 4-1 ELEVATOR POSITION SERVO SYSTEM

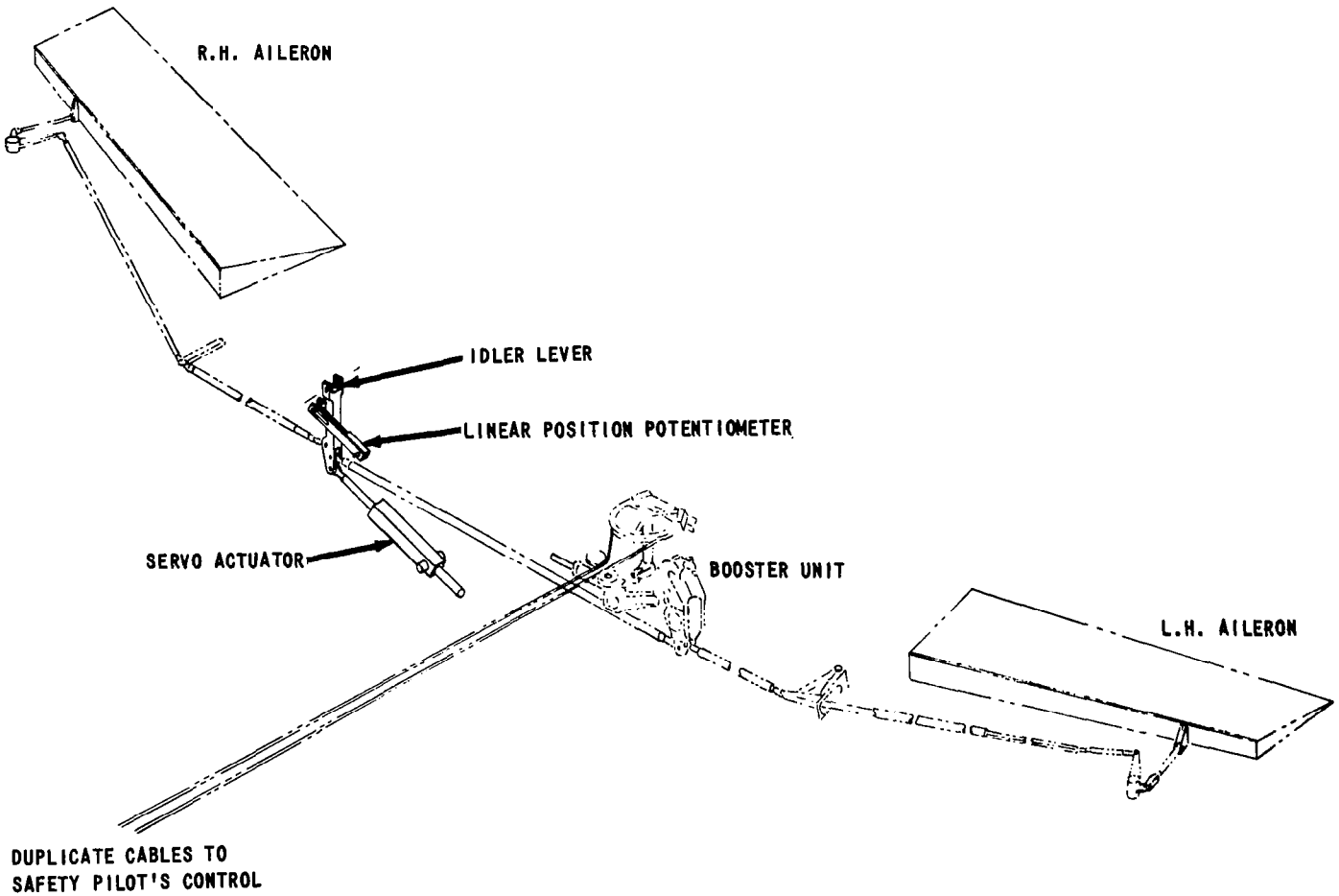

Figure 4-2 AILERON POSITION SERVO SYSTEM

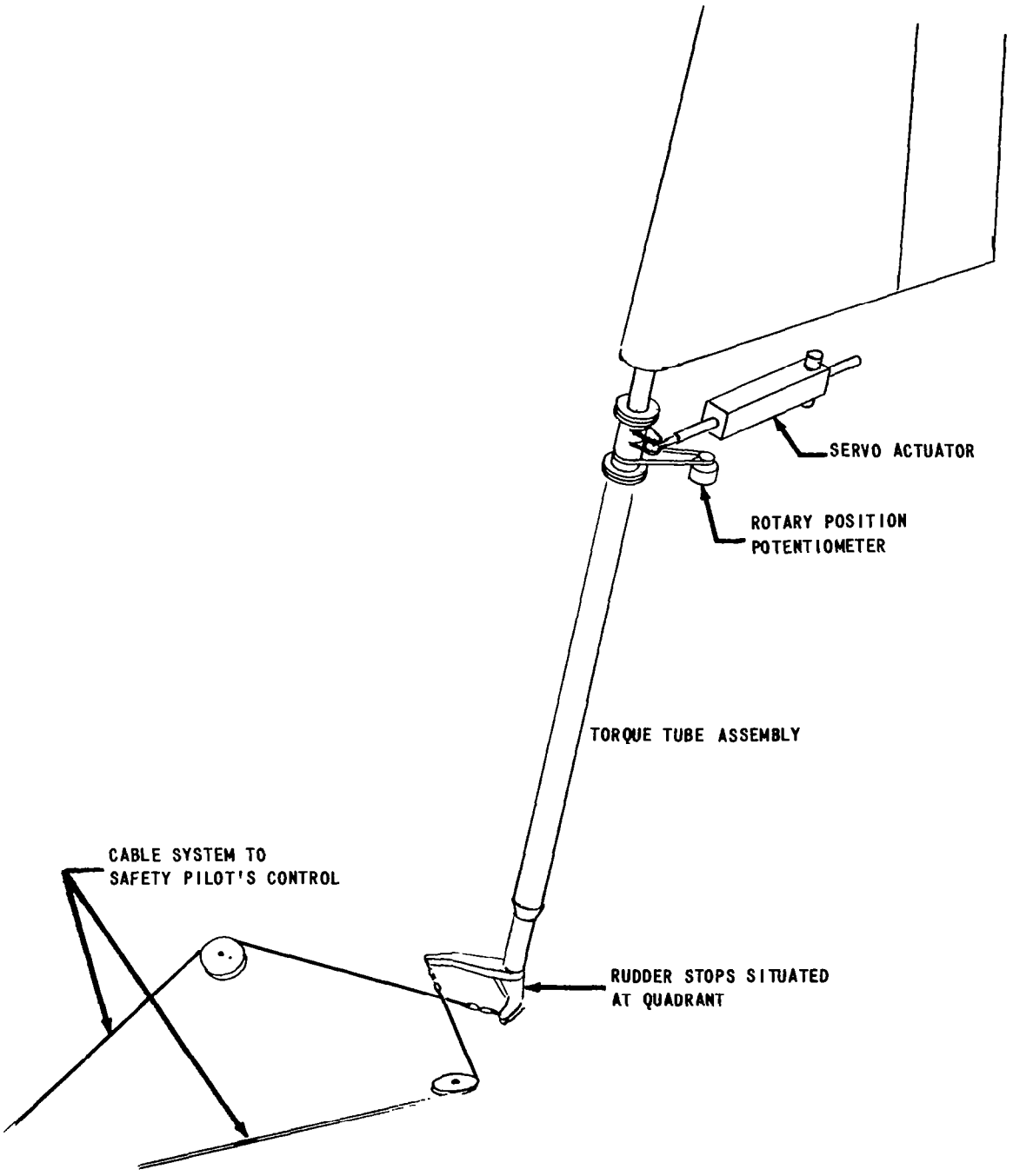

Figure 4-3 RUDDER POSITION SERVO SYSTEM

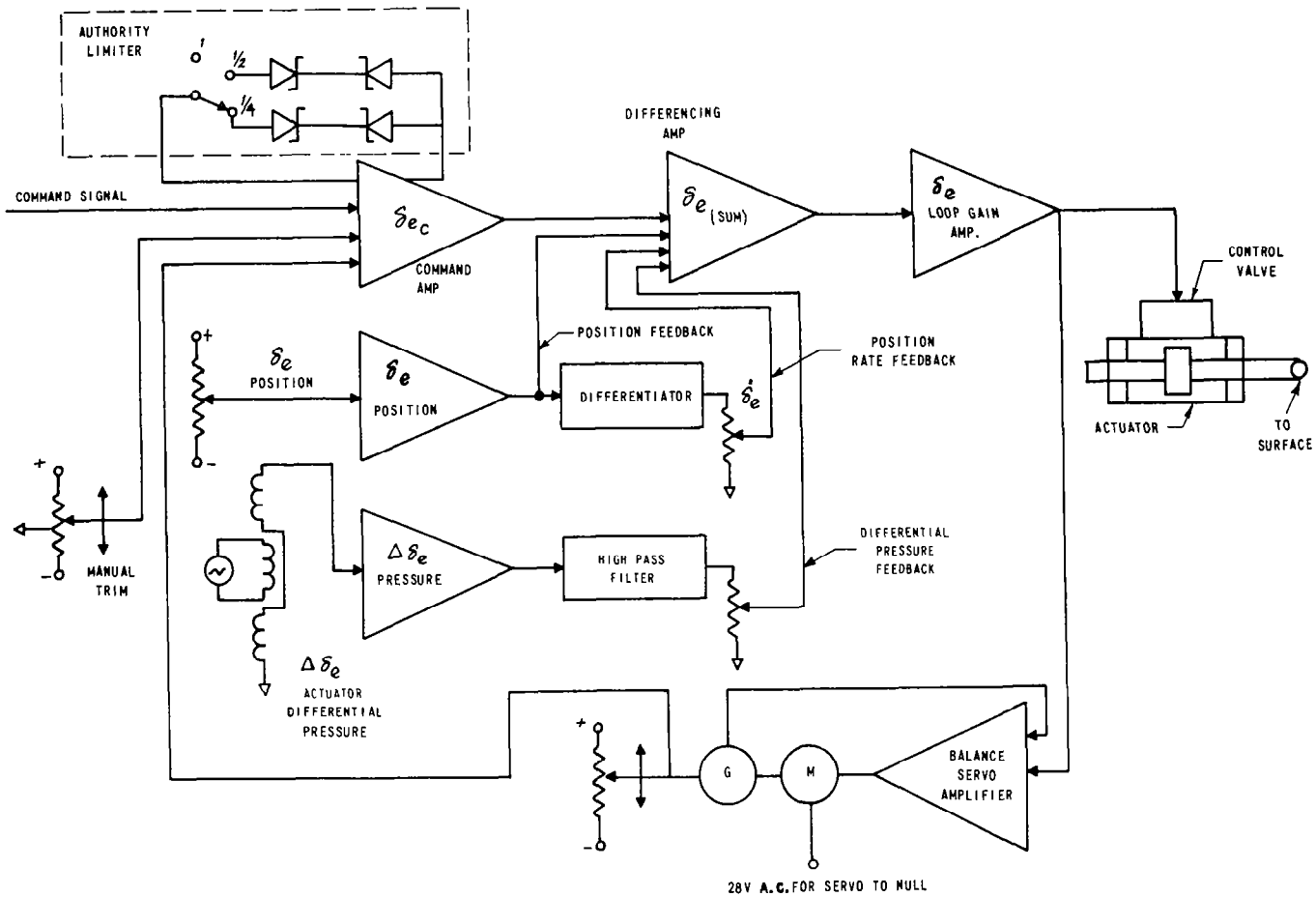

Figure 4-4 ELEVATOR POSITION SERVO BLOCK DIAGRAM

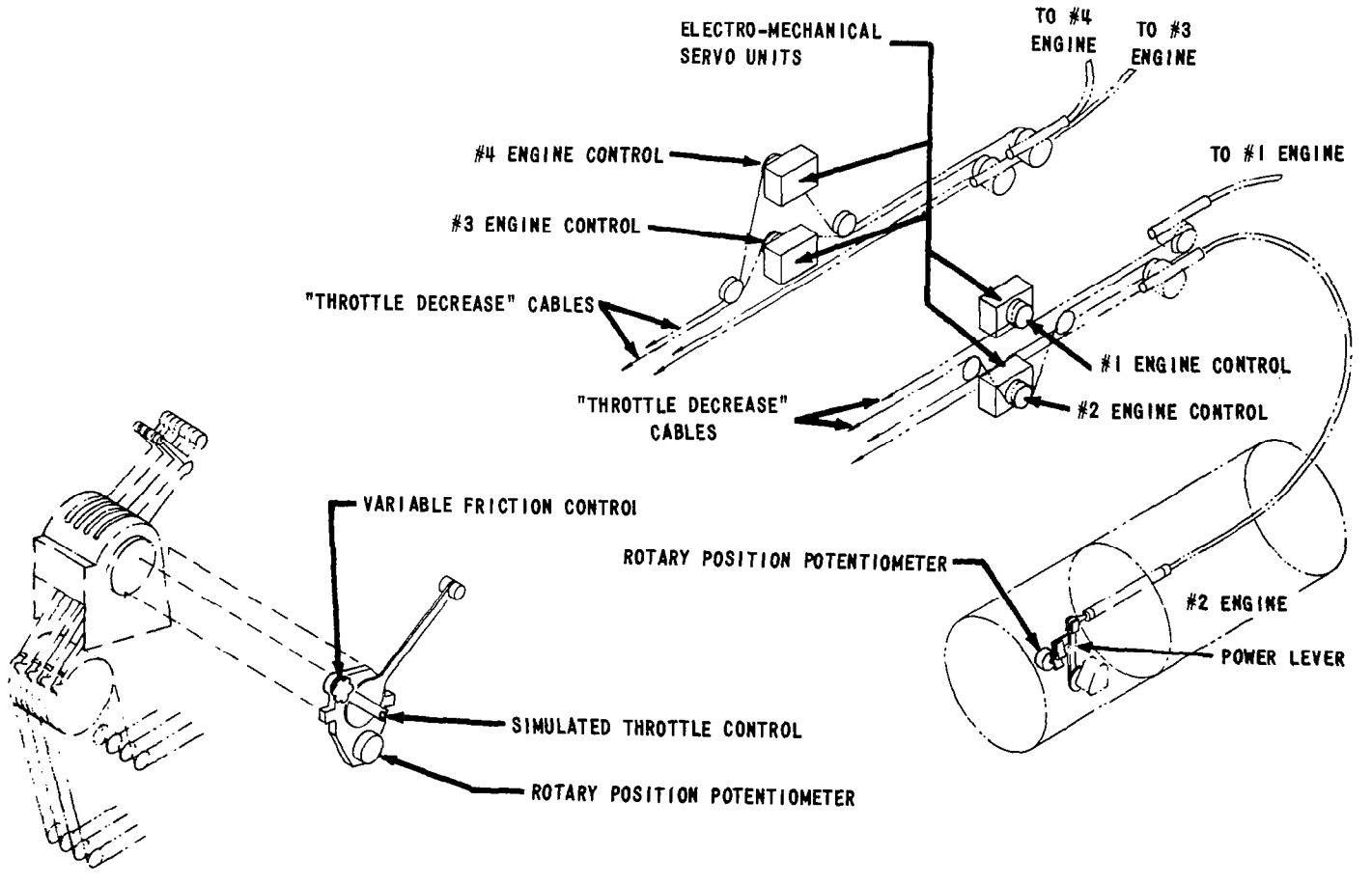

Figure 4-5 THROTTLE SERVO SYSTEM

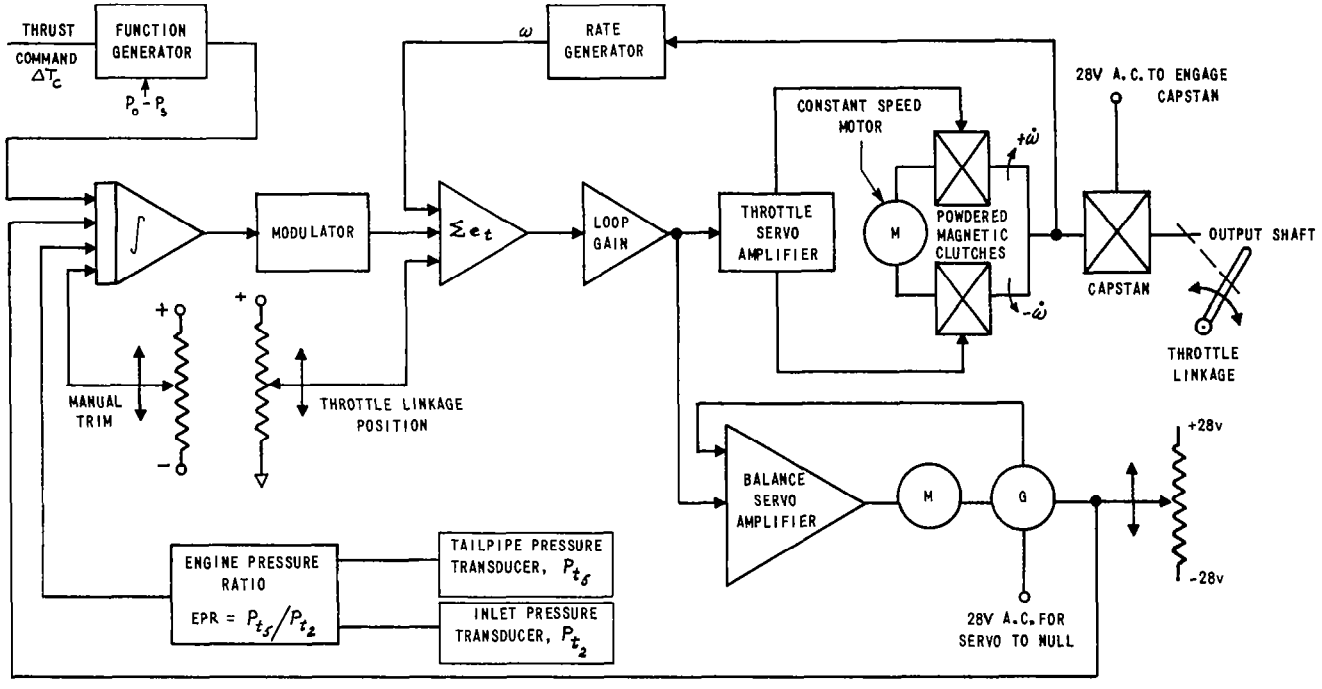

Figure 4-6 TYPICAL THROTTLE SERVO CONTROL LOOP

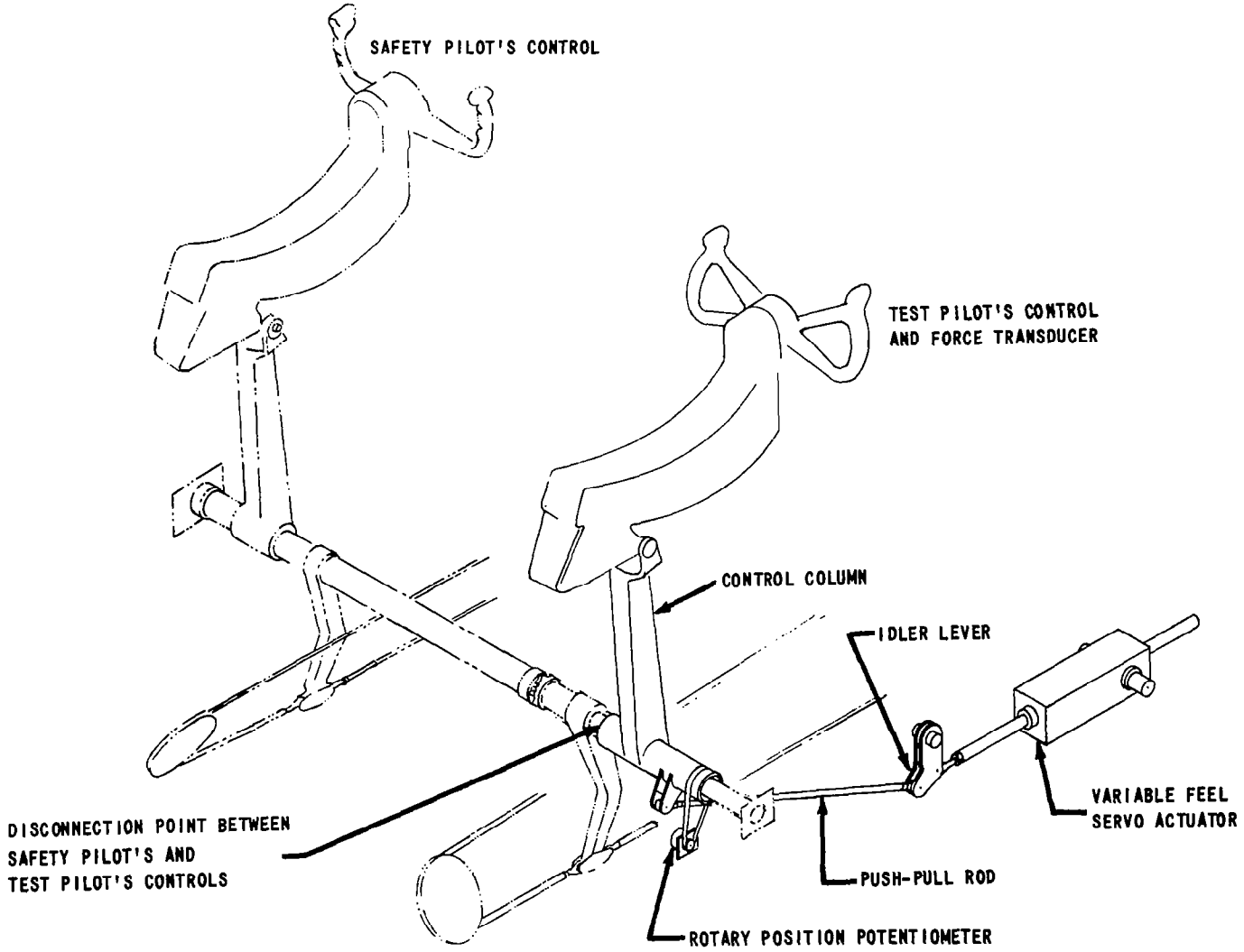

Figure 4-7 ELEVATOR FEEL SERVO SYSTEM

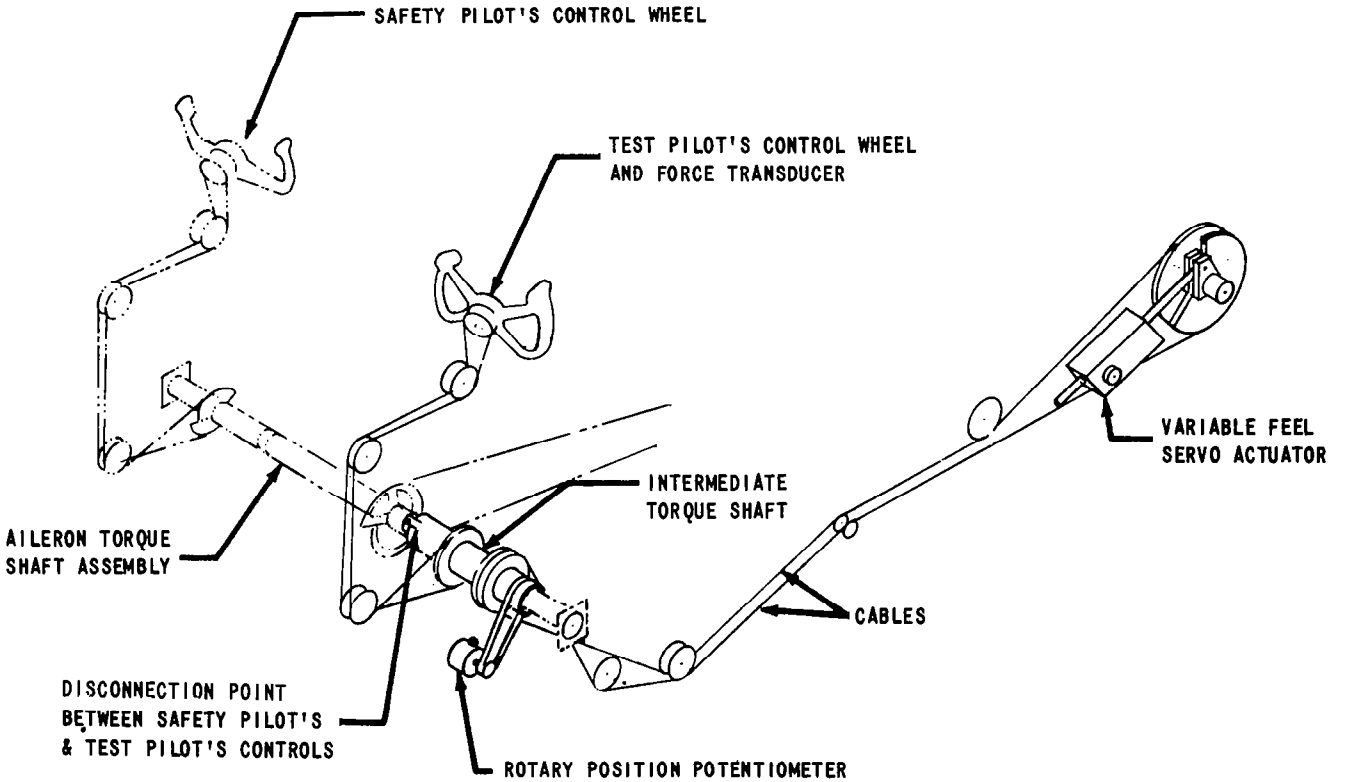

Figure 4-8 AILERON FEEL SERVO SYSTEM

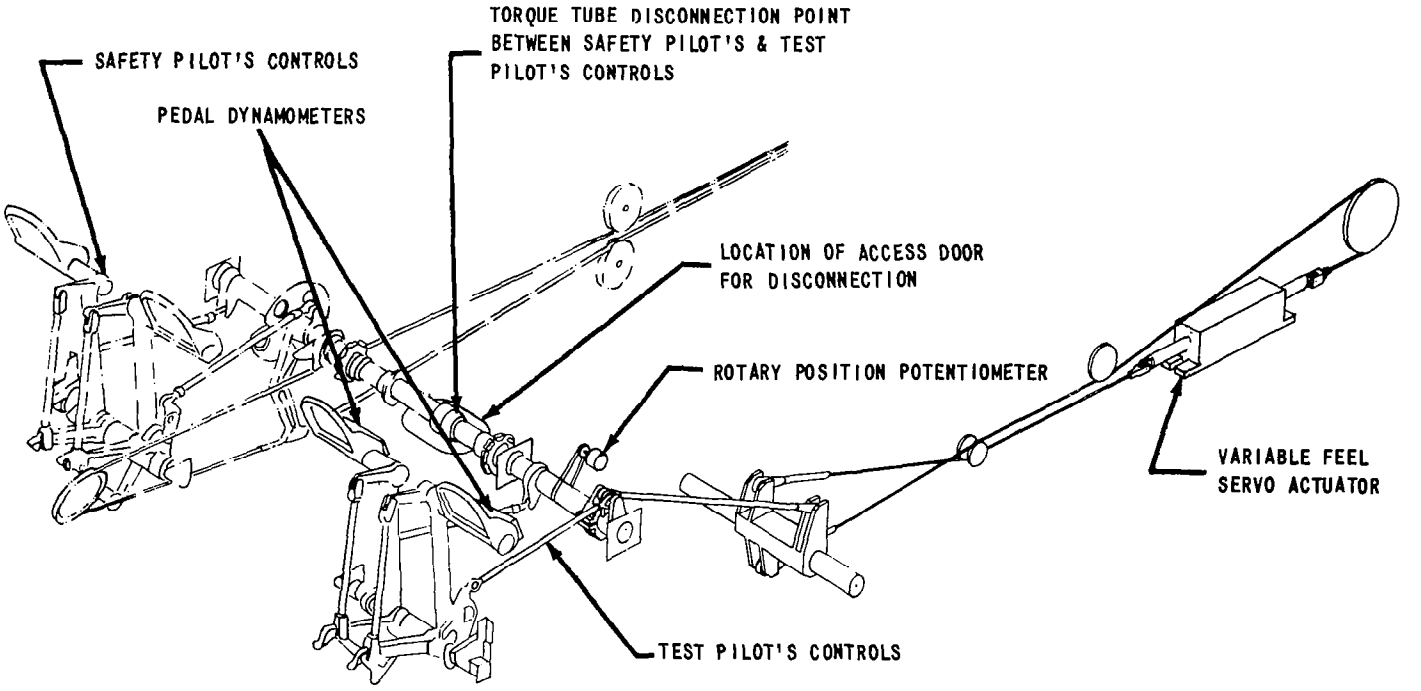

Figure 4-9 RUDDER FEEL SERVO SYSTEM

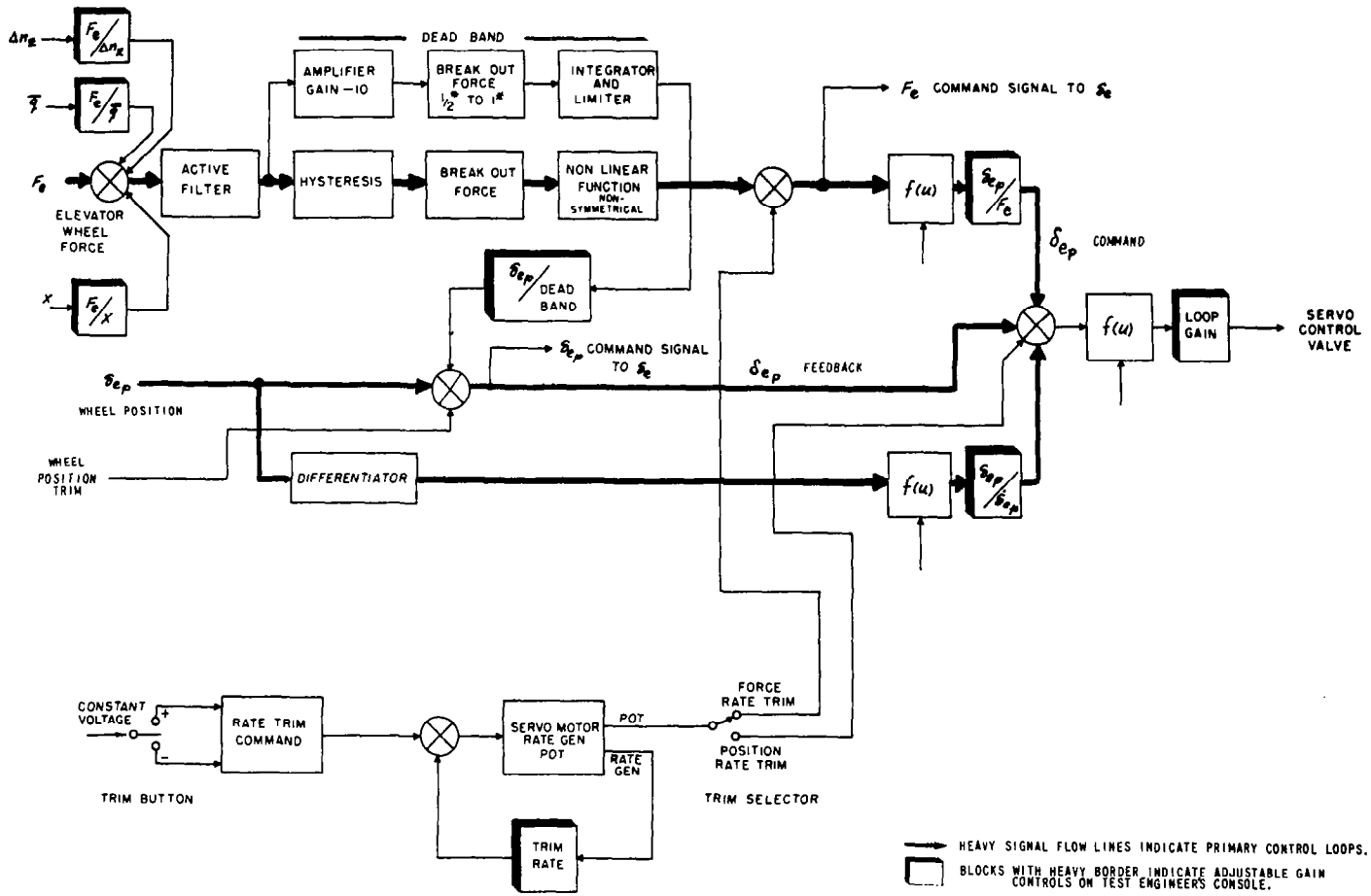

Figure 4-10 ELEVATOR FEEL SYSTEM FUNCTIONAL BLOCK DIAGRAM

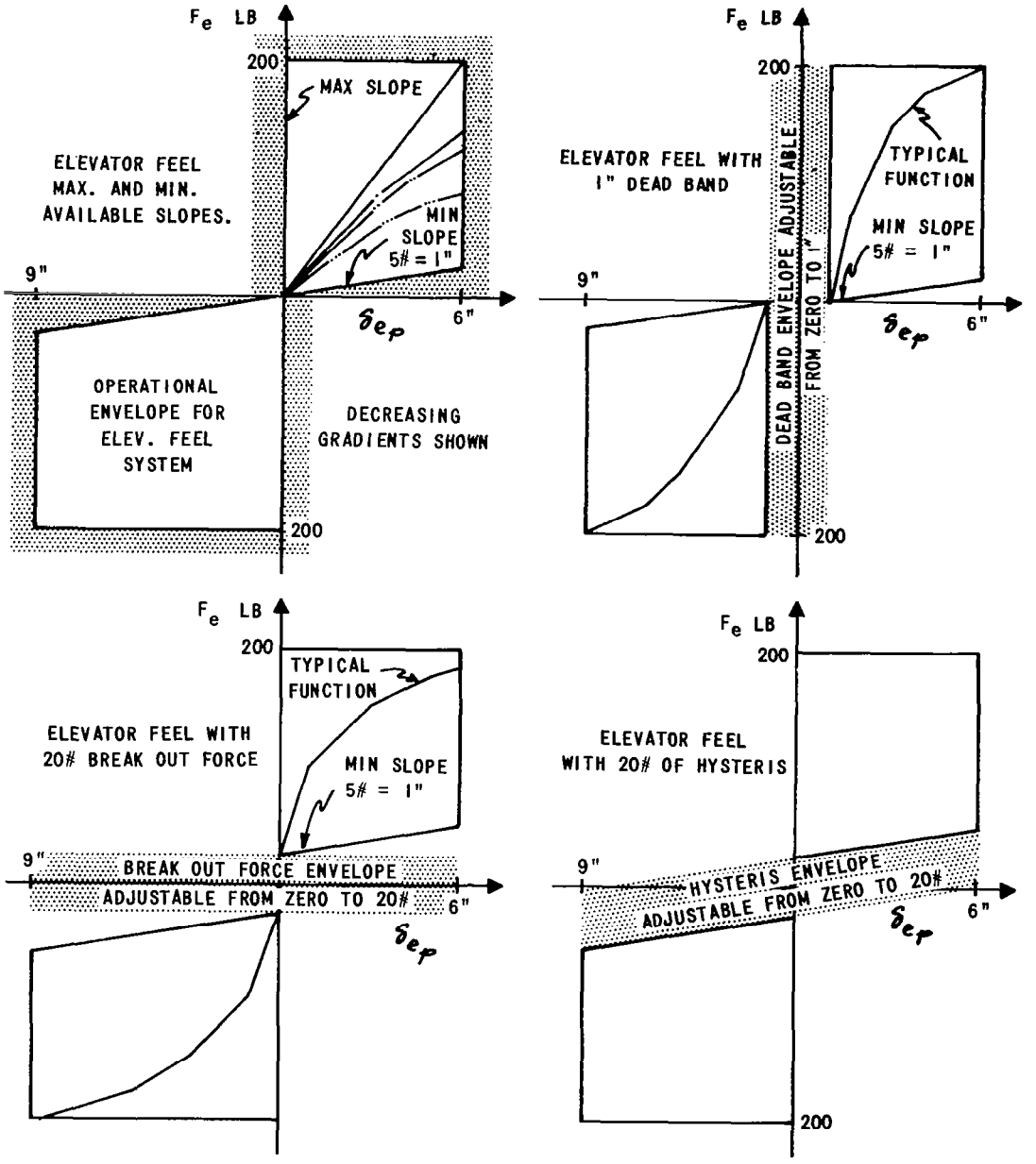

Figure 4-11 PERFORMANCE CAPABILITIES OF ELEVATOR FEEL

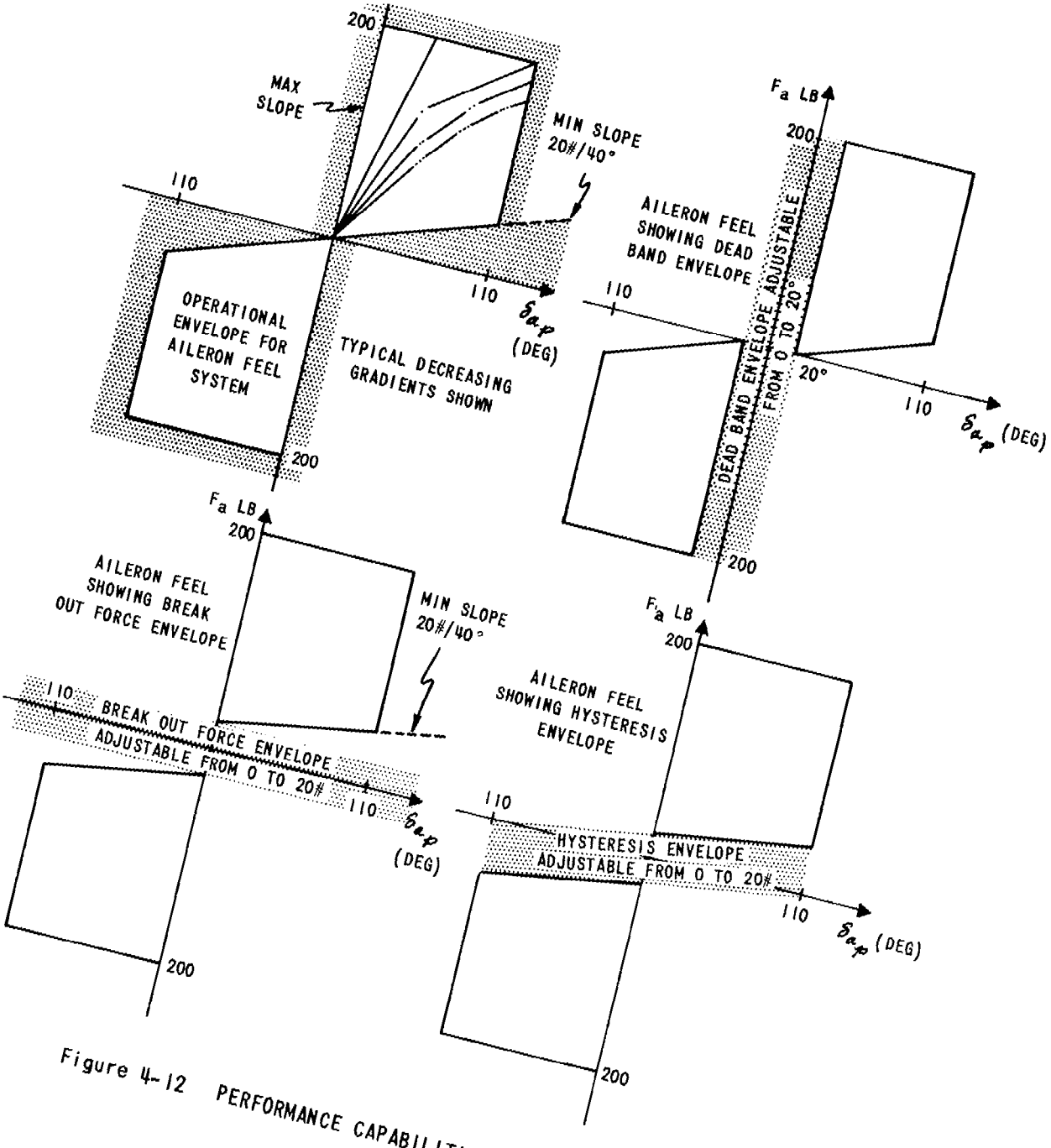

Figure 4-12 PERFORMANCE CAPABILITIES OF AILERON FEEL

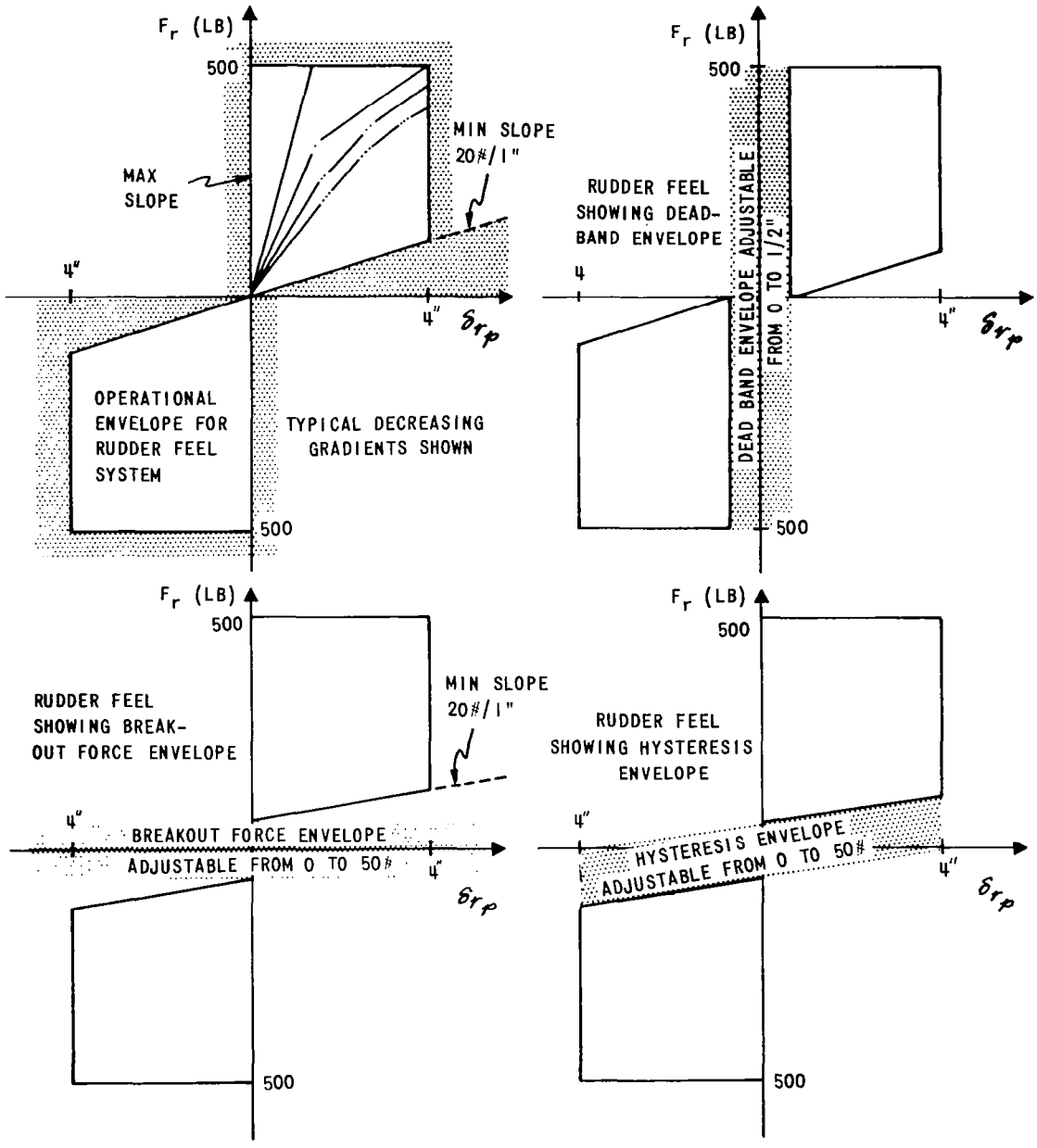

Figure 4-13 PERFORMANCE CAPABILITIES OF RUDDER FEEL

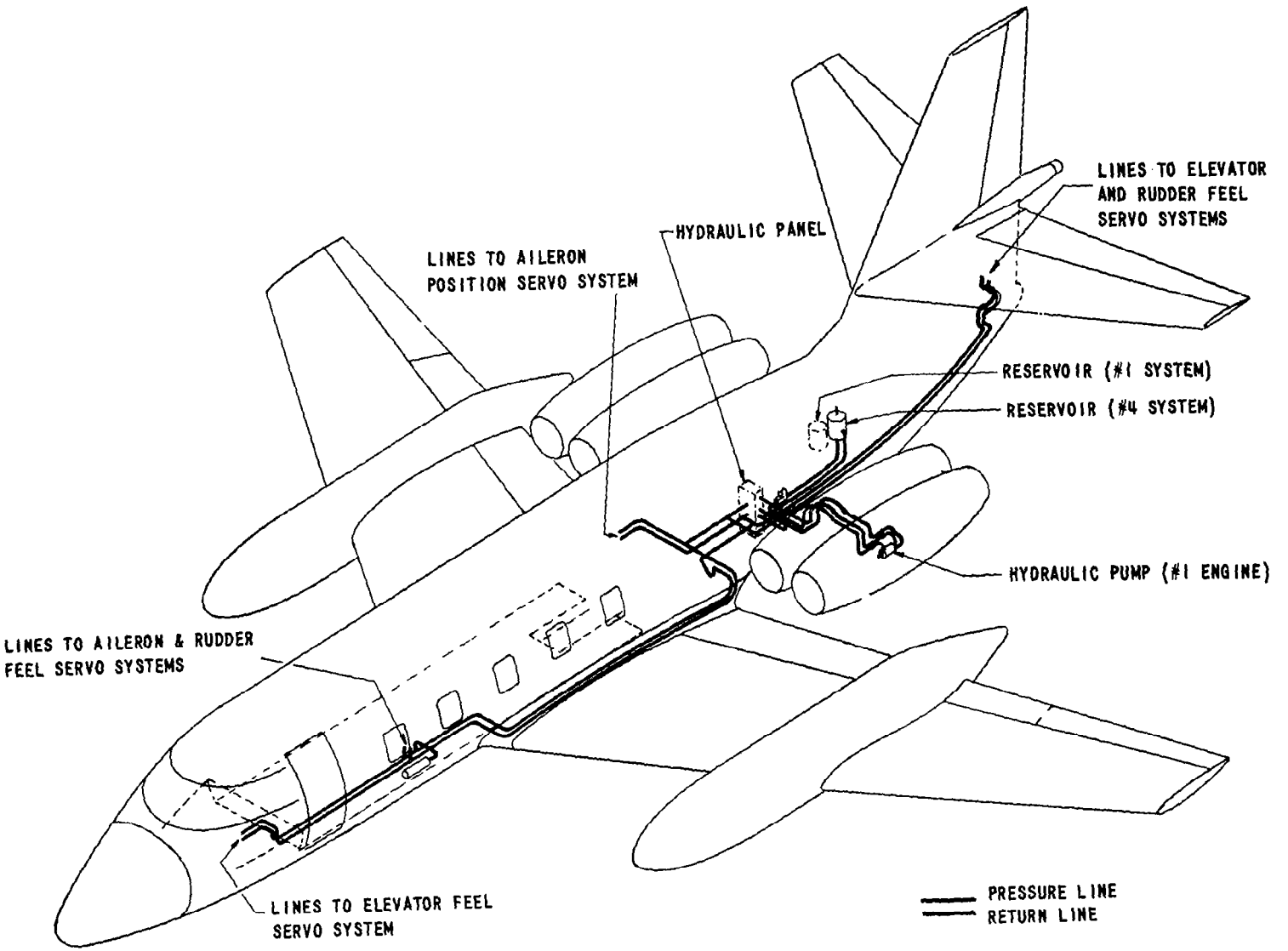

Figure 4-14 #4 HYDRAULIC SYSTEM MAIN SUPPLY LINES

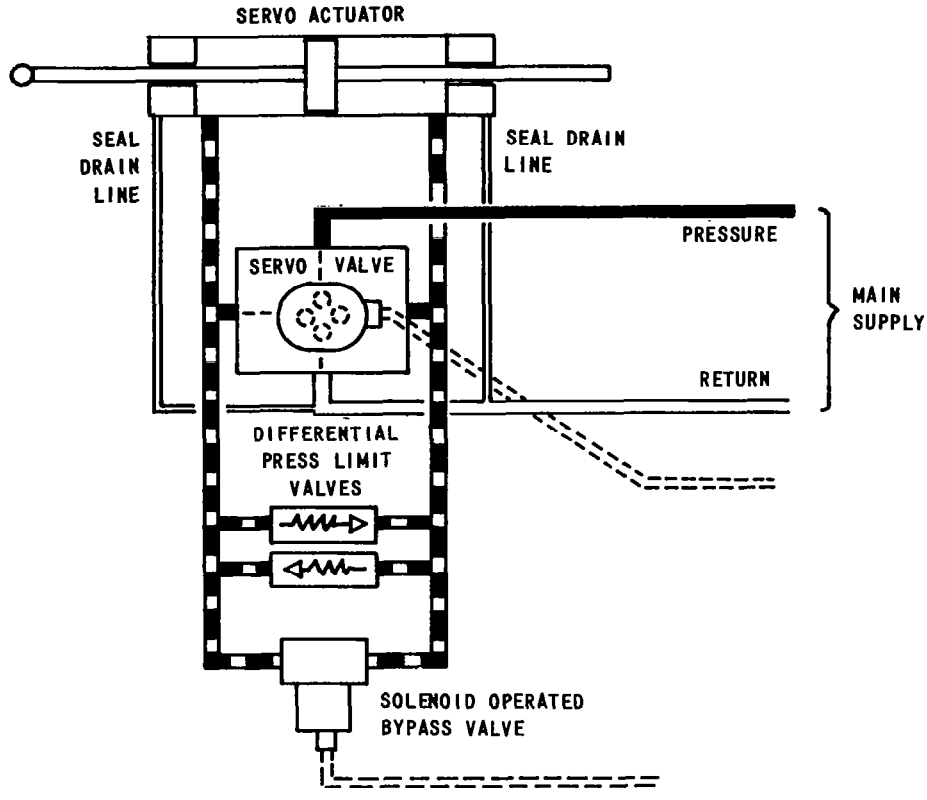

Figure 4-15 SCHEMATIC DRAWING OF TYPICAL FEEL SERVO HYDRAULIC SYSTEM

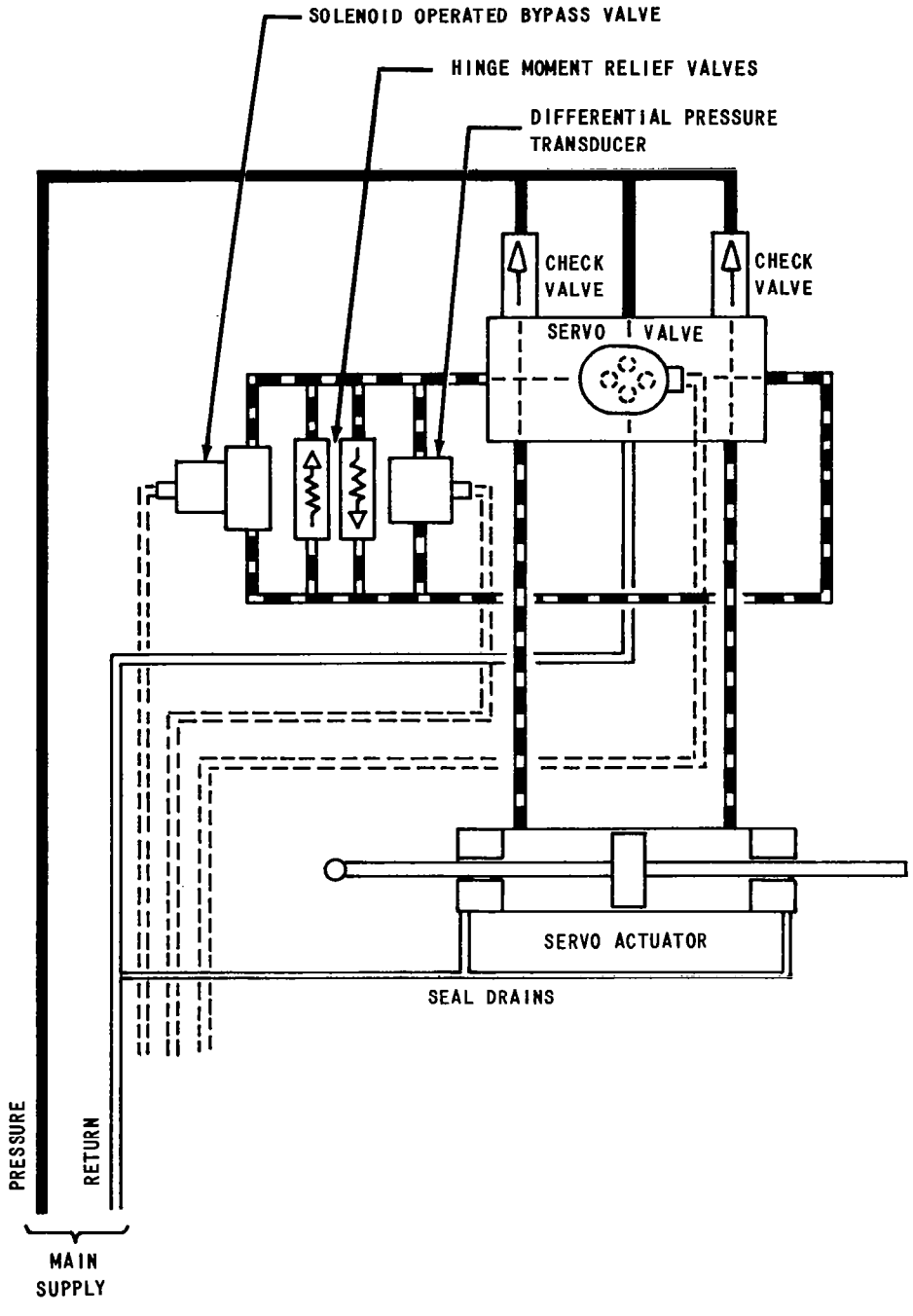

Figure 4-16 SCHEMATIC DRAWING OF TYPICAL SURFACE POSITION SERVO HYDRAULIC SYSTEM

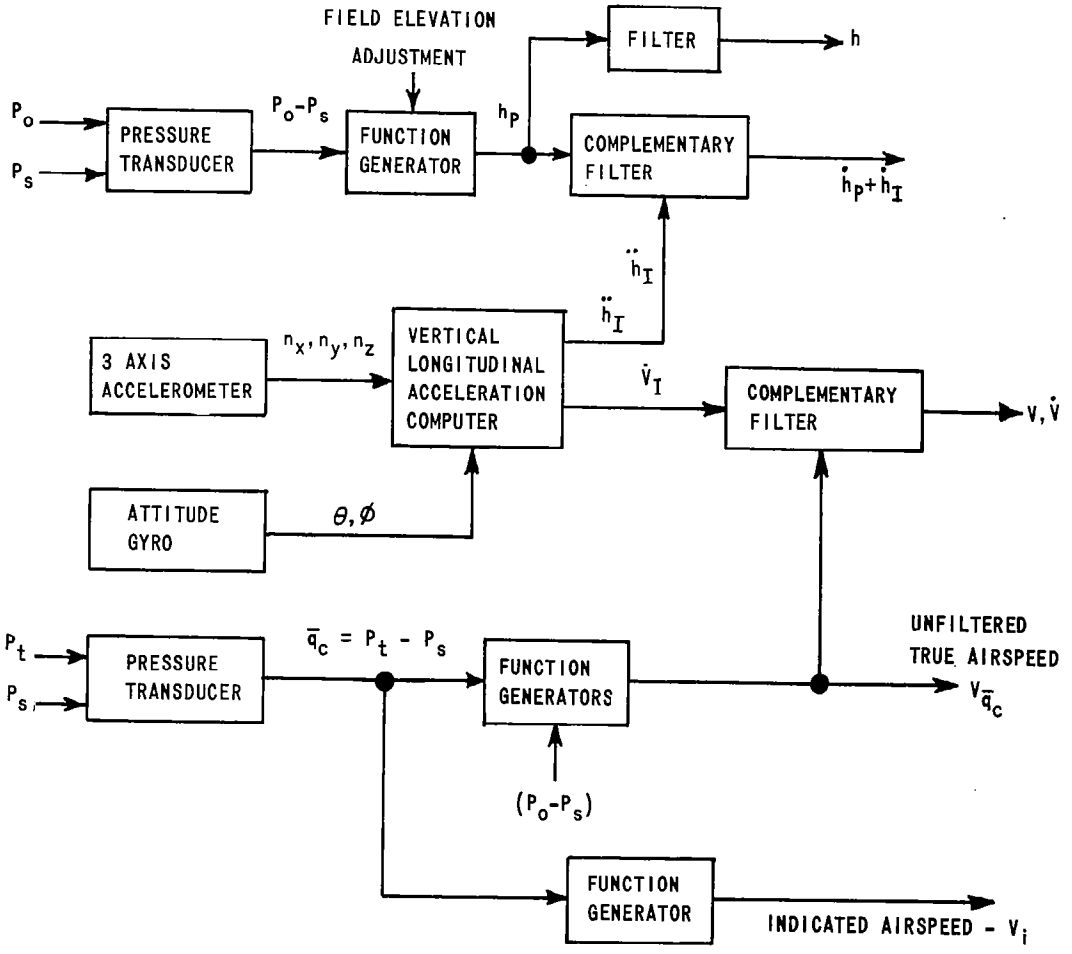

Figure 4-17 SIMPLIFIED BLOCK DIAGRAM OF AIR DATA SYSTEM

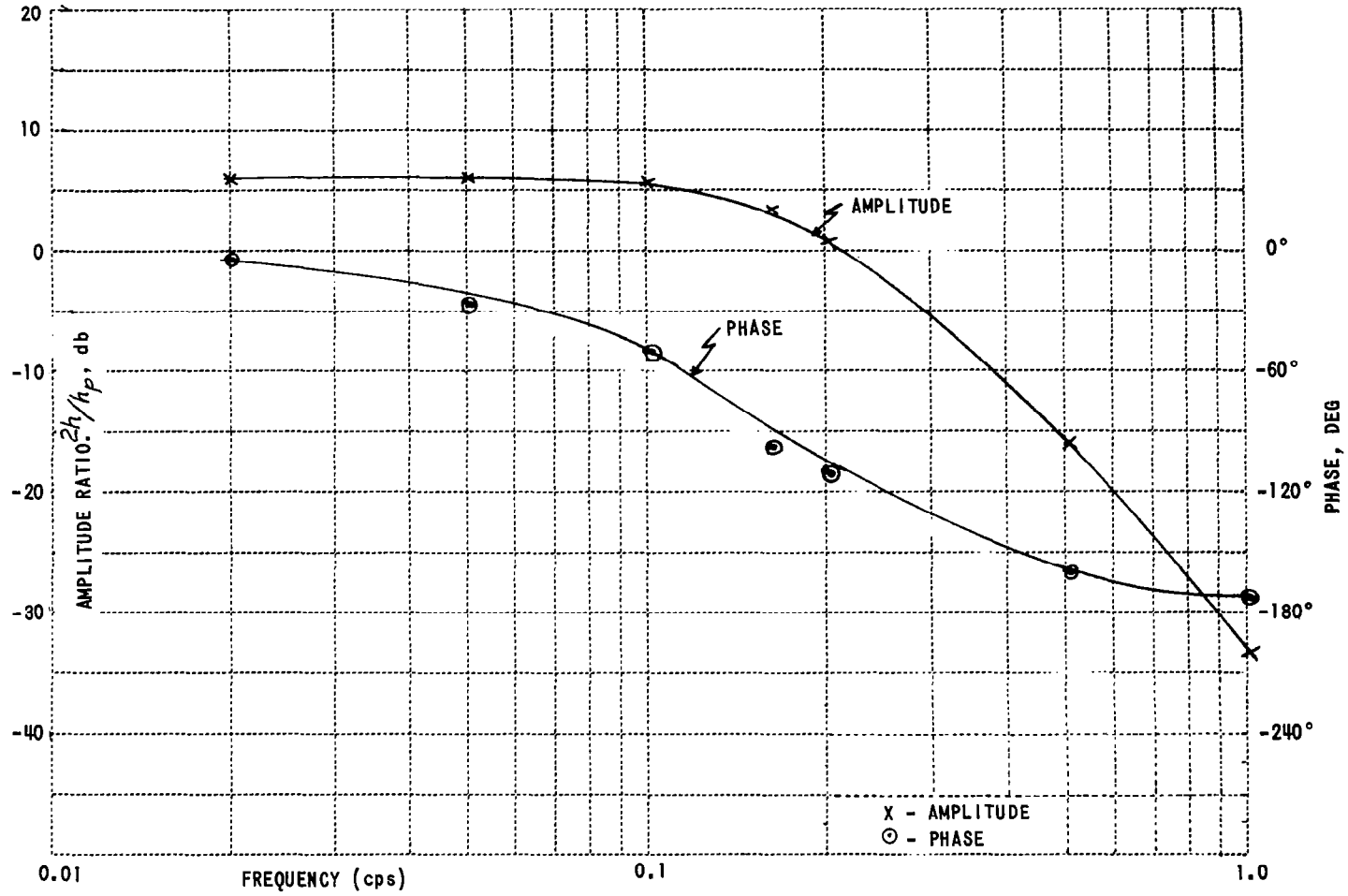

Figure 4-18 FREQUENCY RESPONSE OF PRESSURE ALTITUDE FILTER

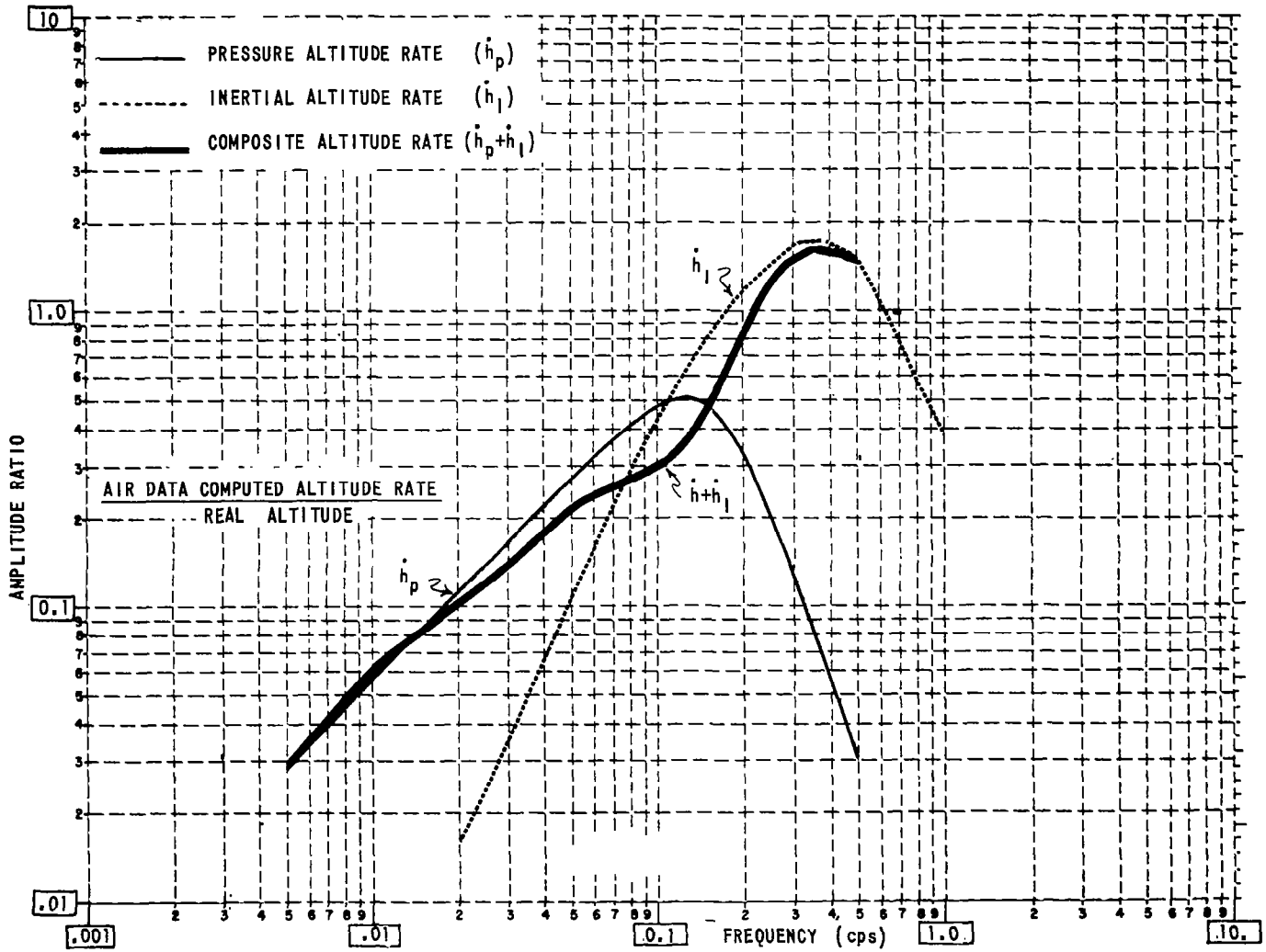

Figure 4-19 MAGNITUDE VS. FREQUENCY OF COMPOSITE RATE OF CLIMB

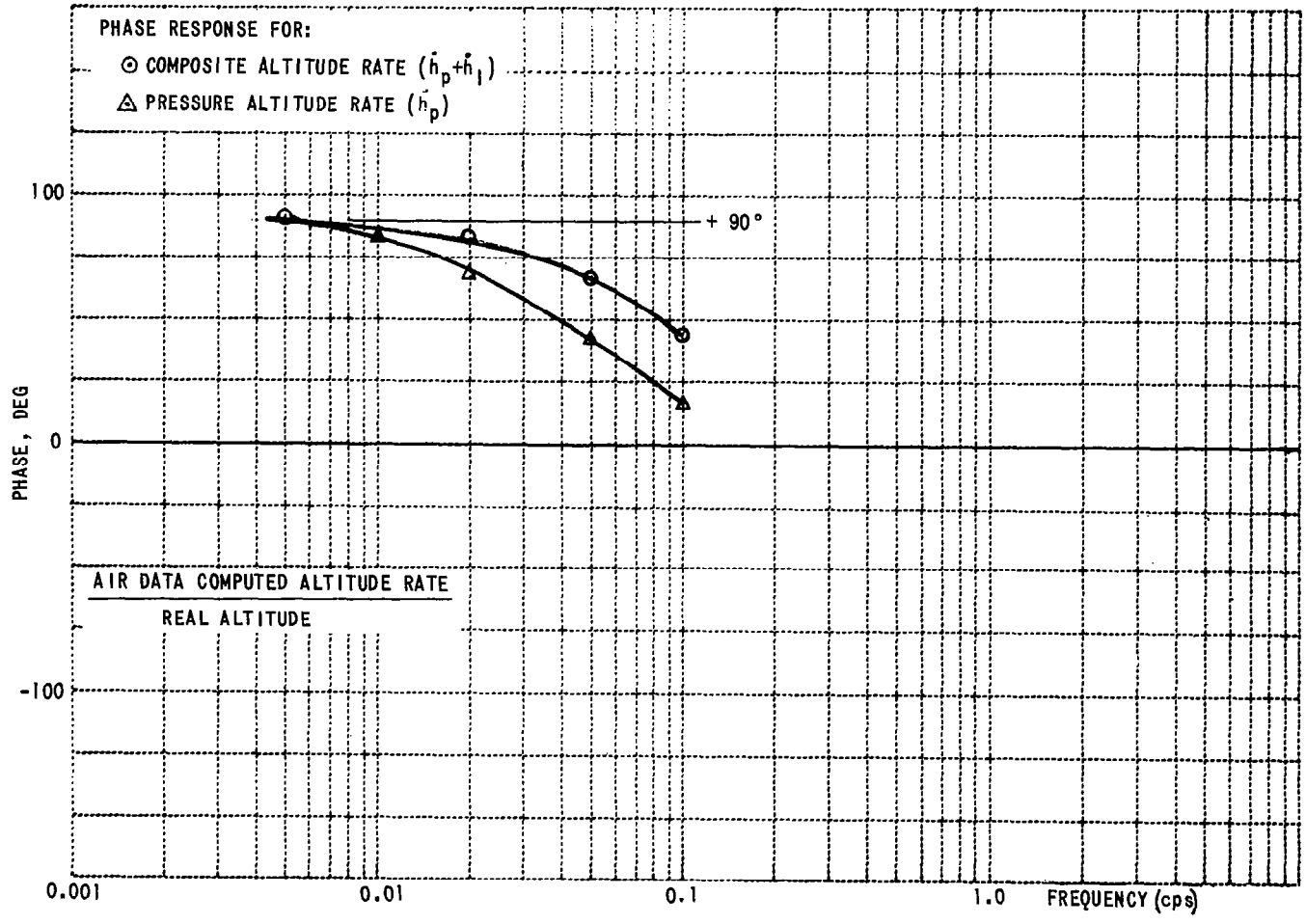

Figure 4-20 PHASE VS. FREQUENCY OF COMPOSITE RATE OF CLIMB

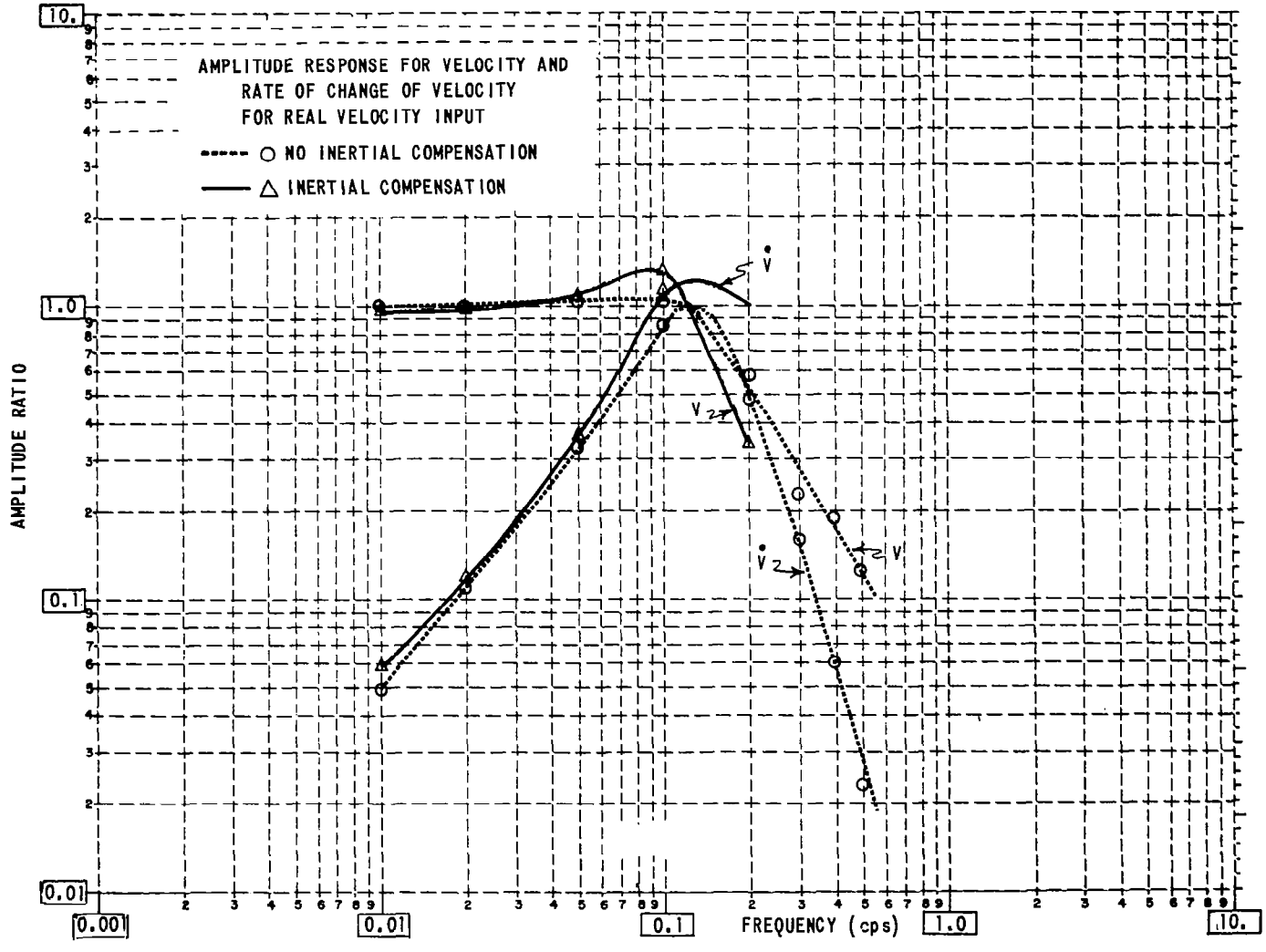

Figure 4-21 MAGNITUDE VS. FREQUENCY OF VELOCITY AND VELOCITY RATE, WITH AND WITHOUT INERTIAL COMPENSATION

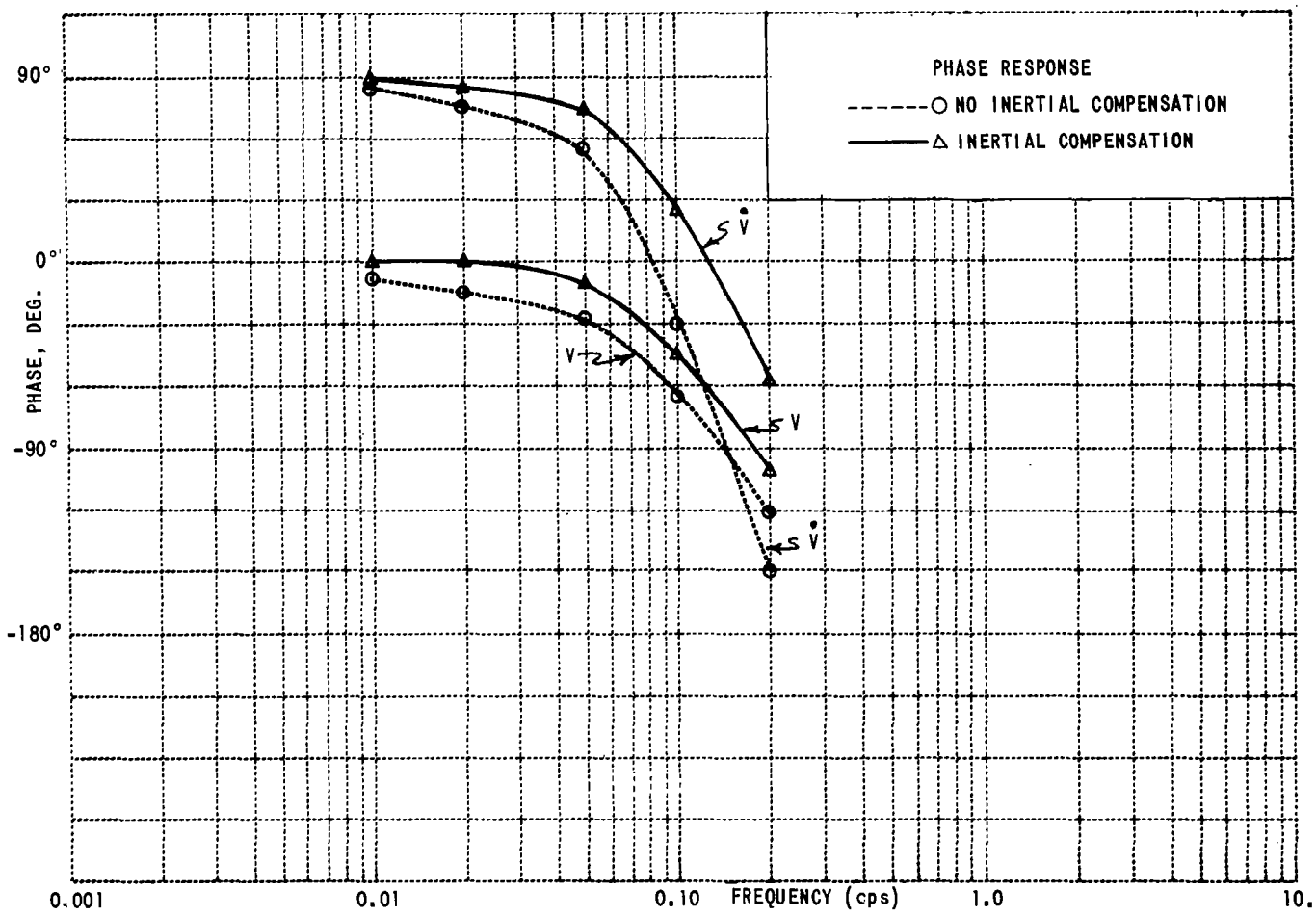

Figure 4-22 PHASE VS. FREQUENCY OF VELOCITY AND VELOCITY RATE, WITH AND WITHOUT INERTIAL COMPENSATION

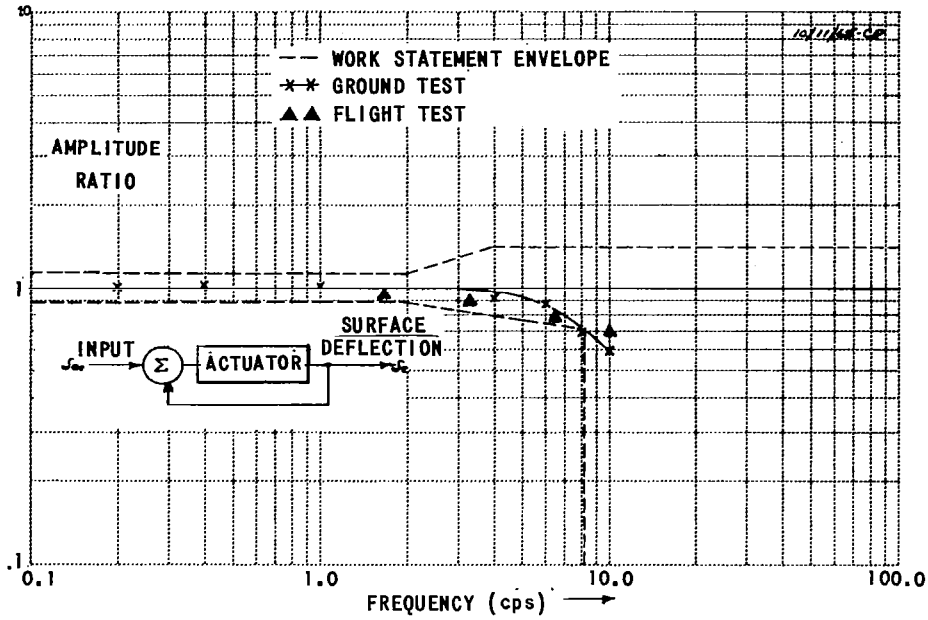

ELEVATOR MAGNITUDE VS. FREQUENCY

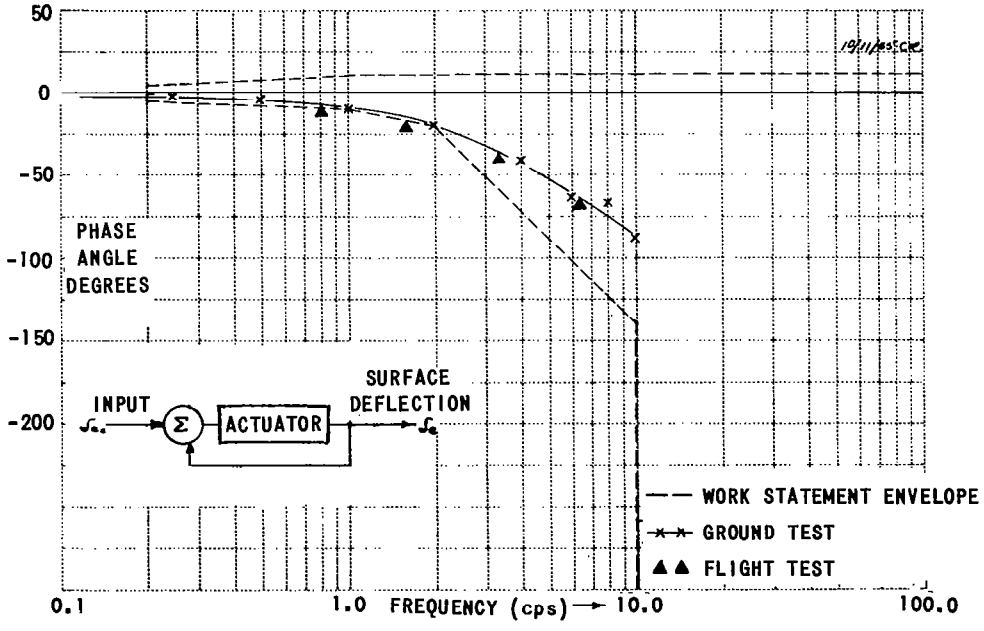

ELEVATOR PHASE VS. FREQUENCY

Figure 5-1 FREQUENCY RESPONSE OF ELEVATOR SIMULATION SERVO SYSTEM

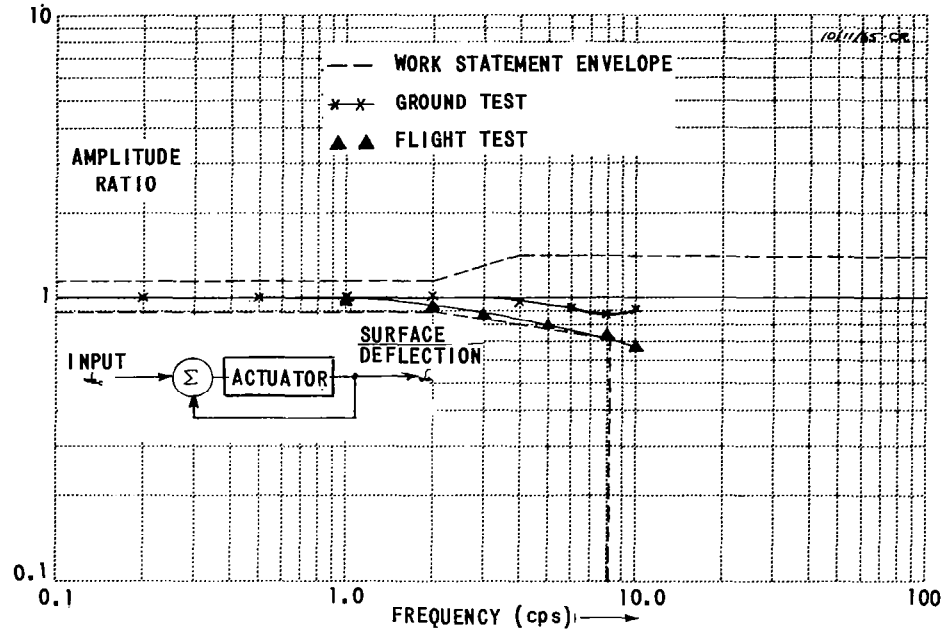

AILERON MAGNITUDE VS. FREQUENCY

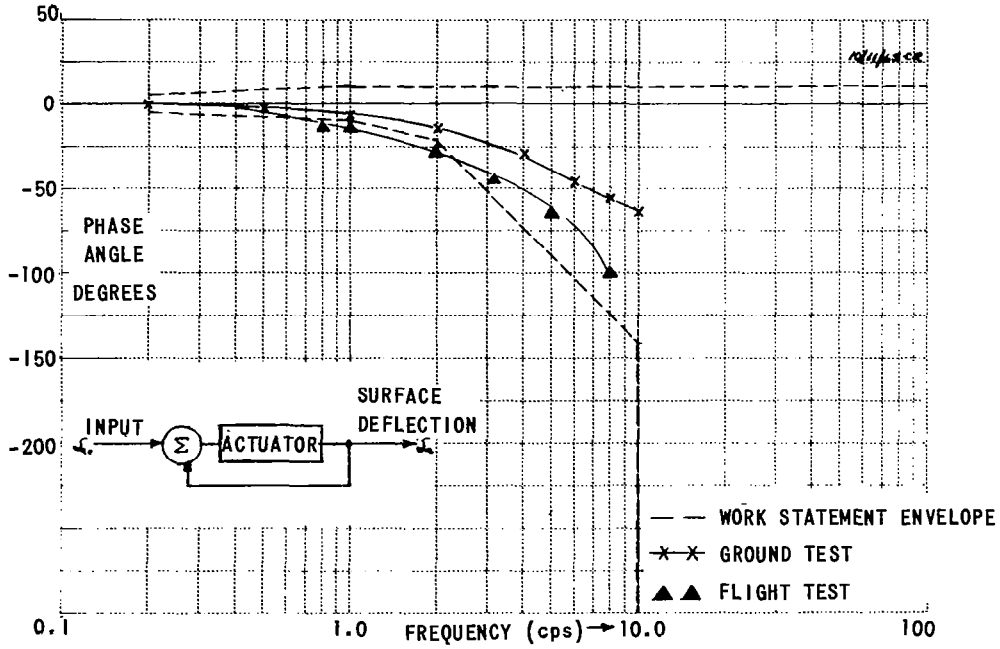

AILERON PHASE VS. FREQUENCY

Figure 5-2 FREQUENCY RESPONSE OF AILERON SIMULATION SERVO SYSTEM

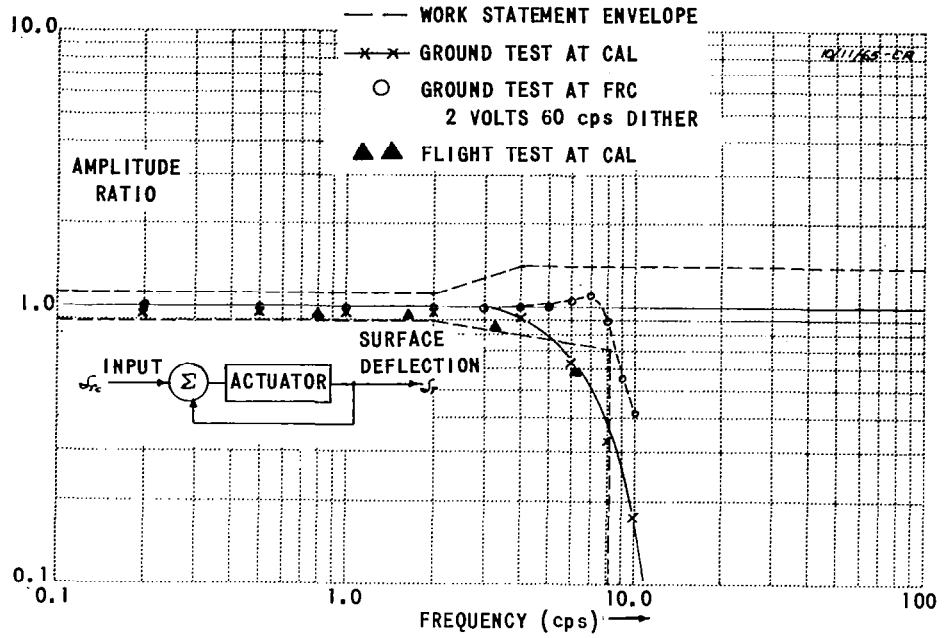

RUDDER MAGNITUDE VS. FREQUENCY

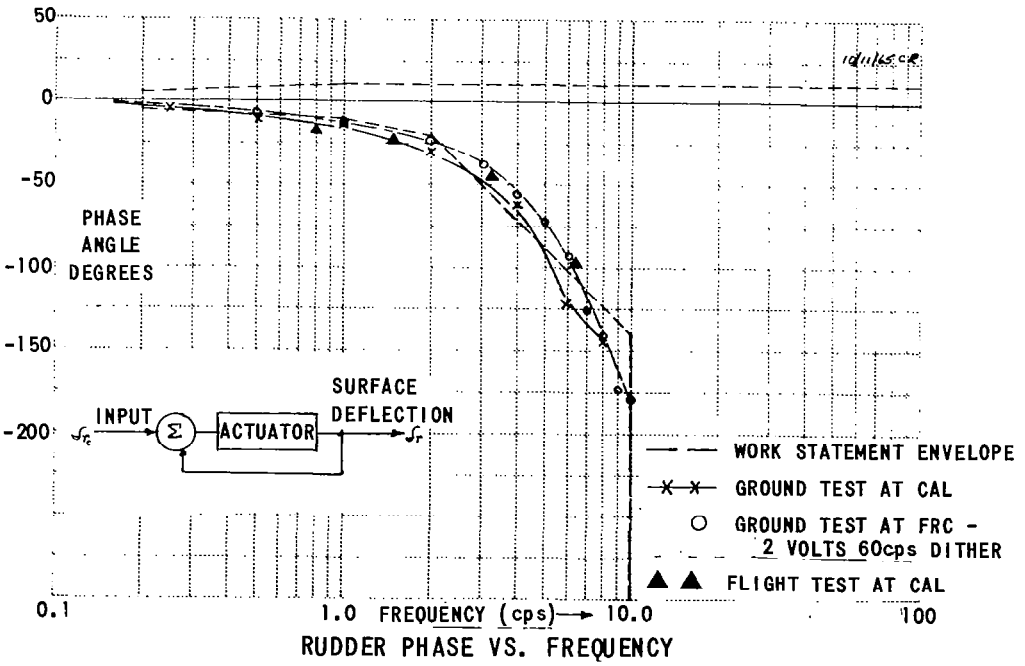

RUDDER PHASE VS. FREQUENCY

Figure 5-3 FREQUENCY RESPONSE OF RUDDER SIMULATION SERVO SYSTEM

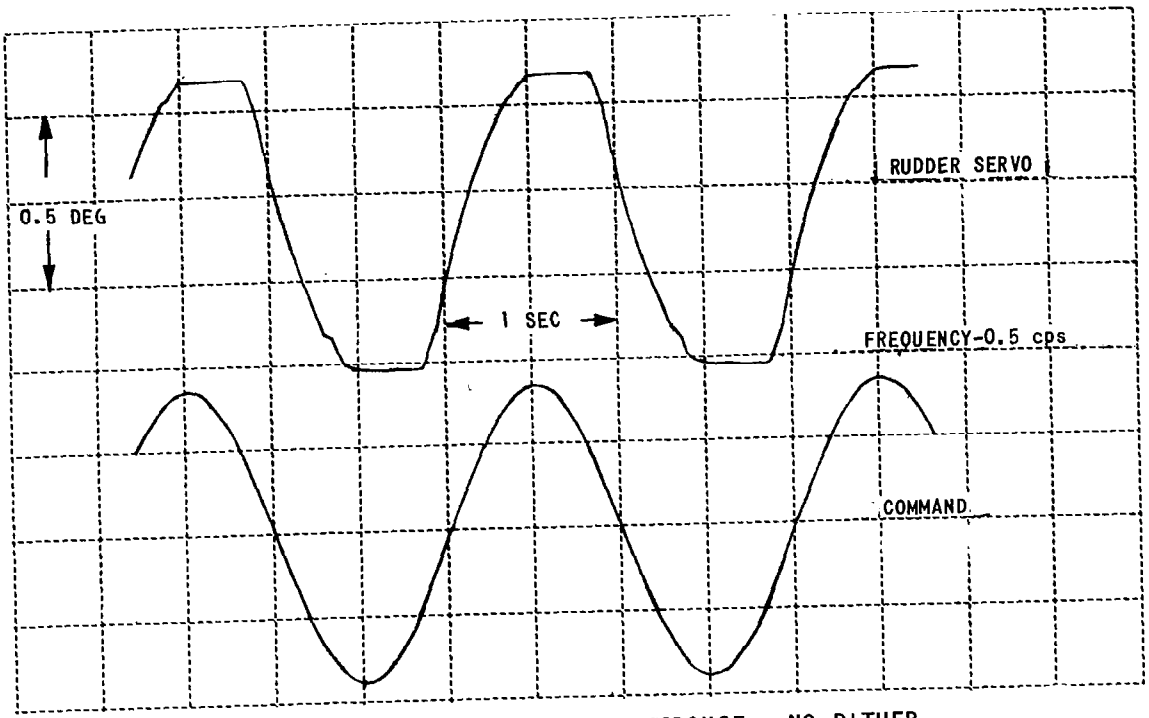

Figure 5-4 RUDDER SERVO RESPONSE - NO DITHER

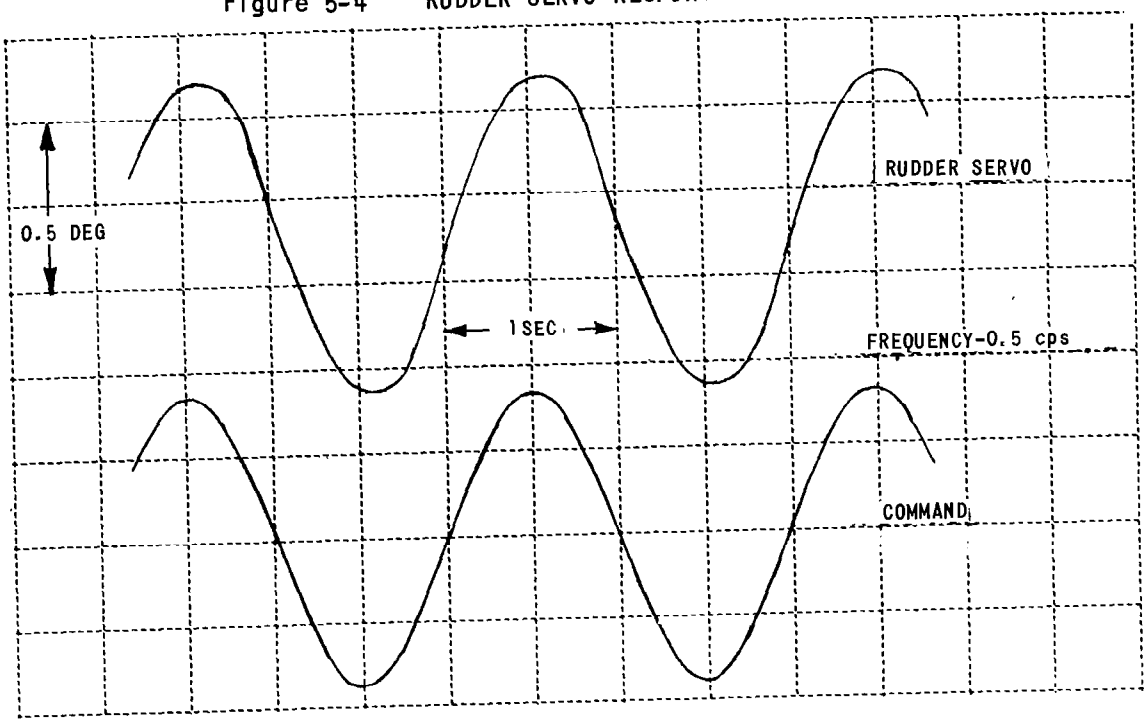

Figure 5-5 RUDDER SERVO RESPONSE - 2.0 VOLTS OF 60 cps DITHER

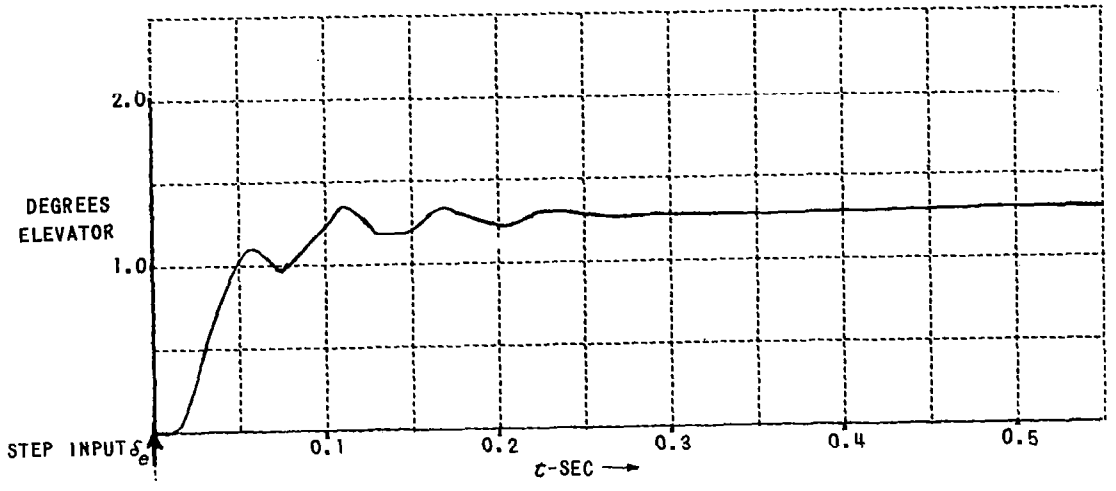

Figure 5-6 ELEVATOR SERVO STEP RESPONSE

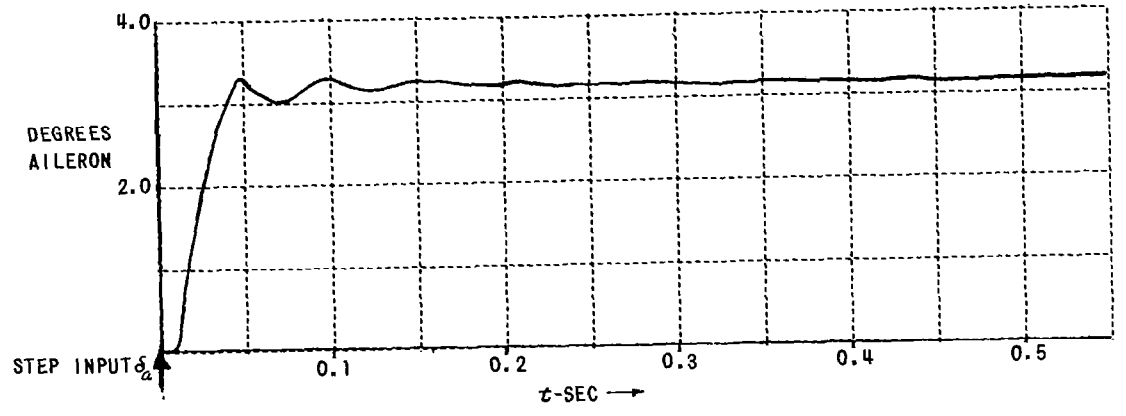

Figure 5-7 AILERON SERVO STEP RESPONSE

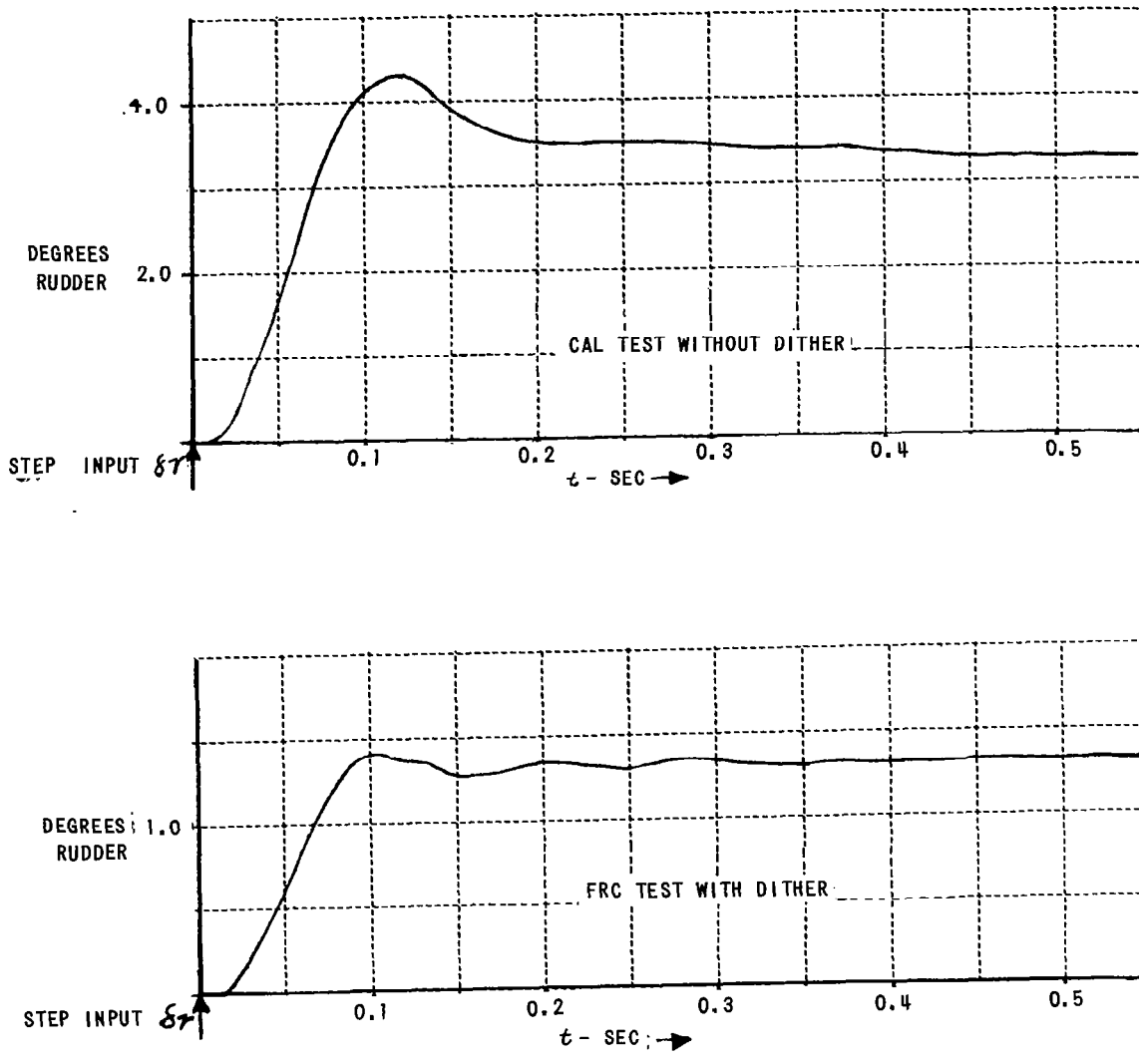

Figure 5-8 RUDDER SERVO STEP RESPONSE

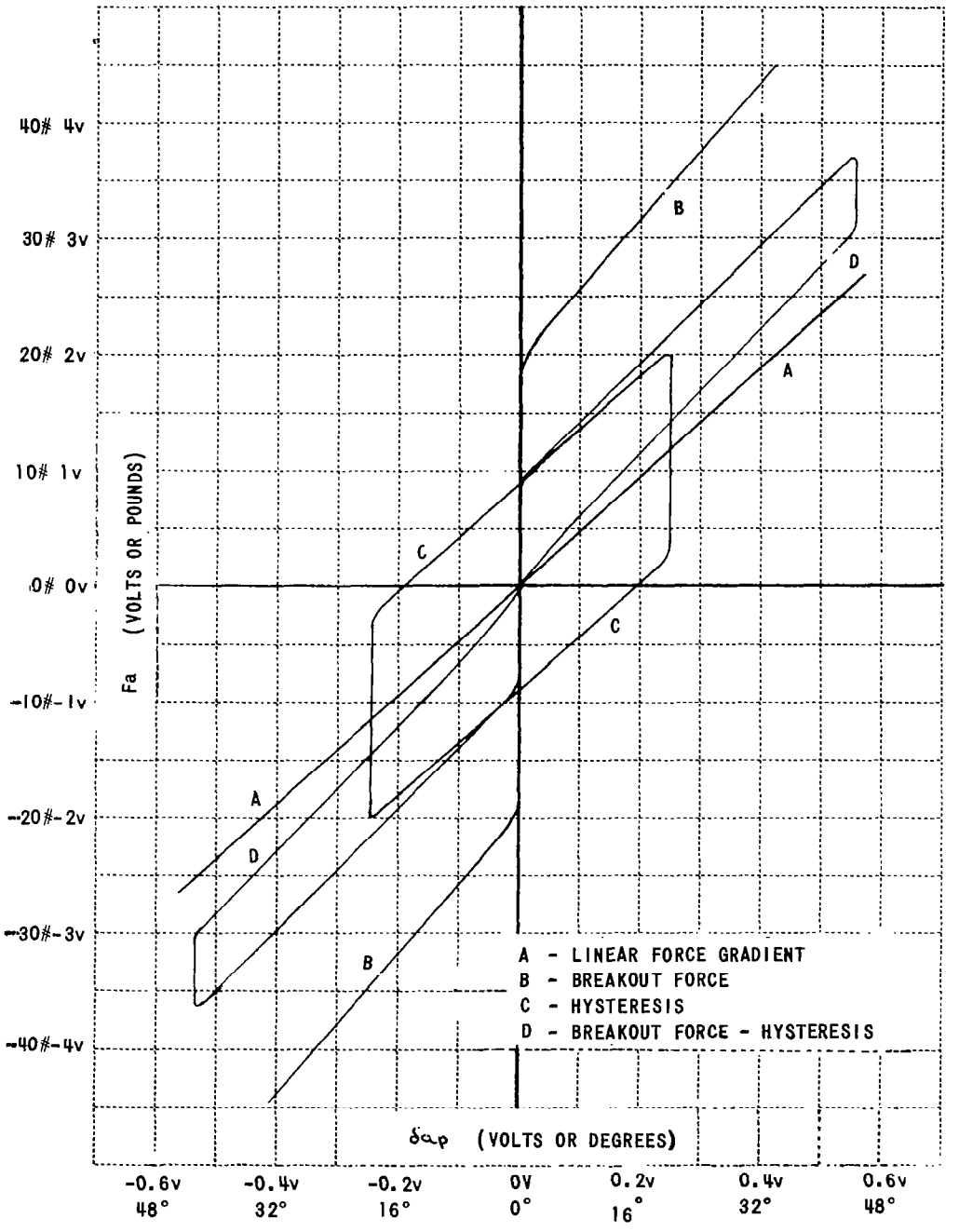

Figure 5-9 MEASURED PERFORMANCE OF AILERON FEEL SYSTEM (SHEET 1 OF 3)

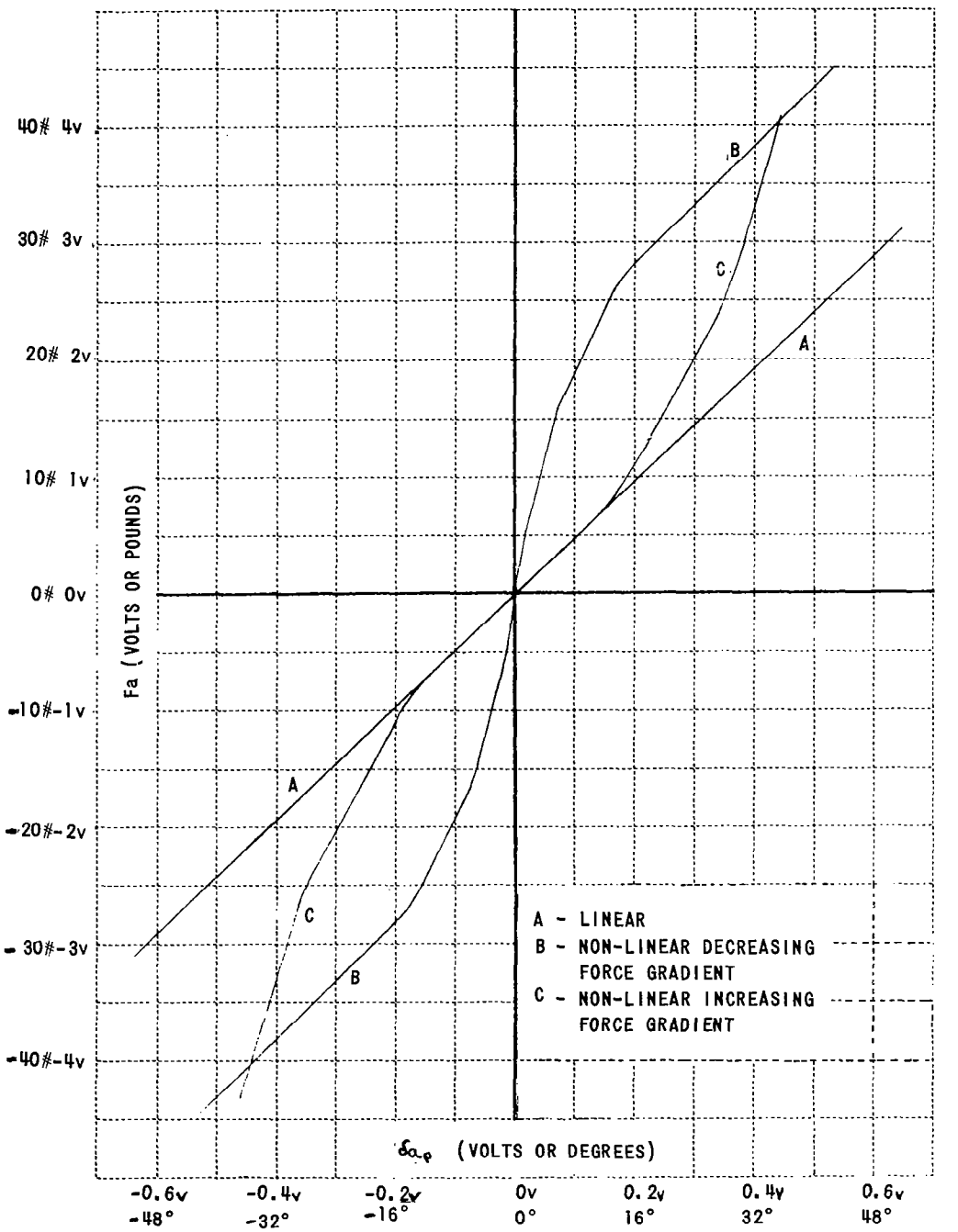

Figure 5-9 MEASURED PERFORMANCE OF AILERON FEEL SYSTEM (SHEET 2 OF 3)

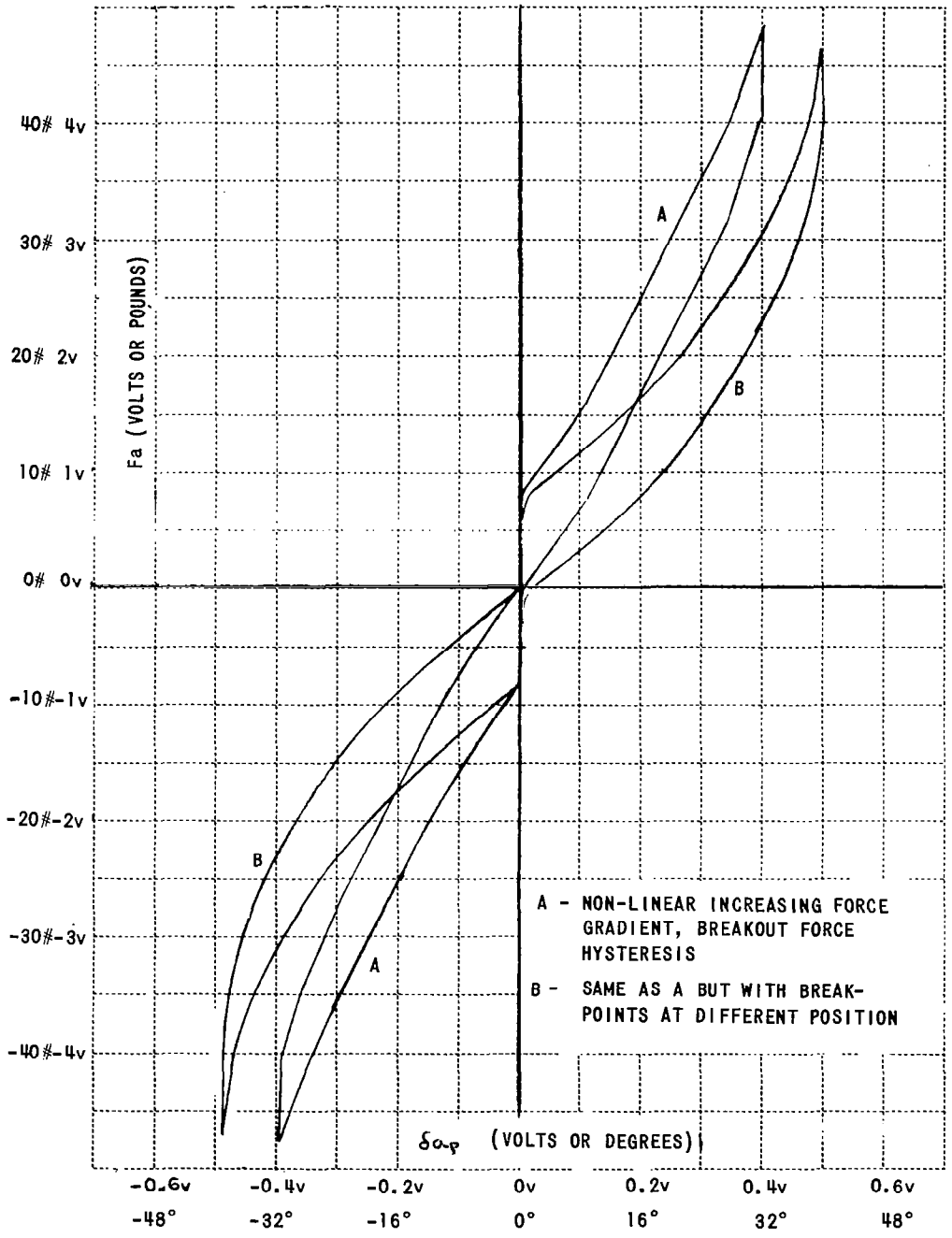

Figure 5-9 MEASURED PERFORMANCE OF AILERON FEEL SYSTEM (SHEET 3 OF 3)

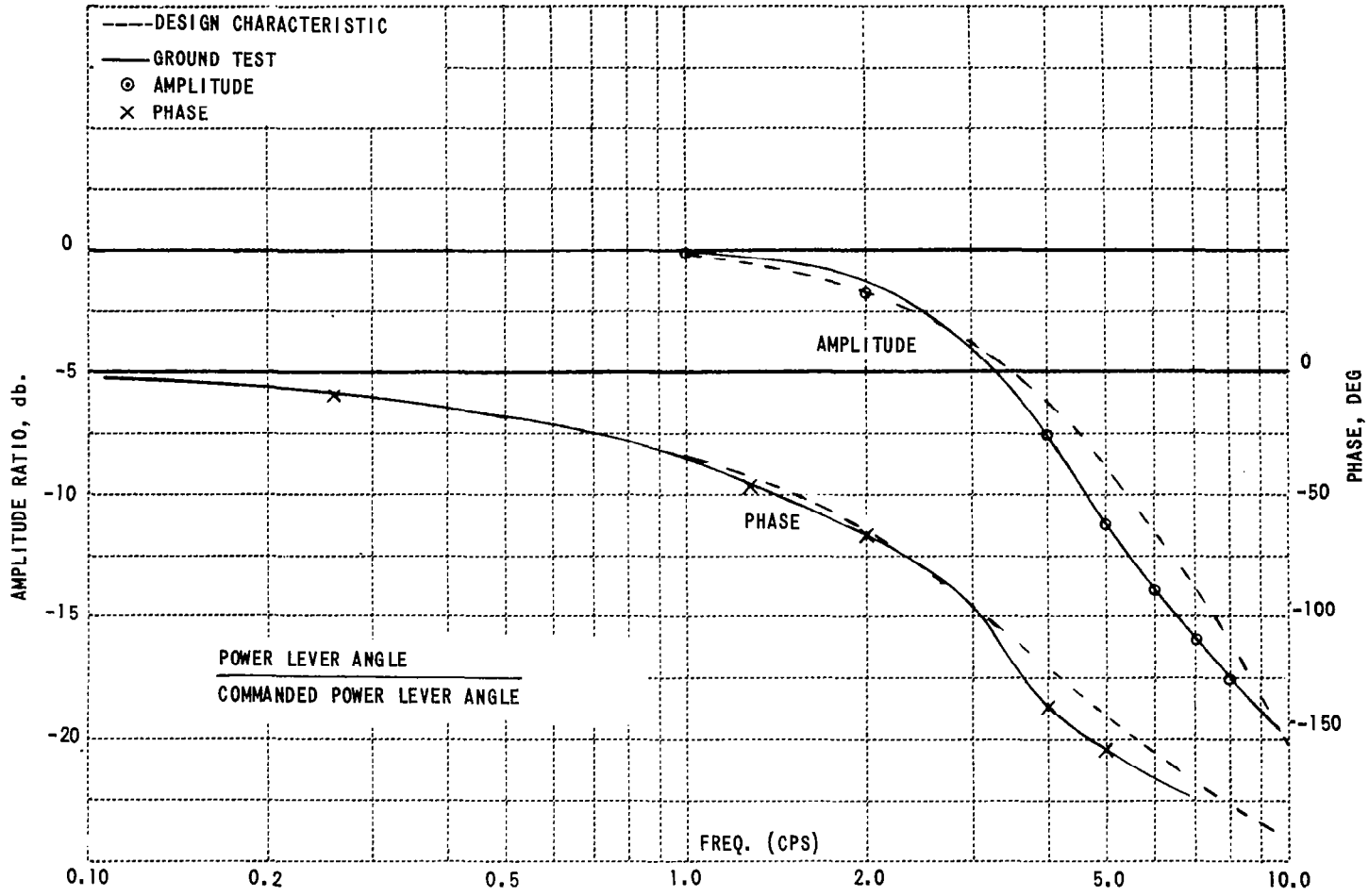

Figure 5-10 FREQUENCY RESPONSE OF GPAS THROTTLE POSITION LOOP

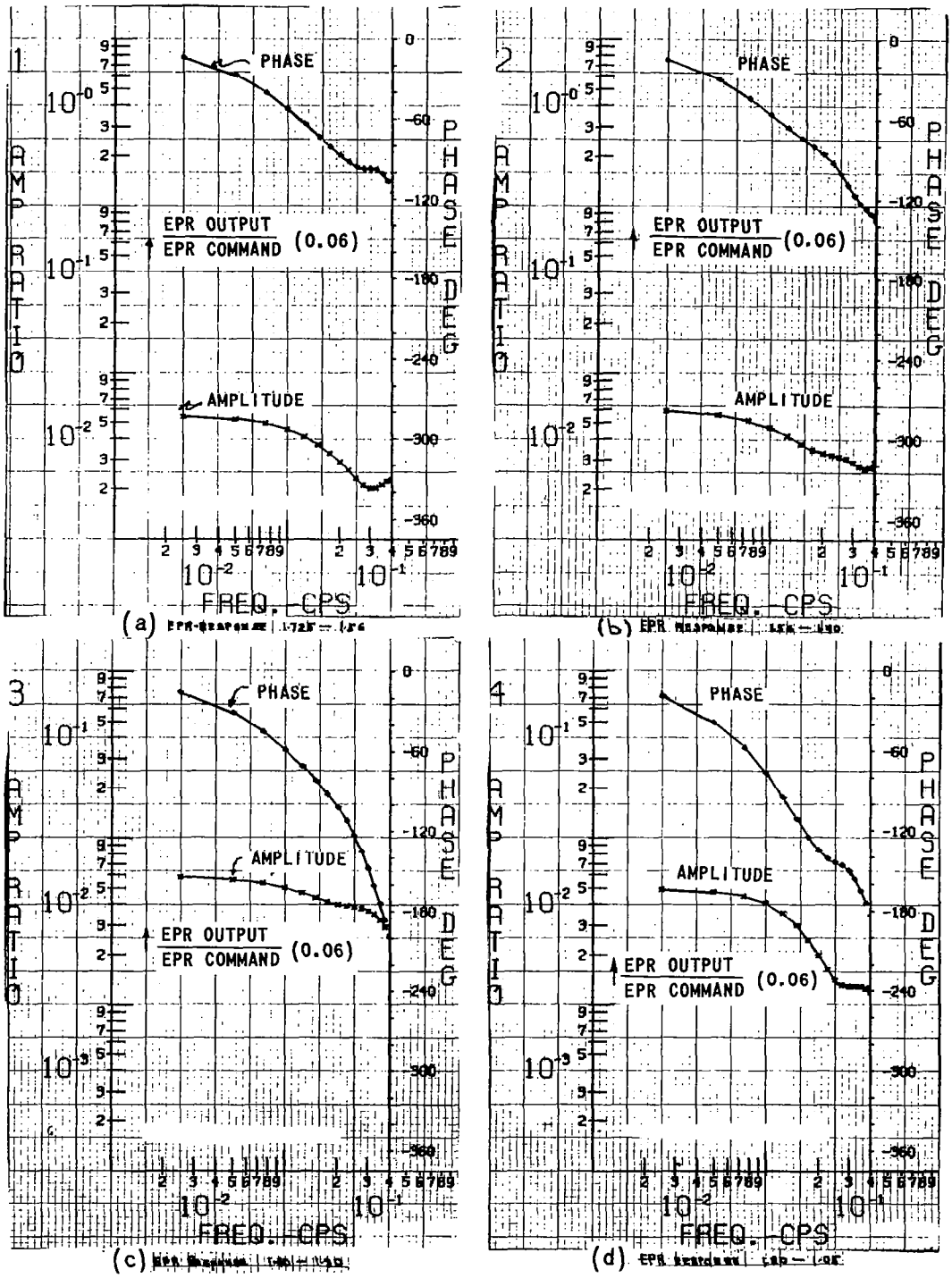

Figure 5-11 GROUND-TEST ENGINE PRESSURE RATIO RESPONSES FOR DESCENDING STEP COMMANDS

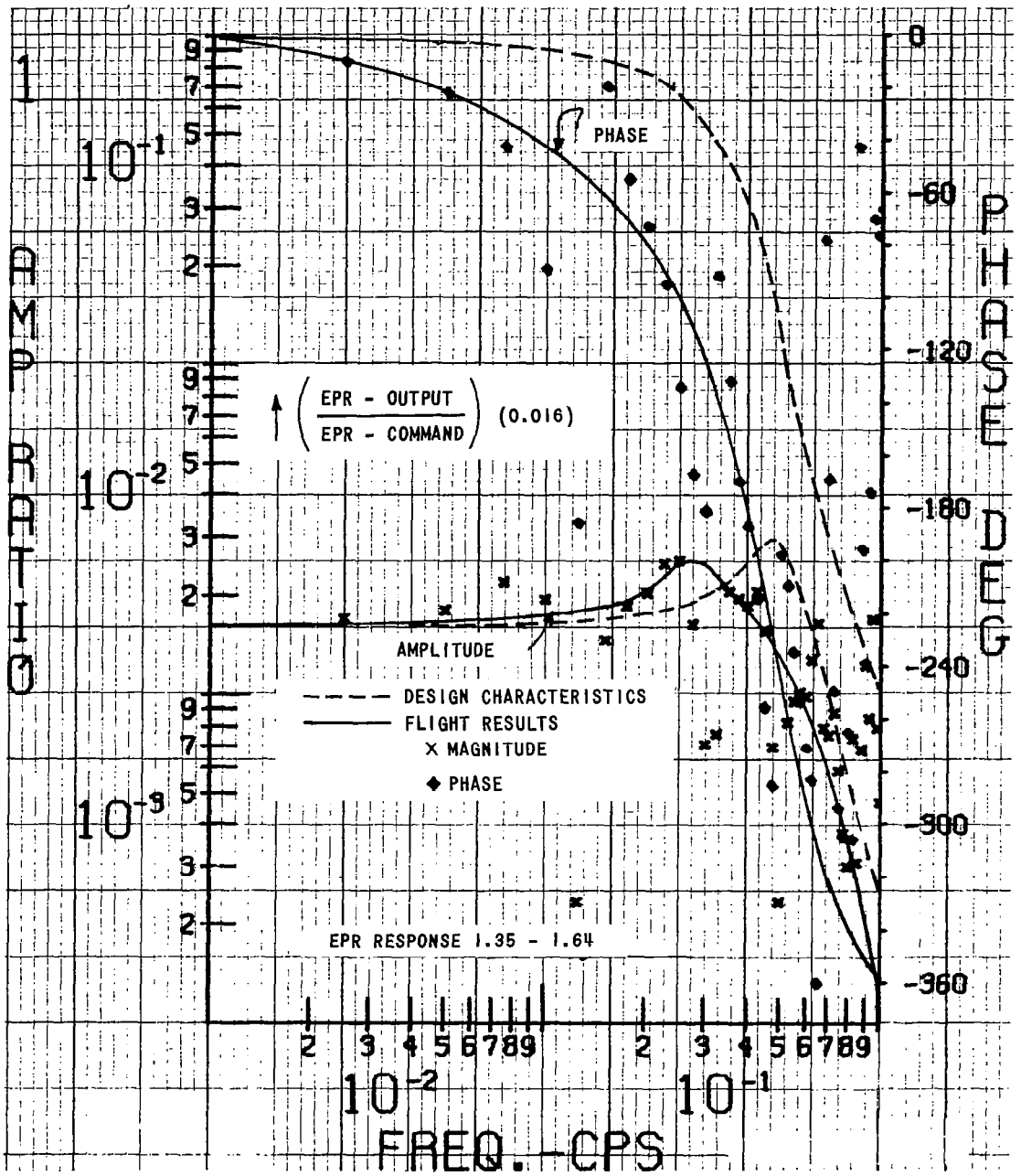

Figure 5-12 FLIGHT-TEST ENGINE PRESSURE RATIO RESPONSE FOR ASCENDING STEP COMMAND

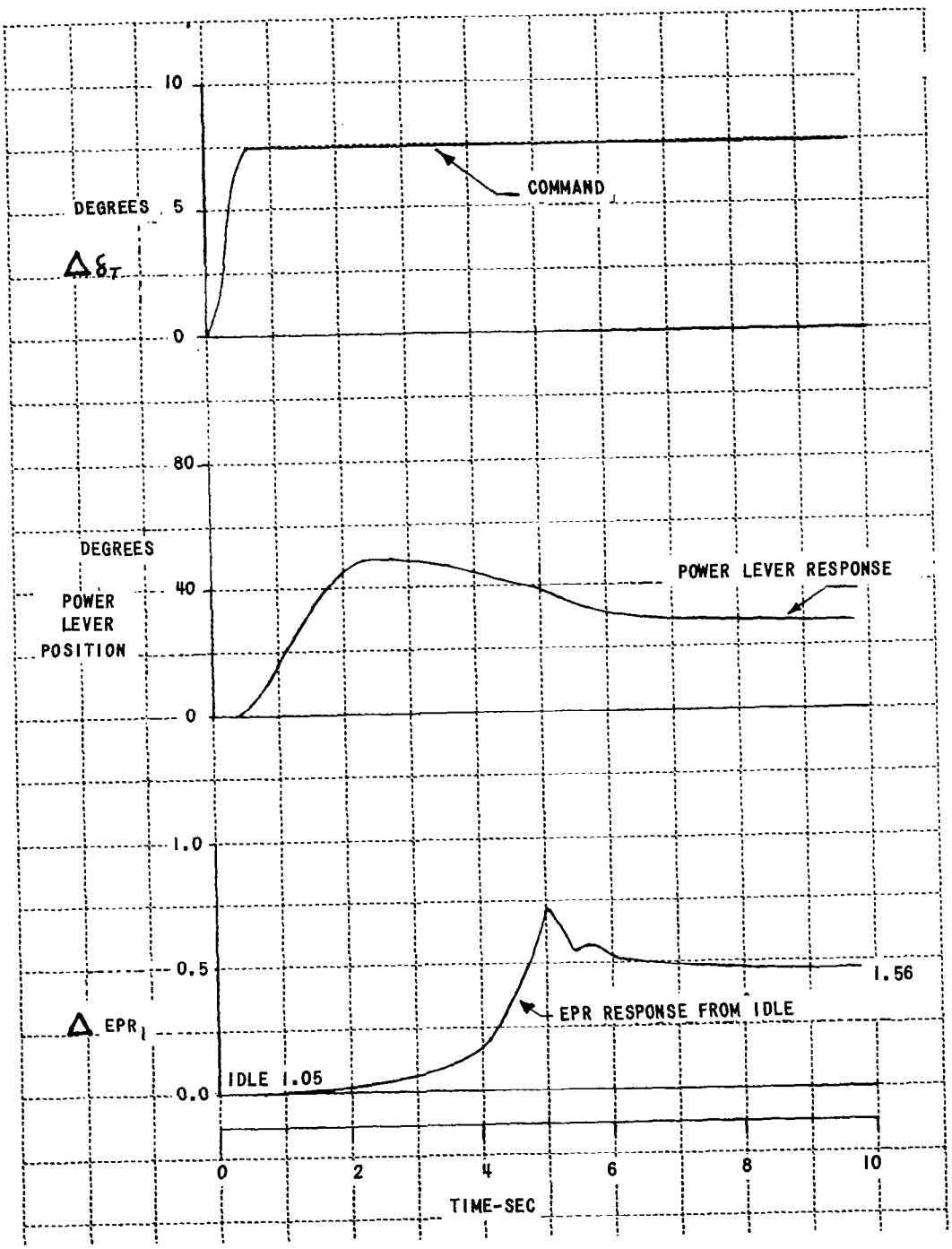

Figure 5-13 GROUND-TEST ENGINE PRESSURE RATIO RESPONSE FOR ASCENDING STEP COMMAND

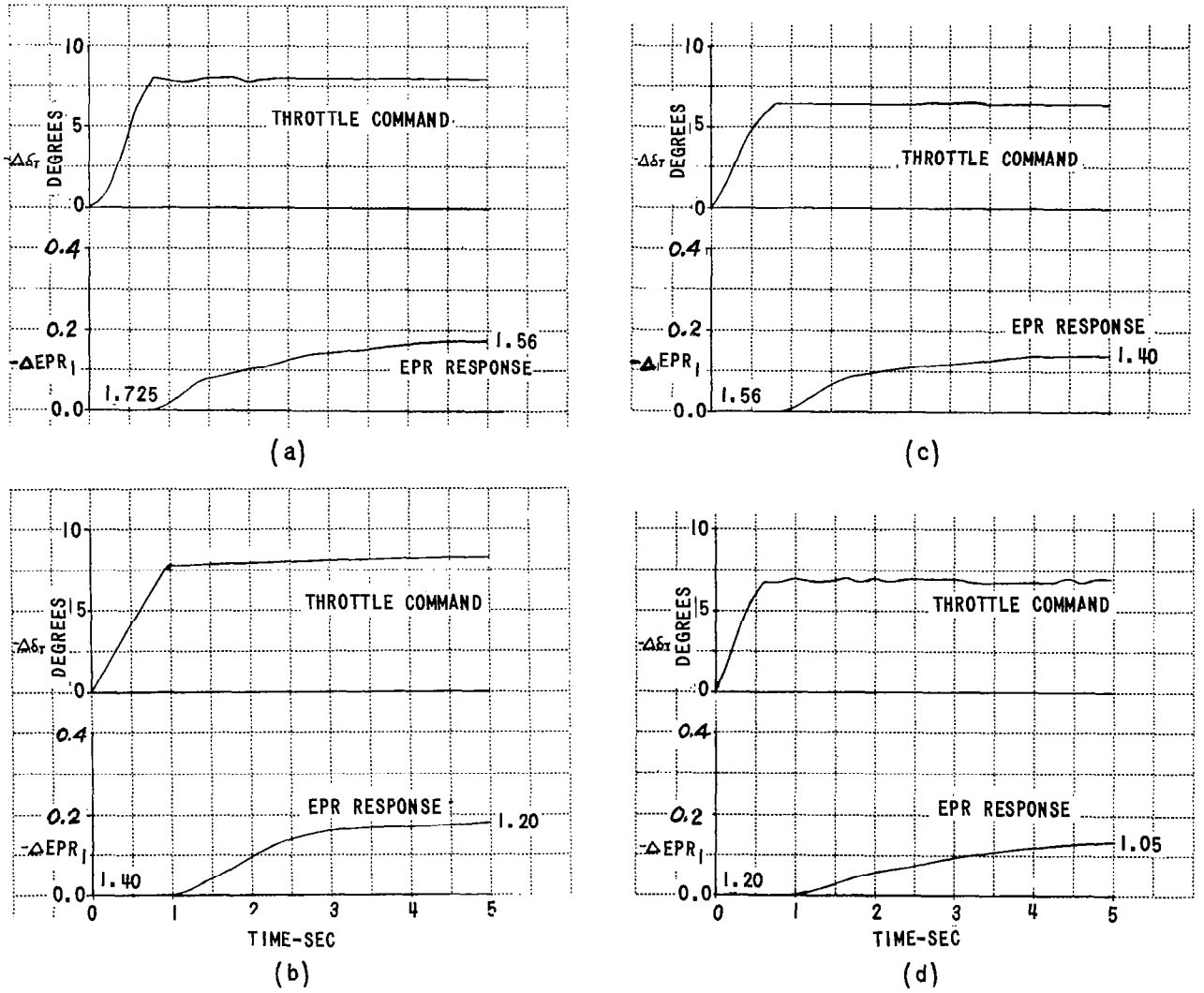

Figure 5-14 TIME HISTORIES OF ENGINE PRESSURE RATIO RESPONSES FOR DESCENDING STEP COMMANDS

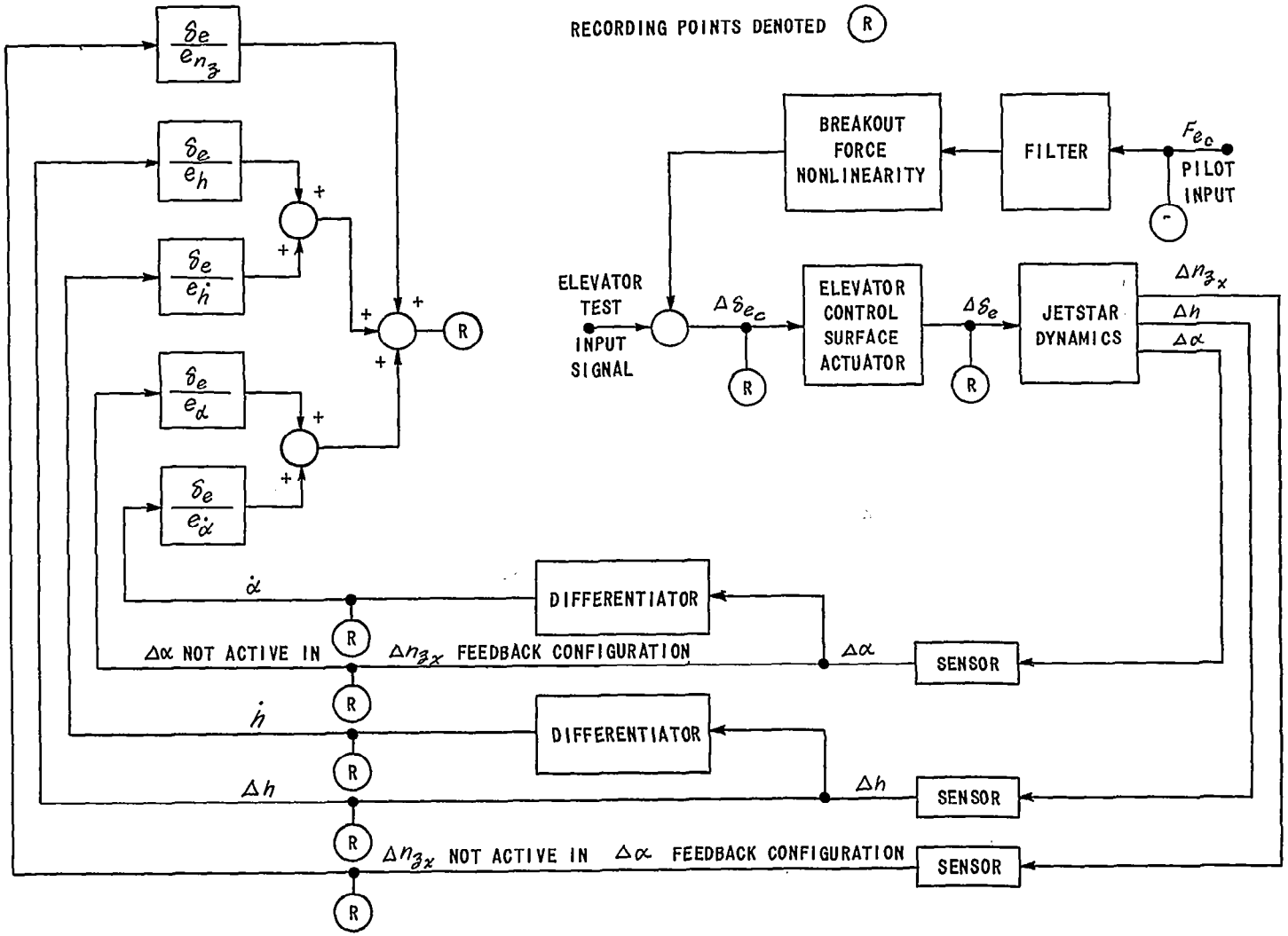

Figure 5-15 GPAS ELEVATOR CONTROL LOOPS

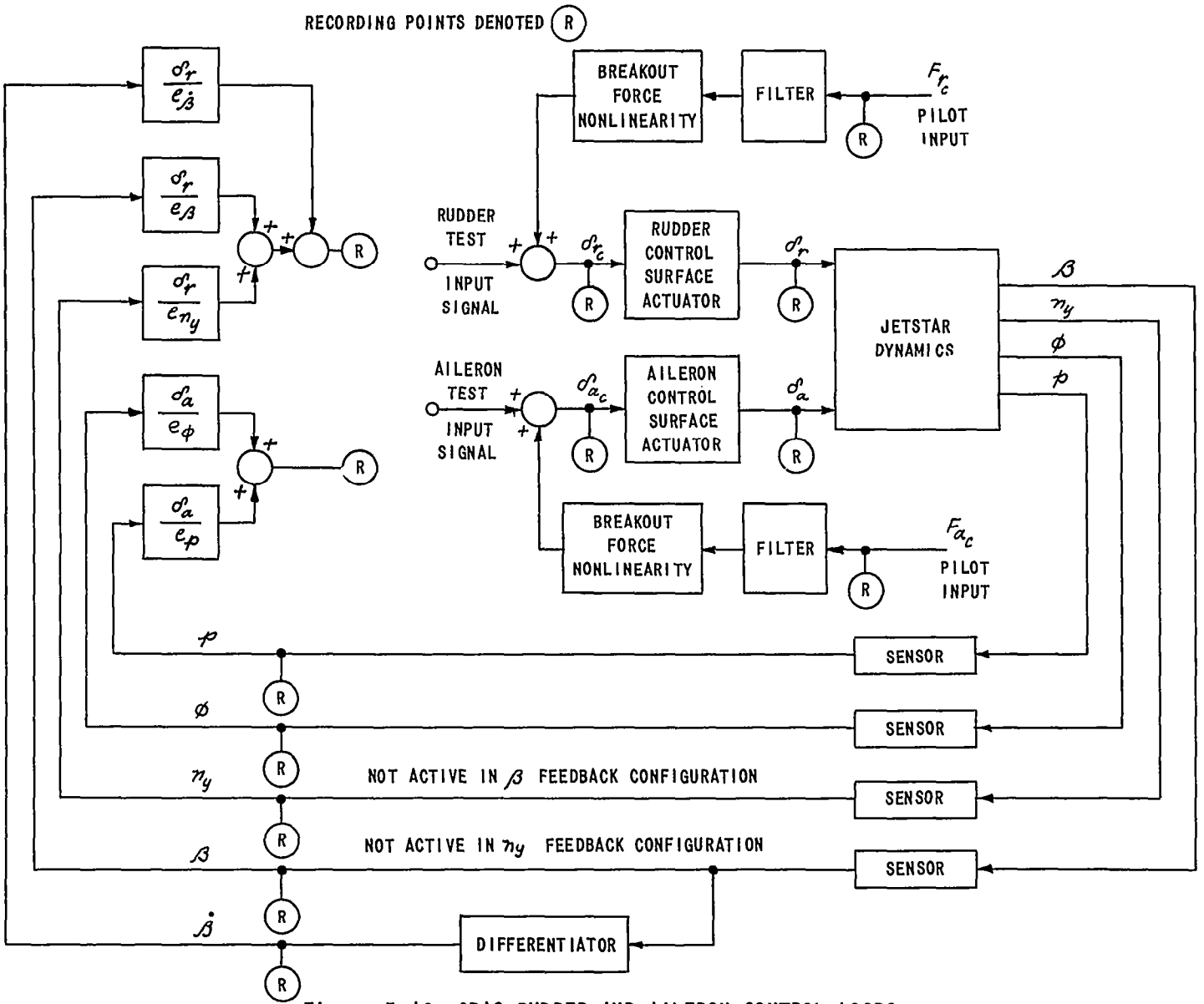

Figure 5-16 GPAS RUDDER AND AILERON CONTROL LOOPS

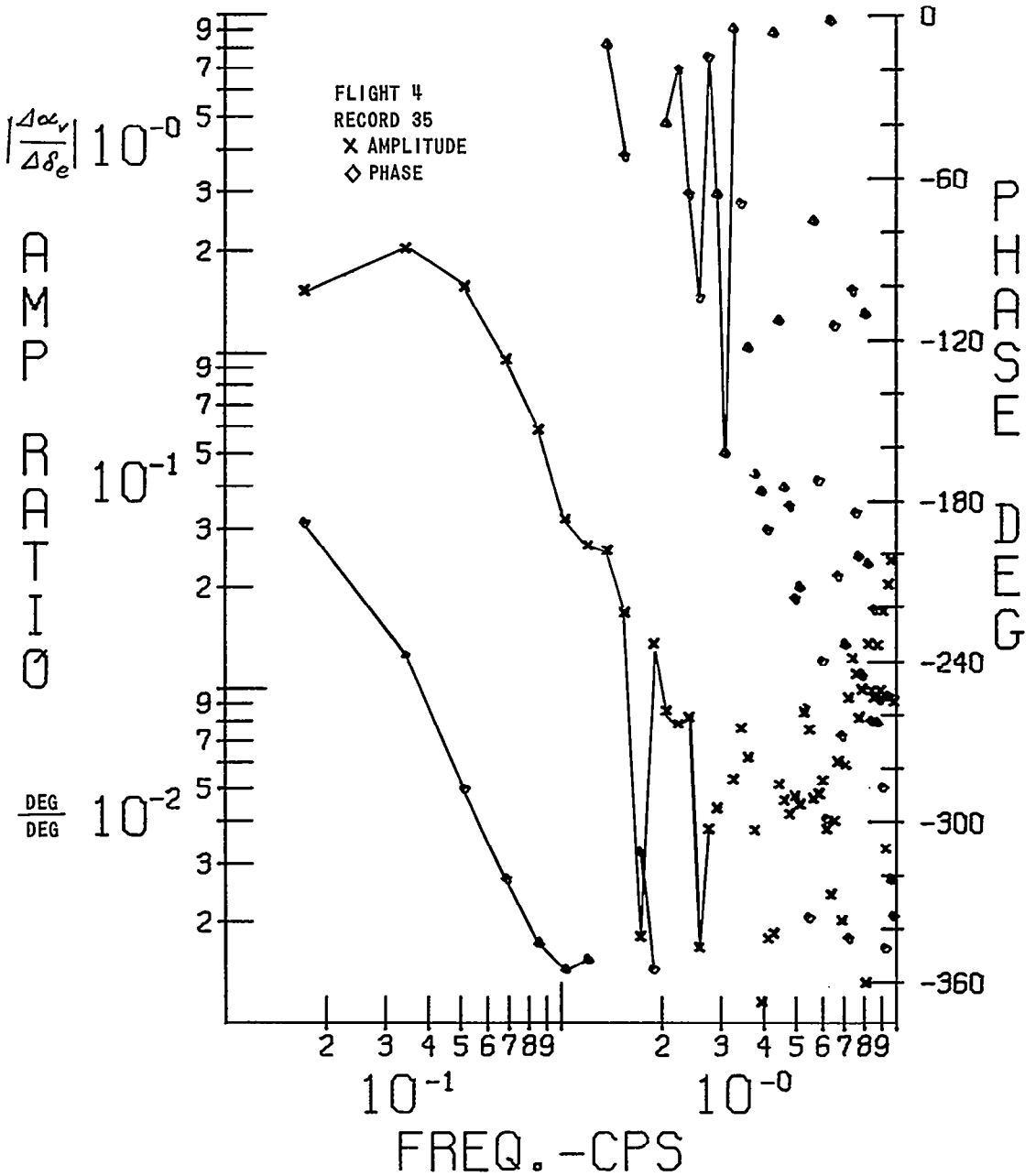

Figure 5-17 ANGLE OF ATTACK TRANSFER FUNCTION FOR ELEVATOR INPUTS

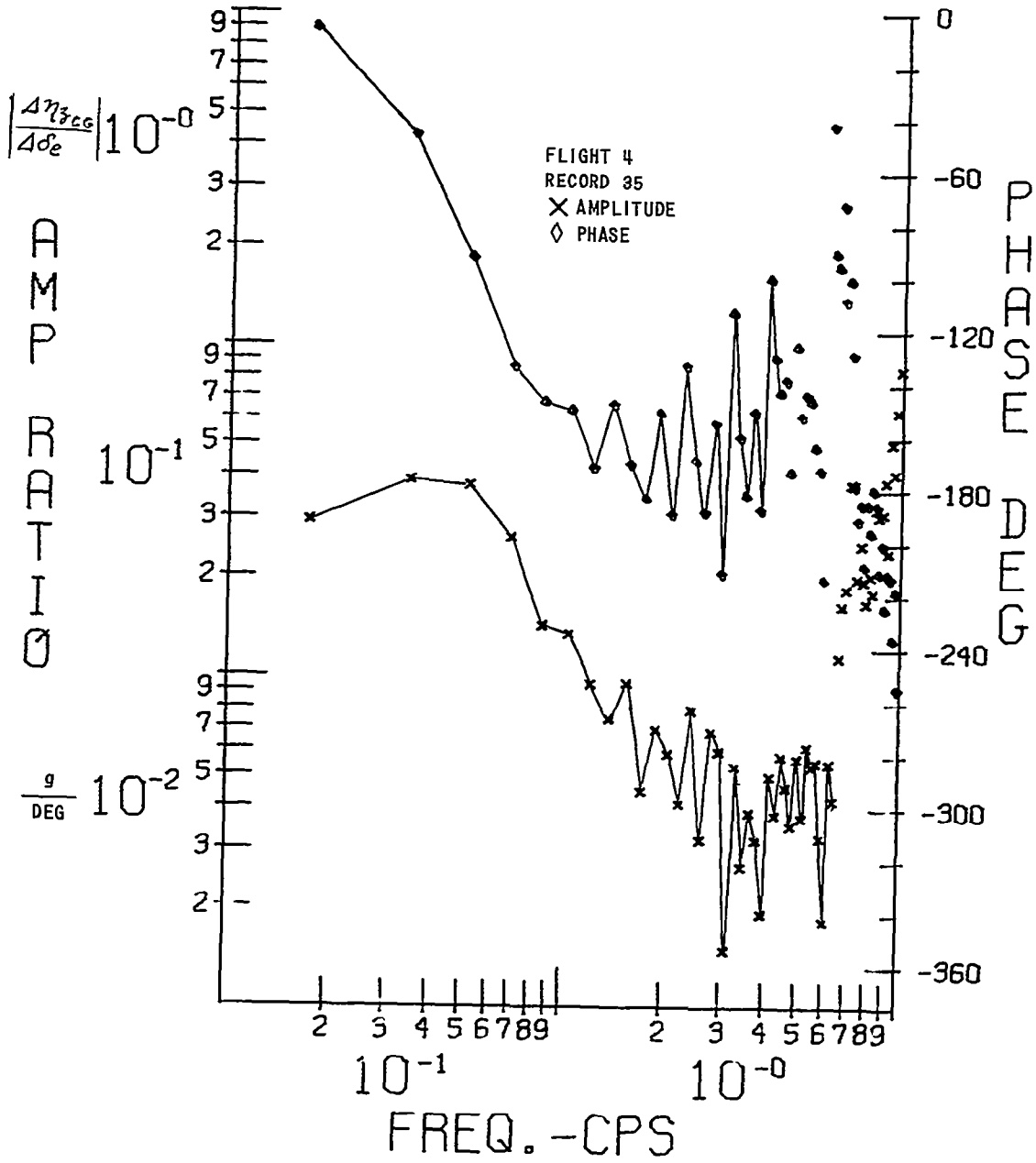

Figure 5-18 NORMAL ACCELERATION TRANSFER FUNCTION FOR ELEVATOR INPUTS

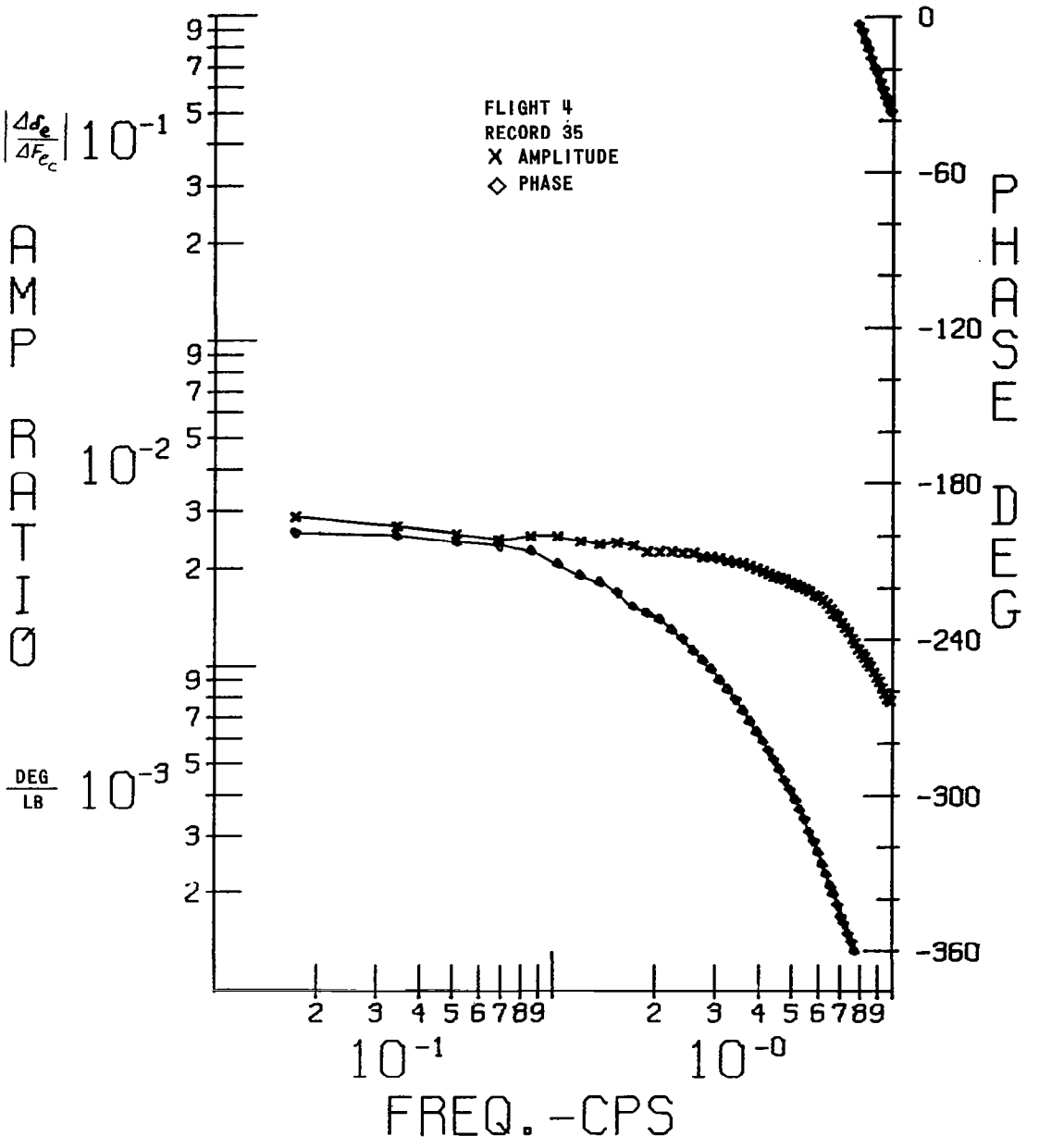

Figure 5-19 ELEVATOR DEFLECTION TRANSFER FUNCTION FOR STICK FORCE INPUTS

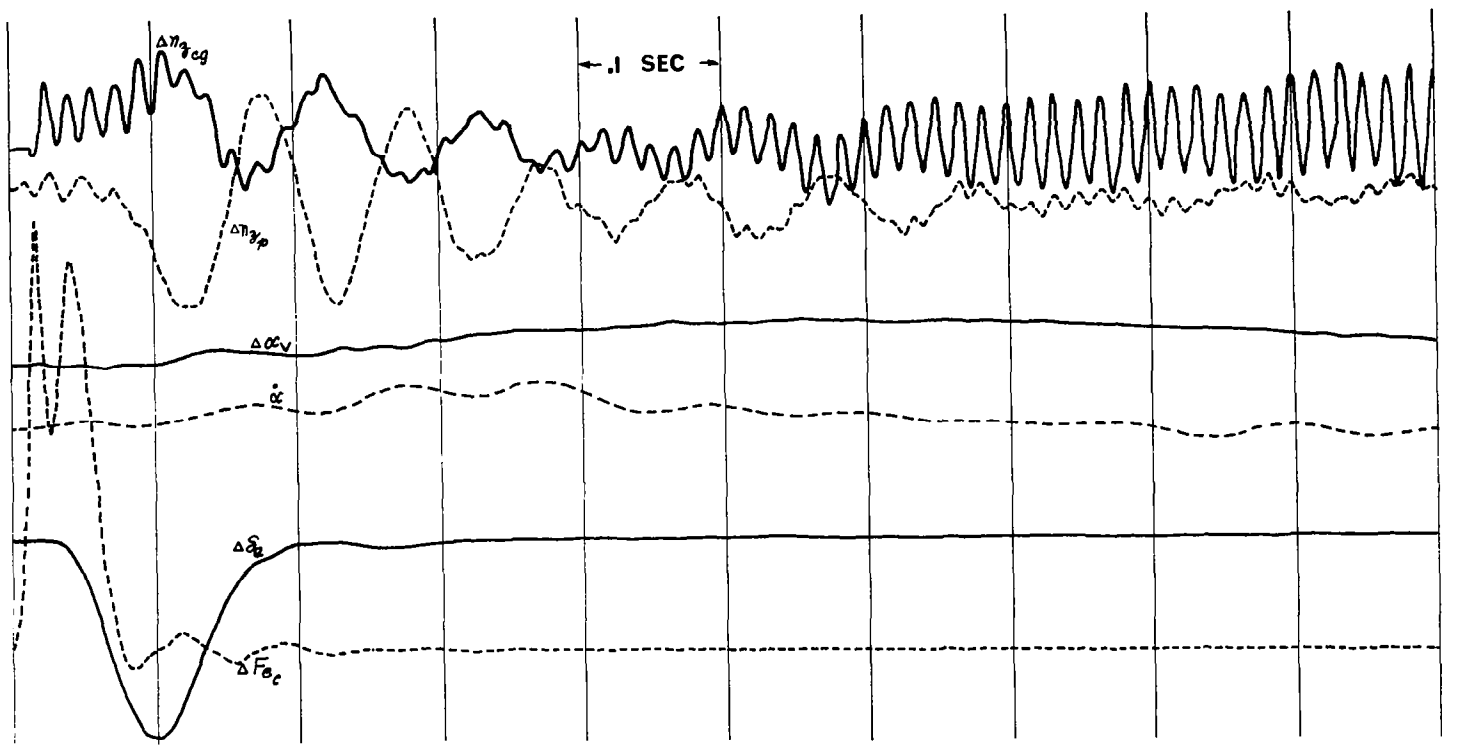

Figure 5-20 PORTION OF FLIGHT 4 , RECORD 35 SHOWING RESPONSE FOR FORCE PULSE INPUT

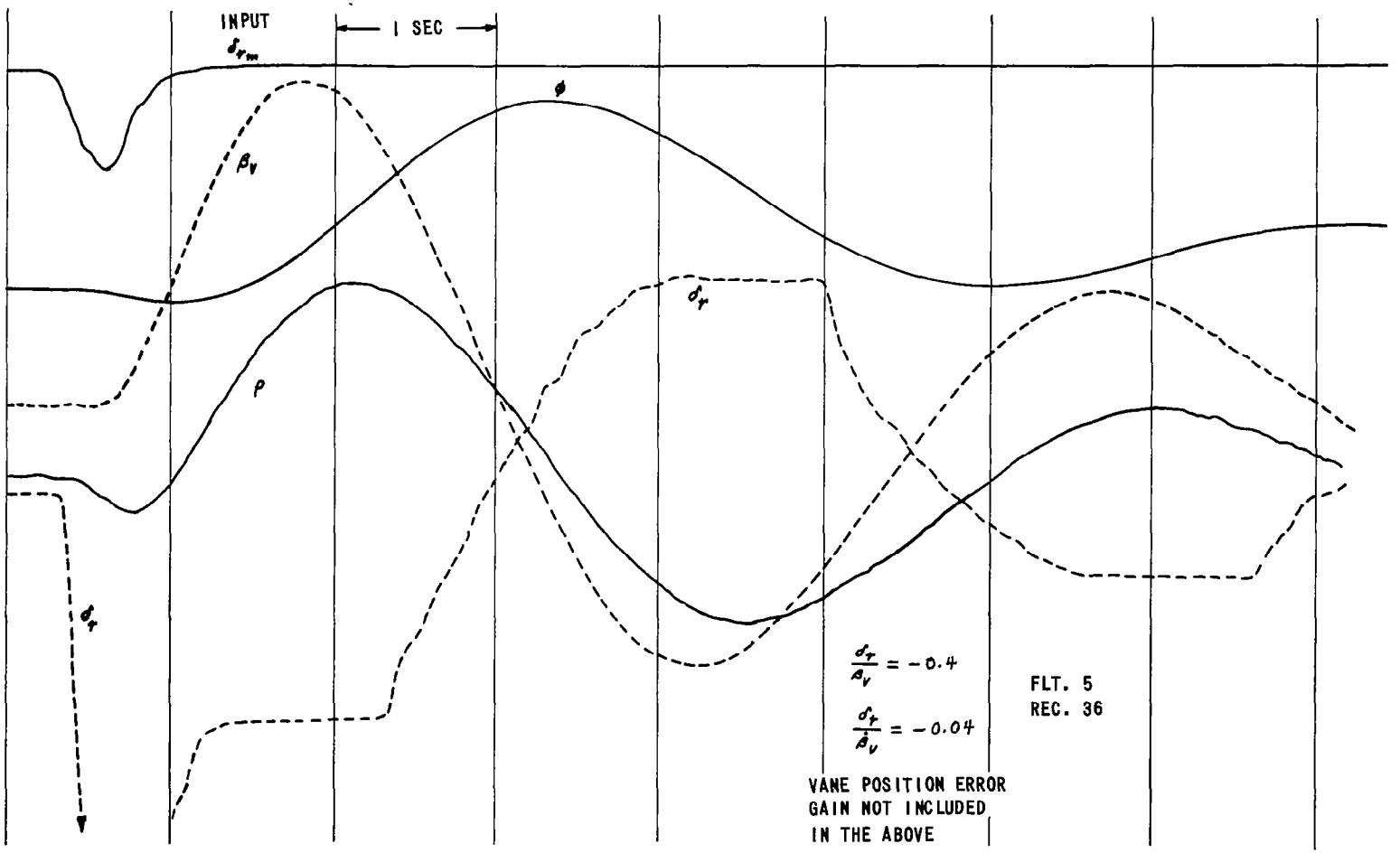

Figure 5-21 RESPONSE FOR PULSE INPUT TO RUDDER CONTROL LOOPS (RFS)

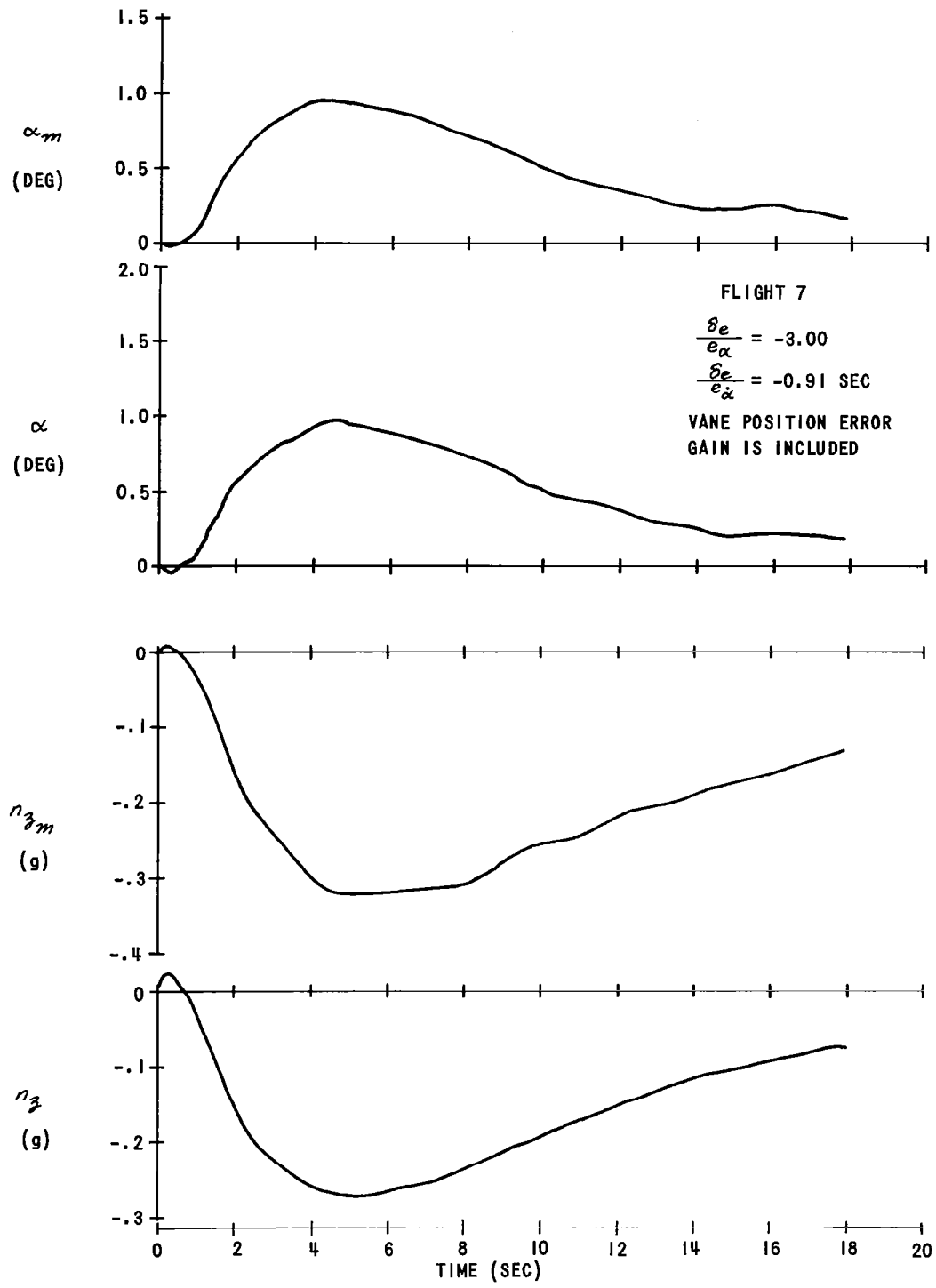

Figure 5-22 FLIGHT-TEST MODEL-FOLLOWING RESULTS - ELEVATOR INPUT

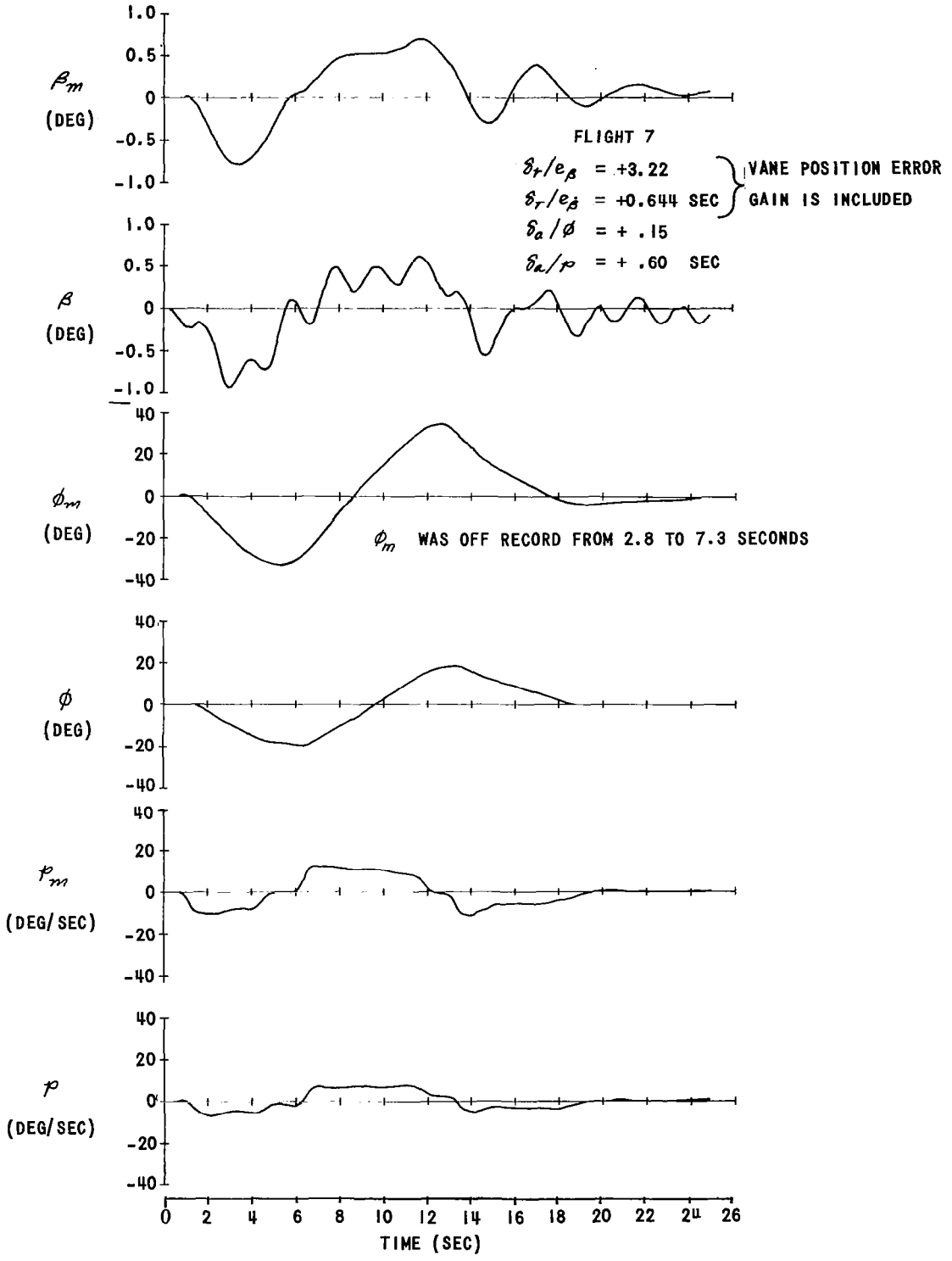

Figure 5-23 FLIGHT-TEST MODEL-FOLLOWING RESULTS - AILERON INPUT